Dissertation

The Hydroclimate of the Upper Colorado River Basin and the Western

United States

Submitted by

Rebecca A. Bolinger

Department of Atmospheric Science

In partial fulfillment of the requirements

For the Degree of Doctor of Philosophy

Colorado State University

Fort Collins, Colorado

Summer 2014

Doctoral Committee:

Advisor: Christian D. Kummerow

Nolan Doesken
Jorge Ramirez
Steven Rutledge
Tom Vonder Haar

ABSTRACT

THE HYDROCLIMATE OF THE UPPER COLORADO RIVER BASIN AND THE WESTERN

UNITED STATES

Understanding water budget variability of the Upper Colorado River Basin (UCRB) is critical, as changes can have major impacts on the region's vulnerable water resources. Using in situ, reanalysis, and satellite-derived datasets, surface and atmospheric water budgets of the UCRB are analyzed. All datasets capture the seasonal cycle for each water budget component. Most products capture the interannual variability, although there are some discrepancies with atmospheric divergence estimates. Variability and magnitude among storage volume change products also vary widely. With regards to the surface budget, the strongest connections exist between precipitation, evapotranspiration (ET), and soil moisture, while snow water equivalent is best correlated with runoff. Using the most ideal datasets for each component, the atmospheric water budget balances with 73 mm leftover. Increasing the best estimate of ET by 5% leads to a better long-term balance between surface storage changes, runoff, and atmospheric convergence. It also brings long-term atmospheric storage changes to a better balance of 13 mm.

A statistical analysis and case study are performed to better understand the variability and predictability of the UCRB's hydroclimate. Results show significant correlations (at the 90% confidence level) between UCRB temperature and precipitation, and El Niño - Southern Oscillation (ENSO) and Pacific Decadal Oscillation (PDO) during the fall. However, correlations are typically not greater than 0.4. ENSO and PDO are associated with the second mode of variability in a Principal Component analysis, while the first mode of variability (57% of variance for precipitation and 74% of variance for temperature) displays a

high year-to-year variability. A case study of a wet and a dry year (with similar ENSO/PDO conditions) shows that a few large accumulation events is what drives the seasonal variability. These large accumulation events are more dependent on a variety of more local synoptic conditions (e.g., location of low pressure, direction and speed of local winds, amount of moisture available). An analysis of ten winters shows that there are generally less than five large accumulating events in drier winters, with closer to ten in wetter winters. Overall, the statistics and case study show that a consistently accurate seasonal forecast for the UCRB is not achievable at this time.

Expanding the ideal datasets selected over the UCRB, an analysis of the errors in atmospheric and surface water budgets is performed for every individual HUC4 basin over the western U.S. Surface water budgets show overall much smaller residual errors than the atmospheric water budgets over the region. Visually analyzing the balances and imbalances, we see that several different areas around the Continental Divide and the Great Basin balance well at the surface, but not as well in the atmosphere; around Arizona, most basins dont balance at either the surface or atmosphere; many of the Pacific coastal basins and basins in the northern Rocky mountains balance well at the surface and in the atmosphere. These balances/imbalances, climate variability, land cover, and topography are combined to delineate five hydroclimate zones. Seasonal and interannual variability is analyzed for each zone. The Pacific Coast zone shows strong agreement amongst the seasonal cycles of all the water budget components, while most of the other zones show an offset in peaks between components during the winter and summer.

TABLE OF CONTENTS

List of Figures

CHAPTER 1

INTRODUCTION

Understanding the water budget and hydrologic variability of a region is of paramount importance to identify the mechanisms of climate variability and change. Analysis of the water budget's variability over time can also shed light on the impacts of extreme events and help improve predictions of future states (Sheffield et al. 2012). This is especially important over the western United States, where water resources are vulnerable, and the population continues to grow.

1.1. WATER BUDGET OF THE UPPER COLORADO RIVER BASIN

For seven states in the western U.S., much of the water supply primarily begins as snow-pack in the Upper Colorado River Basin (UCRB). With sparse vegetation in the basin, changes in temperature and precipitation lead to direct responses in the water budget (particularly storage in snowpack and runoff), thus greatly affecting the water supply. A complete understanding of the water budget is critical, as changes can have major socioeconomic impacts. Though there is still doubt about how climate change will affect precipitation trends in the basin, temperature increases are likely. Seager et al. (2007) have shown that rising temperatures associated with climate change could increase the frequency of severe droughts in arid and semi-arid regions, while other studies have shown shifts in the timing of peak runoff (Miller and Piechota 2008; Hamlet et al. 2007) and reduction in runoff (Christensen and Lettenmaier 2007; Hoerling and Eischeid 2007; McCabe and Wolock 2007) over the region. Several studies have also pointed to positive feedbacks that could have an affect on the basin's water supply. Groisman et al. (1994) showed a positive feedback between warming

temperatures and snow cover extent, and Entekhabi et al. (1992) highlighted several positive feedbacks (as a result of precipitation deficits propagating down through all components of the water budget) that prohibit the generation of precipitation and result in prolonged droughts.

In addition to sensitivity due to feedbacks and climate change, the UCRB is also sensitive to climate variability. Several studies have identified a correlation between hydroclimatic variability in the region and large-scale climate forcings such as the El-Nino Southern Oscillation (ENSO) and Pacific Decadal Oscillation (PDO) (Hurkmans et al. 2009; Kim et al. 2005; McCabe and Dettinger 2002). Other studies have found strong relationships between UCRB climate variability and sea surface temperature (SST) variability in other ocean regions not related to ENSO and PDO (Aziz et al. 2010; Switanek et al. 2009; Tootle and Piechota 2006). Some studies have shown that UCRB climate is dominated by variances on decadal to multidecadal timescales (Nowak et al. 2012; Ault and George 2010). With the sensitivities of the water budget to climate change, climate variability, and land-atmospheric feedbacks, it is essential to have a thorough knowledge of the variability of each water budget component and how they relate to each other in the region's hydrologic cycle.

Ideally, one would study the different components of the water budget using perfect observations taken at a continuous and high spatial and temporal resolution. This is unfortunately impossible. Though *in-situ* observations are the most direct way to take measurements of the water variables, they are only point measurements that cannot be easily (or accurately) extrapolated to other areas throughout a larger basin (Kustas et al. 1991). In addition, direct measurements may not yield the most accurate and representative datasets. For example, snowpack measurements cannot be made above treeline (due to wind contamination), where

the heaviest amounts of snow can accumulate throughout the winter; precipitation obser-
vations tend to be more concentrated in populated areas; soil moisture measurements are
sparse given the hard soils found throughout much of the basin; evaporation measurements
rely on some set of assumptions that may only apply at a local scale. The weaknesses of
in-situ observations point to the necessity of utilizing model, reanalysis, and satellite-derived
datasets.

Reanalysis and satellite-derived datasets have an advantage over *in-situ* observations in
that they provide spatially and temporally consistent global measurements of all atmospheric
and surface hydrologic variables. However, each gridded dataset comes with their own set
of weaknesses. Reanalysis data, though initially forced by direct or remotely sensed obser-
vations, are continuously modified and confined by model physics. Each reanalysis product
has its own set of model parameterizations and data assimilation methods to simulate land
and atmospheric variables. Reanalysis products are also released at a relatively coarse spa-
tial resolution that is ideal for global climate studies and may not be as ideal for regional
analysis. Satellite-derived datasets tend to be available at much higher spatial resolutions.
But they each rely on different algorithms to translate raw retrievals into water variables.
These generalized (i.e. imperfect) models and algorithms add some degree of uncertainty to
each gridded dataset.

In Chapter 3, a suite of *in-situ*, reanalysis, and satellite-derived datasets will be compared
for each component of the surface and atmospheric water budgets. The objectives are to
gain a better understanding of the UCRB's hydroclimatic variability and to identify a set of
consistent datasets to use for each water budget component. These objectives will be met
through analysis of each water budget component and by attempting water budget closure.

1.2. Hydroclimatic Prediction of the UCRB

In addition to understanding the water budget, a more thorough analysis of the hydroclimatic variability of the UCRB is necessary in order to improve predictability. The Colorado Basin River Forecast Center (CBRFC) currently releases seasonal streamflow and water supply forecasts beginning in January (forecasting for the spring runoff and summer water demand seasons), but there is a greater desire from water managers and planners to have forecasts beginning in October of the previous year (i.e., the beginning of the water year). Franz et al. (2003) stated that earlier in the water year, the main source of forecasting uncertainty is meteorology. Later in the season (close to spring), meteorology has less of an impact as existing conditions (i.e. snowpack) increasingly play a larger role in forecasting streamflow and water supply.

Many studies have tried to improve long-term predictions of streamflow in the region. Franz et al. (2003) detail the Ensemble Streamflow Prediction (ESP) forecasts used by the National Weather Service (NWS) River Forecast Centers (RFCs, CBRFC included). The ESP forecasts combine a soil moisture accounting model with a snow model and a streamflow routing algorithm. Starting with current basin conditions, a range of historical temperature and precipitation values are input into the model to produce an ensemble of possible streamflow scenarios. Werner et al. (2004) found that adding ENSO conditions to the model does not improve forecasts for the UCRB. Other studies have found only weak to no lag correlations between the UCRB hydroclimate and ENSO/PDO indices (Hurkmans et al. 2009; McCabe and Dettinger 2002).

Some older studies have focused on more local, synoptic scale statistics of winter season precipitation in the region, without regard to ocean indices. Rasmussen (1968) found that

winter storm periods over the UCRB were generally associated with 500 hPa southwesterly flow, while northerly 500 hPa flow was more dominant during dry periods. Similarly, Changnon et al. (1993) found an overall higher number of 500 hPa southwest troughs and a lower occurrence of dry ridge patterns during wet snowpack years over the Rocky Mountains. Although both studies identified a statistical relationship between the 500 hPa pattern and the region's winter precipitation, neither study focused on specific storms or attribution.

Until now, the majority of studies have focused on identifying statistical relationships between the regional climate variability and large-scale climate drivers and using those statistical relationships as a basis for predictability. Chapter 4 will go into more detail on the UCRB's variability by focusing on the eight sub-basins that make up the UCRB separately, and also focusing in on monthly contributions as opposed to variability in the seasonal total. Because of the ambiguous large-scale statistical relationships that exist, one objective, in Chapter 4, is to gain a better understanding of the local drivers that modulate wet seasons versus dry seasons. A detailed case study of one wet and one dry year, with similar ENSO/PDO conditions, will shed more light on what controls the variability in the UCRB.

1.3. Water Budget of the Western United States

In Chapter 5, analysis is expanded from the smaller domain UCRB to the larger region of the western U.S. Many previous studies have looked at the hydroclimate of the western U.S. A vast number of studies (including Harpold et al. 2012; Nolin 2012; Regonda et al. 2005; Barnett et al. 2004; Stewart et al. 2005; and Dettinger and Cayan 1995) have looked at how climate change has impacted the hydroclimate of the region; other studies focused on the large-scale variability (e.g., Pederson et al. 2011; Abatzoglou 2011; Cayan 1996; and Redmond and Koch 1991). In addition to previously mentioned research over the UCRB,

several studies have presented research for other watersheds within the western U.S. Hamlet and Lettenmaier (1999) studied how the water resources of the Columbia River Basin respond to climate change; MacDonald et al. (2011) studied the impacts of climate change on snow in the St. Mary watershed in Montana; and changes in streamflow patterns were found in Idaho, Nevada and Wyoming watersheds (Clark 2010). While the aforementioned studies have either looked over the larger region, focused in on smaller watersheds, or limited the scope to one or two components of the water budget, it is uncommon to find research that analyzes every hydrologic component over the entire western United States coupled with a watershed approach.

While Chapter 3 quantifies the errors in the water budget, it highlights the importance of identifying the strengths and weaknesses of the different dataset measurements over a larger region. Several studies have quantified the inconsistencies and errors in measurements of certain variables. Sheffield et al. (2012) identified discrepancies in the North American Regional Reanalysis's (NARR) surface water budget closure over more complex topography, while Bosilovich et al. (2011) and Trenberth and Guillemot (1998) both provide examples of the difficulties that reanalyses have in depicting the water budget. Errors in modeled evapotranspiration have been found by Mueller et al. (2011) and Jimenez et al. (2011), and challenges still remain in accurately depicting modeled or satellite-derived soil moisture (Reichle et al. 2004), snowpack (De Lannoy et al. 2012), and terrestrial water storage changes (Lorenz et al. 2014). Because errors are inherent with most datasets, it will be necessary to determine a dataset's performance over different areas with different topography, land cover, and climate.

Chapter 5 provides a more qualitative "bigger picture" representation of the water budget, with the identification of self-similar regions within the western U.S. The selection of

these regions, through the analysis of the water budget of individual watersheds, will help pinpoint the causes for inconsistencies amongst the different variables and datasets. Analysis of the seasonal cycle and variability within each region will also provide further insight into the mechanisms, controls, and sensitivities of the local hydroclimatic variability of the western U.S.

1.4. OVERALL OBJECTIVES

Athough previous studies have analyzed the variability in the UCRB, this is the first study analyze the variability of each water budget component. This is also the first study to identify self-consistent datasets in the goal of attaining water budget closure over the UCRB.

In terms of improving seasonal prediction of water supply over the basin, many studies have already identified the statistical connections between global climate circulations and UCRB variability. This is the first study goes further by looking at what can drive the differences between wet and dry winters during similar large-scale climate regimes.

With regard to expanding over the western U.S., a large number of studies have already looked at the impacts of climate change and variability over specific regions of one or two specific components of the water budget. This is the first study to analyze every component of the water budget for every watershed of the western U.S. using a water budget closure approach.

With the accomplishment of the above research, we hope to gain a more thorough understanding of 1) water budget variability in the west, 2) how different datasets are consistent amongst each other, 3) the strengths and weaknesses of individual datasets in specific regions, and 4) how to improve the long-term seasonal prediction of the region.

CHAPTER 2

DATA AND METHODOLOGIES

Table 2.1 details the resolutions, time periods, and references for all of the datasets used in this study. Data are monthly totaled and presented in terms of water years (October - September). For the third and fifth chapters, the inclusion of all components of the water budget requires a shorter time period of study, so research is mainly limited to WY1999 - WY2008. For the temperature and precipitation analysis in Chapter 4, a longer time period is chosen (WY1911 - WY2010).

Chapters 3 and 4 focus in on the Upper Colorado River Basin (UCRB), which covers portions of Colorado, Utah, and Wyoming, with an areal size of about 2.9 x 10^5 km^2. Elevations in the UCRB range from 1400 m around the rivers to the highest peaks along the Continental Divide of over 3500 m (see Fig. 2.1, bottom panel). In Chapter 3, one basin average is calculated for all of the hydroclimate variables. This allows for easier comparisons across datasets with differing spatial resolutions. The differing spatial resolutions of the many different products could lead to disagreements that are beyond the scope of this research. While one basin average may eliminate important details from some of the datasets, it was considered the most ideal way to cross-compare and still provides informative and realistic results. In Chapter 4, sub-basin averages are calculated for each of the eight sub-basins within the UCRB (Fig. 2.1, top panel).

Chapter 5 expands the analysis to the 44 sub-regional hydrologic units (Seaber et al. 1987) that comprise the United States, west of the Continental Divide (Fig. 2.2). For each HUC4 sub-region, one basin-averaged value is calculated for the monthly hydroclimate variables.

Before datasets can be chosen, it is important to understand all components of the atmospheric and surface water budget equations. As shown by Peixoto and Oort (1992), the atmospheric water budget is defined as

$$\frac{\partial W}{\partial t} + \nabla \cdot \mathbf{Q} = (E - P),$$

(1)

where the difference between $\nabla \cdot \mathbf{Q}$ (the divergence of water vapor) and $(E - P)$ (evaporation minus precipitation) will equal the change in total column atmospheric water vapor, W, over time $(\frac{\partial W}{\partial t})$. $\frac{\partial W}{\partial t}$ can vary widely over shorter time periods. However, on an annual timescale, $\frac{\partial W}{\partial t}$ will be small, therefore $\nabla \cdot \mathbf{Q}$ and $(E - P)$ should essentially balance.

The surface water budget is defined as

$$\Delta S = P - R - ET,$$

(2)

where R is the surface runoff, and ΔS is the change in terrestrial water storage. ΔS is estimated from changes in snow water equivalent (annually this equals zero), changes in soil moisture storage, and changes in deep ground water and surface reservoir storage (assumed to be negligible for the western U.S.).

For Chapter 5, it will be important to look at how well each HUC4 balances, at the surface and in the atmosphere, by looking at the magnitude of the error. On annual and longer time scales, the atmospheric water budget in Eq. (1) becomes

(3)
$$\varepsilon_A = (ET - P) - \nabla \cdot \mathbf{Q},$$

where $\nabla \cdot \mathbf{Q}$ (atmospheric runoff) essentially balances with $(ET - P)$, and the remainder is the residual error, ε_A. Similar to Eq. (3), Eq. (2) now becomes

(4)
$$\varepsilon_S = P - R - ET - \Delta S.$$

Precipitation varies largely over the western U.S. (HUC4 annual precipitation can be as low as 250 mm to as high as 1500 mm or higher), therefore residual errors could also vary widely amongst the HUC4 basins. In order to accurately compare the HUC4 residuals in Chapter 5, all residual errors are normalized by dividing by the HUC4 precipitation, then multiplied by 100, and presented as percent residual error.

Now that each component of the water budget has been identified, a complete inventory of datasets for every component is necessary.

2.2. In-situ Datasets

2.2.1. Precipitation. National Weather Service Cooperative Network stations (COOP), located within the UCRB, provide direct observations of precipitation. Because COOP data are not spatially consistent, the question of representativeness is raised. In order to obtain one basin-averaged precipitation value over time, one could average the 105 stations together for one value. However, this might not be reasonable for a basin where precipitation is heavily dependent on elevation. Analysis of long-term averaged monthly precipitation at all sites show that precipitation amounts can vary by over an inch between the lower and higher

elevation stations. To test the representativeness of the COOP stations, a frequency distribution of the elevations in the basin (found by taking an average elevation for every $^1/_4^\circ$ by $^1/_4^\circ$ gridbox in the basin) is compared to the frequency distribution of the 105 COOP station elevations (Fig. 2.3). The spatially continuous gridpoint elevations are normally distributed with a mean elevation of 2149 m. The COOP stations' distribution is also normal, but shifted to lower elevations, with a mean elevation of 1921 m. Higher elevations are not well represented for COOP station data, therefore basin-averaged precipitation could be an underestimate. Instead of averaging the stations, an average precipitation is calculated for each 150 m elevation bin. These are then weighted based on the frequency distribution of the gridded elevations and totaled for one basin value.

Previous studies have shown the usefulness of incorporating elevation influences when spatially gridding station precipitation. External drift kriging and cokriging have been used to statistically interpolate precipitation based on elevation (Haiden and Pistotnik 2009). Daly et al. (1994) found that the PRISM dataset (Precipitation-elevation Regressions on Independent Slopes Model, released by the PRISM Climate Group at Oregon State University), performed better than any kriging method over the Willamette River Basin in Oregon. When spatially interpolating precipitation from point data in mountainous regions, elevation rather than distance is very important, and the use of elevation dependent data (such as PRISM) is ideal. For this study, it is only necessary to define one basin-wide precipitation value (monthly or annually), therefore spatially gridding the data first may be needlessly and computationally intensive. Additionally, the weighting technique (which captures the elevation dependence) removes the need for linear interpolation and simply uses the actual precipitation values from the COOP stations.

Figure 2.4 shows the comparison of annual precipitation using a simple basin average compared to using the weighting technique. The weighting technique results in annual totals that are 10% to 25% higher than the basin-averaged precipitation. When comparing one year of monthly basin-averaged precipitation, weighted precipitation, and averaged PRISM precipitation (not shown), PRISM values match more closely with the weighted totals than with the basin-averaged totals. However, the PRISM totals are 10% to 20% higher than the weighted totals for many of the months. The biggest discrepancies occur during months when the higher elevation station precipitation totals are anomalously less than the lower elevations. The weighting technique captures this anomaly, where a technique using a linear interpolation (PRISM in this example) did not.

2.2.2. EVAPOTRANSPIRATION. Direct measurements of evapotranspiration (ET) in the western U.S. are not common. The Colorado Agricultural Meteorological Network (CoAg-Met) provides ET data at 18 sites in UCRB (all in western CO). These sites are located in lower elevation locations that are irrigated during the warm season. Reference ET measurements at CoAgMet sites are calculated using the Penman-Monteith or Kimberly-Penman equations (which rely on maximum and minimum temperature, relative humidity, daily wind, and solar radiation measurements) and are based on a standardized reference crop (alfalfa or short grass). Weather data required for the ET measurements are collected in well-irrigated grass areas, therefore are only accurate for croplands. Land cover data over the region (not shown) indicate that irrigated/cultivated croplands only cover a small percentage of the region, so reference ET measurements will not be representative, therefore will not be used in the analysis.

2.2.3. SNOW WATER EQUIVALENT. The Natural Resources Conservation Service's snow telemetry sites (SNOTEL) directly measure and automatically report snow water equivalent (SWE, also known as snowpack). Similar to the COOP dataset, SNOTEL data are not spatially continuous and may not be representative of the entire basin. SWE values are also heavily dependent on elevation. Since the goal of the SNOTEL network is to monitor snowpack in the mountains, most stations are high elevation. It is the frequency distribution of the SNOTEL elevations which is higher than that of the gridded elevations, with a mean elevation of over 2923 m (Figure 2.3). Calculating a simple average of all the SNOTEL sites would result in an overestimate of basin-averaged SWE. A similar methodology as presented in the precipitation section (weighting the values based on elevation bins) was used to weight the SNOTEL SWE values across the basin. Although the methodology generally reduces the SWE peaks by approximately 50%, it also changes the inter-annual variability in those peaks (possibly as a result of the linear interpolation that is required for the lower elevation bins that contain no actual SNOTEL sites). Maintaining the actual inter-annual variability is very important for comparison with the other water variables in the basin. Therefore, the simple basin average of SNOTEL SWE values will be used in Chapter 3.

2.2.4. SOIL MOISTURE. Soil moisture measurements in the western U.S. are limited. The Natural Resources Conservation Service maintains the Soil Climate Analysis Network (SCAN) dataset. There are 12 SCAN sites in the UCRB (all in eastern UT), and most do not have data for more than five years. The majority of SCAN sites are at elevations below 2100 m, thus they are not representative for much of the region.

2.2.5. STREAMFLOW AND RESERVOIR STORAGE. Raw monthly streamflows (in cubic feet per second) are provided by the United States Geological Survey. For Chapter 3, monthly

data are obtained for two sites along the Colorado River: the gauge at the Colorado - Utah state line and the gauge at the base of the UCRB at Lee's Ferry, just below Lake Powell. Because the UCRB is an entirely closed system, the only runoff out of the basin is from the Lee's Ferry gauge and the several different trans-mountain diversion tunnels to the east side of the Continental Divide. The sum of all the annual trans-mountain volume diversions is more than an order of magnitude less than the annual volume runoff at Lee's Ferry, so it is assumed that volume runoff recorded at Lee's Ferry represents total runoff for the UCRB.

Monthly surface runoff for each HUC4 is also provided by the United States Geological Survey (available online at http://waterwatch.usgs.gov). HUC4 runoff for the 44 HUC4 basins in the western U.S. are analyzed in Chapter 5.

Data from eight major reservoirs, provided by the U.S. Bureau of Reclamation, are used to calculate the water storage of the UCRB, with a total capacity of 39.5 km^3. Storage volumes are sensitive to climate variability, with actual volumes fluctuating between 30% and 60% of capacity over the past decade.

2.3. Reanalysis and Gridded Datasets

2.3.1. Precipitation. NASA's Modern-Era Retrospective Analysis for Research Applications (MERRA) utilizes satellite rain retrievals over the ocean as input to the GEOS-5 data assimilation system, however Reichle et al. (2011) states that this has little effect on the system over land. The precipitation estimates over land are not the result of the data assimilation of surface rain-gauge data but rather the assimilation of *atmospheric* data and model physics. Globally, MERRA reproduces annual precipitation rates and spatial variability fairly well (Bosilovich et al. 2011; Reichle et al. 2011), though it tends to underestimate mid-latitude precipitation.

The European Centre's Medium-Range Weather Forecasts ERA-Interim (ERA-I) also shows improved skill from older generation reanalyses at reproducing global precipitation patterns (Bosilovich et al. 2011), partly as a result of the modification of the convection scheme in the model (Dee et al. 2011). Precipitation estimates from ERA-I are also based on model physics forced by temperature and humidity in the assimilation scheme.

The National Center for Environmental Prediction's Climate Forecast System Reanalysis (CFSR) combines the Noah land surface model with the GFS atmospheric model and is the only reanalysis product to include a fully-coupled ocean model. Over land, daily observations of precipitation are combined with gauge analysis and CMAP 5-day mean precipitation to drive the land surface model, making it the only reanalysis product out of the three to rely on precipitation observations in its precipitation dataset.

In Chapter 3, the above referenced reanalysis precipitation products are analyzed over the UCRB. For Chapters 4 and 5, PRISM precipitation is used to calculate sub-basin and HUC4 averaged monthly precipitation.

2.3.2. EVAPOTRANSPIRATION. The land surface model in the GEOS-5 data assimilation system (used by MERRA) divides the land-surface variables into catchments instead of gridboxes (Decker et al. 2012). MERRA also uses the highest time resolution for inputs into the land surface model, thus making it likely to be the most ideal dataset to use for ET. The ERA-I land surface analysis requires 6-hourly inputs of temperature and relative humidity to model near surface fluxes at a 3-hourly interval (Decker et al. 2012). Land surface assimilation for the CFSR only occurs once a day. Reanalysis ET measurements have not been validated over the UCRB, but other regions have been studied. When compared to flux towers, all reanalyses showed good agreement at many locations, though all had a tendency to overestimate latent heat flux (Decker et al. 2012). Mueller et al. (2011) showed

that in the Mississippi River basin, reanalysis land surface fluxes tended to be greater than satellite-derived land surface fluxes.

2.3.3. WATER VAPOR DIVERGENCE. Using reanalysis data, total column flux of water vapor can calculated at each gridpoint:

$$\text{(5)} \qquad\qquad Q_i = \frac{1}{g} \int_{p=1000}^{p=200} q_p u_p \partial p,$$

$$\text{(6)} \qquad\qquad Q_j = \frac{1}{g} \int_{p=1000}^{p=200} q_p v_p \partial p.$$

The divergence operator can be applied to equations (2) and (3) to obtain the divergence of water vapor flux at each i,j gridpoint,

$$\text{(7)} \qquad\qquad \nabla \cdot \mathbf{Q} = \frac{\partial Q_i}{\partial x} + \frac{\partial Q_j}{\partial y}.$$

The time element of the equations (s^{-1}) are removed by accumulating over a one-month or one-year period, therefore each component is in units of kg m^{-2}. Calculated $\nabla \cdot \mathbf{Q}$ is totaled up over every gridpoint (in the UCRB for Chapter 3 and for every HUC4 in Chapter 5) and can be compared to basin-averaged $(E - P)$. Chapter 3 calculates water vapor divergence over the UCRB using the MERRA, ERA-I and CFSR reanalysis data. In Chapter 5, water vapor divergence is calculated for each HUC4 using ERA-I and NARR reanalysis data.

Trenberth et al. (2000) were one of the first to examine global divergence using reanalysis data, and found that reanalysis could reliably reproduce the global monsoon and the

divergent circulation. Since then, several regional studies have specifically examined wind and humidity data from reanalysis (the two variables needed to calculate vapor divergence). Decker et al. (2012) found that ERA-I winds had the lowest error and bias when compared to flux tower observations across North America; they also found that the CFSR performed the worst of the reanalysis products. Over the Tibetan Plateau, Bao and Zhang (2012) found that ERA-I and CFSR had large positive biases and errors in humidity, while Kennedy et al. (2011) found that MERRA had a slight dry bias in humidity compared to ARM sites in the midwestern U.S. Both studies also pointed to different biases in the reanalyses at lower levels compared to the middle and upper troposphere.

2.3.4. Soil Moisture. The Climate Prediction Center's Soil Moisture V2 dataset (CPC Soil) uses a one-layer leaky bucket model, with temperature and precipitation as inputs, to model soil moisture (Fan and van den Dool 2004). Though difficult to validate over the UCRB, it has done reasonably well at simulating soil moisture when compared to the limited observations available (Huang et al. 1996; Fan and van den Dool 2004). It is likely to compare well with precipitation observations over the UCRB since it is forced by precipitation from the U.S. Historical Climate Network (USHCN).

MERRA's reanalysis includes a root-zone soil wetness variable, which represents the wetness of the top meter of soil (as a fraction). It has been shown to compare well with ERA-I soil moisture (Rienecker et al. 2011). Reichle et al. (2011) have pointed out that MERRA's precipitation estimates may sometimes be underestimated due to less intense precipitation rates and that solar radiation could be overestimated, thus leading to an overall underestimate of soil moisture. Additionally, Rienecker et al. (2011) have pointed to systematic differences in high latitude soil moisture because it cannot be adjusted by evaporation and runoff during long periods of the year with frozen conditions.

2.3.5. SEA SURFACE TEMPERATURE. Correlations between UCRB variables and ocean sea surface temperatures (SST) are performed in Chapter 4. SST data are taken from the Hadley Centre (Rayner et al. 2003). To eliminate small scale variability, SSTs are spatially averaged using a 10° latitude by 10° longitude moving window.

2.4. SATELLITE-DERIVED DATASETS

2.4.1. PRECIPITATION. High resolution global precipitation datasets are widely used in studies and are also useful for comparison with *in-situ* data. For higher latitude land regions, satellite-derived precipitation datasets are limited. Microwave precipitation estimates are not as accurate over land (particularly over mountainous regions), and land infrared (IR) precipitation estimates aren't provided over regions with snow-cover due to the brightness temperature of the snow closely matching the brightness temperature of cloud tops. Over the UCRB, snow-cover is an issue for over six months of the year, limiting the amount of satellite precipitation observations. The Tropical Rainfall Measuring Mission (TRMM) Multi-satellite Precipitation Analysis (TMPA) dataset is unique amongst many high resolution satellite-derived precipitation products as it combines precipitation estimates from multiple satellites with gauge data to produce precipitation data for the lower and middle latitudes (Huffman et al. 2007; Sapiano and Arkin 2009). Because it utilizes gauge analysis, it provides data even during snow-cover times, and is therefore suitable for this study.

2.4.2. EVAPOTRANSPIRATION. Some recent studies have done global comparisons of satellite- and model-derived land heat flux products (e.g. Jimenez et al. 2011; Mueller et al. 2011). This study uses several of the higher resolution latent heat flux datasets presented in the aforementioned articles. The University of California-Berkeley dataset (UCB) combines satellite retrievals with Priestley-Taylor estimates which transform potential ET values to

actual ET values. The Max Planck Institute for Biogeochemistry (MPI) utilizes direct eddy-covariance measurements from flux towers (FLUXNET) and globally grids the data using an approach called model tree ensemble. The Paris Observatory dataset (PAO) empirically derives latent heat fluxes using satellite-derived reflectances, emissivities, backscatter, and temperature as inputs.

Jimenez et al. (2011) have shown that, globally, reanalyses produce the highest ET values (with the exception of the UCB dataset). They also found good agreement between MPI and PAO. While they found good spatial consistency amongst all the products, the magnitudes of ET vary widely from product to product. It was found that the mountainous and desert regions (where ET values are relatively smaller) displayed the greatest amount of variability between products.

2.4.3. SNOW WATER EQUIVALENT. Storage in the form of SWE is measured by the Advanced Microwave Scanning Radiometer for the Earth Observing System (AMSR-E) on the Aqua satellite. The data have a coarse resolution for SWE, which is highly variable in the mountainous terrain. De Lannoy et al. (2012) showed that in low elevation flat areas, AMSR-E values can exceed nearby SNOTEL SWE values by an order of magnitude, while the higher elevation peak SNOTELs can exceed the AMSR-E values by an order of magnitude.

2.4.4. TOTAL WATER STORAGE. The Gravity Recovery and Climate Experiment (GRACE) satellites measure changes in the gravity field caused by changes in mass. Over land, these mass changes are primarily the result of changes in terrestrial water storage (ΔTWS). Land data processed by University of Texas's Center for Space Research (CSR, Release 04) were processed from the raw gravity fields using spherical harmonics(Swenson and Wahr 2006).

The mass of the atmosphere is removed using ECMWF fields, and then the data are de-striped and smoothed using a 300 km Gaussian filter. The data are ideal for basins 200,000 km^2 or larger (Zaitchik et al. 2008). Land water content from the Noah land surface model in the Global Land Data Assimilation System (GLDAS) can be compared to the CSR measurements over land (Rodell et al. 2004b). Both datasets are available through the Jet Propulsion Laboratory's GRACE website (http://grace.jpl.nasa.gov).

ΔTWS over land can be the result of changes in soil moisture, deep ground water, reservoir storage, or storage in SWE. Using *in-situ*, gridded, and satellite data, ΔTWS can be estimated by calculating basin-averaged monthly volume changes in SWE, reservoir storage, and soil moisture and then taking the sum of the three. This can then be compared to ΔTWS from CSR and GLDAS, which will be done in Chapter 3.

2.5. SPI and Z-score

In Chapter 4, a standardized precipitation index (SPI) is calculated for each 4 km grid-point in the UCRB. SPIs are calculated by taking the 100 years of precipitation data (which follows a gamma distribution) and normalizing it into a Gaussian distribution (McKee et al. 1993). A cumulative distribution function is then calculated, and from that an index is created (similar to a Z-score) which ranks precipitation from around -3 (extremely dry) to +3 (extremely wet), with 0 representing the 50th percentile ranking. This study analyzes the 9-month SPI from October - June (marking the beginning of the water year and capturing critical snow accumulation and snow melt time frames).

A temperature Z-score is calculated for maximum temperatures at each 4 km gridpoint over the UCRB. Z-scores are calculated by computing the 100-year average for each individual month, removing the average from that specific month and dividing by the standard

deviation. A winter Z-score is then calculated by averaging the monthly Z-scores for October - June.

Monthly and seasonal SPIs and temperature Z-scores are used to examine the interannual and spatial variability in the UCRB and to identify the connections with larger scale climate variability. The monthly statistics are also used to analyze each month's contribution to the basin's variability.

TABLE 2.1. Summary of the different datasets used, including their temporal and spatial resolutions, the time period used, and the reference for the dataset.

Data	Time Res	Space Res	Period	Reference
In-situ				
COOP	daily	105 datapoints	2002-2010	NWS
SNOTEL	daily	112 datapoints	2002-2010	NRCS
CoAgMet	daily	point	1992-2008	Colorado Climate Center
SCAN	daily	1 m depth, point	2010-2012	NRCS
Reanalysis/gridded				
MERRA	hourly	$2/3°$ x $1/2°$	1999-2008	Rienecker et al. (2011)
	6-hourly	72 levels		
ERA-I	hourly	1.5° x 1.5°	1999-2008	Dee et al. (2011)
	6-hourly	37 levels		
CFSR	hourly	$1/2°$ x $1/2°$	1999-2008	Saha et al. (2010)
	6-hourly	37 levels		
NARR	monthly	32 km x 32 km	1999-2008	Mesinger et al. (2006)
		29 levels		
CPC Soil V2	monthly	$1/2°$ x $1/2°$	2002-2012	Fan and van den Dool
		1 m depth		(2004)
PRISM	monthly	4 km x 4 km	1911-2010	Daly et al. (1994)
Hadley SST	monthly	1.0° x 1.0°	1911-2010	Rayner et al. (2003)
Satellite derived				
TMPA	monthly	$1/4°$ x $1/4°$	2002-2010	Huffman et al. (2007)
UCB	monthly	$1/2°$ x $1/2°$	1986-1995	Fisher et al. (2008)
MPI	monthly	$1/2°$ x $1/2°$	1986-2008	Jung et al. (2009)
PAO	monthly	$1/4°$ x $1/4°$	1993-1999	Jimenez et al. (2011)
AMSR-E	monthly	25 km	2002-2010	Kelly (2009)
		equal area grids		
CSR	monthly	1.0° x 1.0°	2002-2010	Swenson and Wahr (2006)
GLDAS	monthly	1.0° x 1.0°	2002-2010	Rodell et al. (2004b)
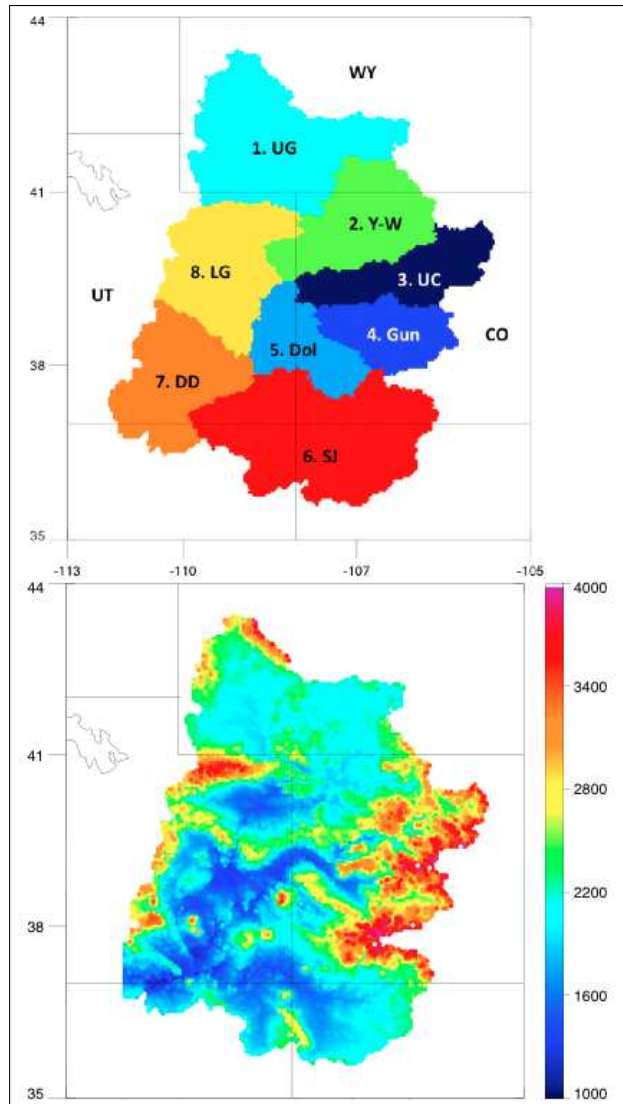
FIGURE 2.1. Top: Upper Colorado River Basin location, with each of its sub-basins represented by a different color. Starting at the top and moving clockwise: Upper Green, Yampa-White, Upper Colorado, Gunnison, Dolores, San Juan, Dirty Devil, and Lower Green. Bottom: elevations from the USGS Digital Elevation Model (reduced to 4 km resolution) over the UCRB, in meters above sea level.

FIGURE 2.2. Western United States with 44 hydrologic sub-basins (4-digit HUCs) west of the Continental Divide outlined in grey.
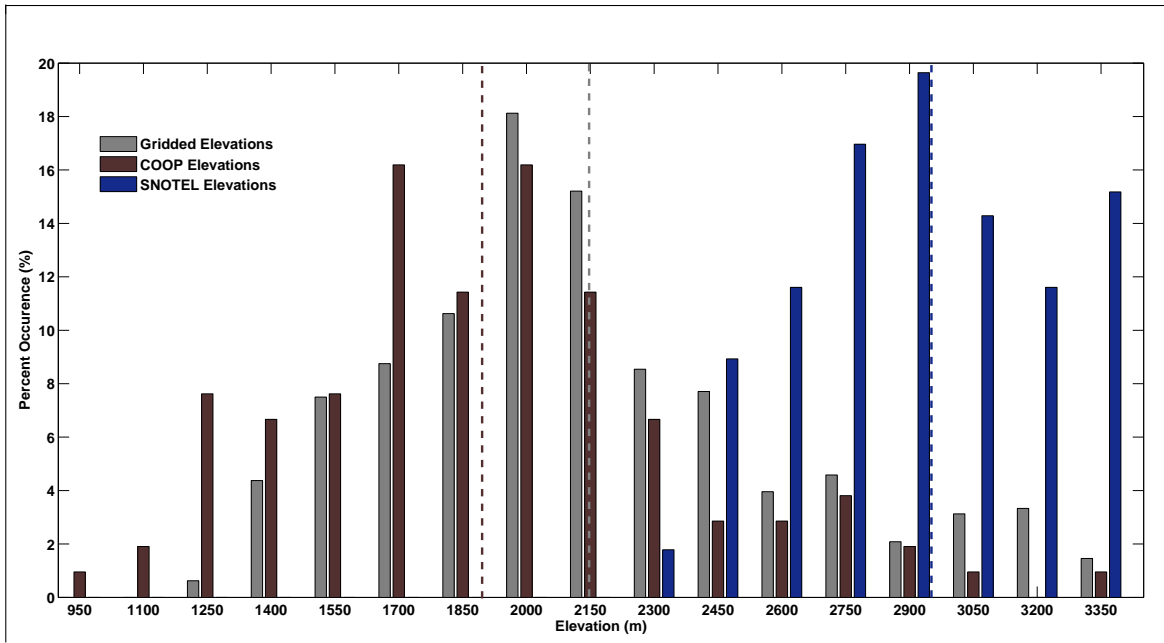
FIGURE 2.3. Frequency distribution of elevations (150 m bins) in the UCRB for $1/4$ ° by $1/4$ ° gridpoints (grey), COOP stations (maroon), and SNOTEL sites (blue). Dashed lines represent average elevation for each dataset.
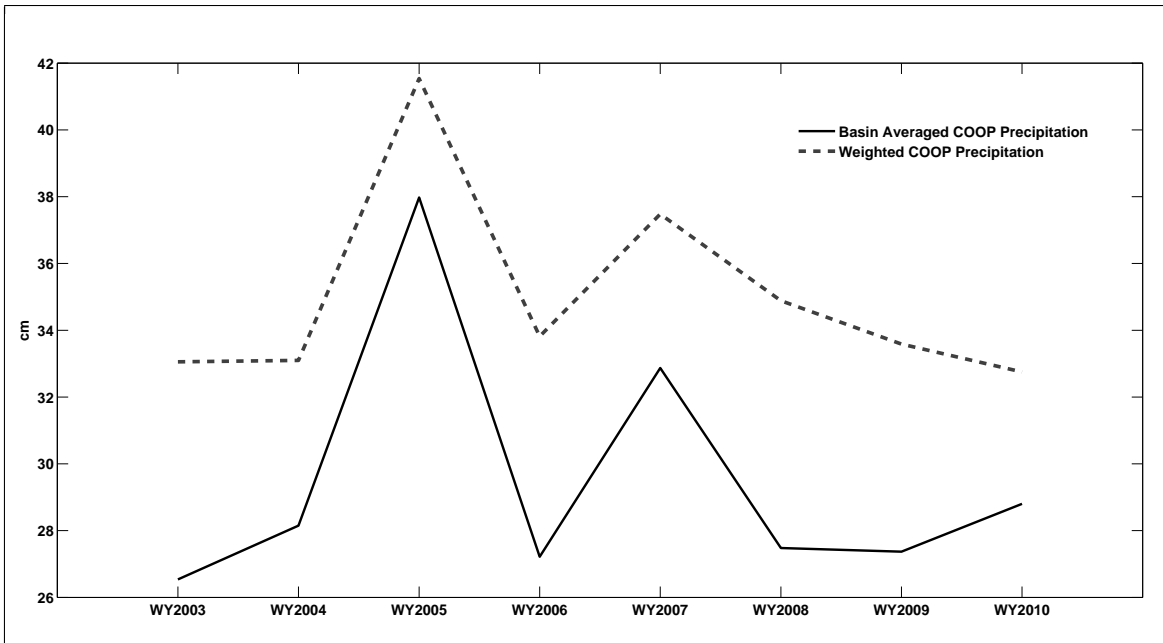
FIGURE 2.4. Annual accumulated precipitation using a simple basin-average of the 105 COOP stations compared to weighting the COOP stations based on elevation.

CHAPTER 3

Water Budget of the UCRB

3.1. Water Budget Components

3.1.1. Precipitation. The *in-situ* precipitation timeseries is overlaid with MERRA, ERA-I, CFSR, and TMPA precipitation timeseries in Fig. 3.1. Based on the location and topography of the UCRB, two seasonal peaks would be expected - the first during the cold season, when the higher elevations receive their largest amounts of precipitation; a second peak would be expected in the late summer, coinciding with the onset of the North American Monsoon (NAM). The northernmost fringes of the NAM results in increased precipitation over the southern portion of the UCRB (Vera et al. 2006).

When looking at the *in-situ* monthly precipitation timeseries (Fig. 3.1, top) no consistent seasonal cycle with two peaks is apparent. In this case, using one value for the basin could be obscuring the signal. A simple k-means cluster analysis of every COOP stations' precipitation timeseries separated the basin into northern and southern regions. But analysis of the separate clusters' precipitation timeseries yielded minimal differences (not shown). When the COOP stations were binned according to elevation and then averaged over each bin, larger seasonal differences became apparent (Fig. 3.2). The highest elevation bin's seasonal cycle shows a precipitation maximum in July - September, another maximum in December and a third maximum in April. The middle and lower elevation bins' seasonal cycles show a precipitation maximum for August - October. It appears as if all elevations are in some way influenced by the NAM (though the lower elevations lag the higher elevations), and the higher elevations are more influenced by larger cold-season snowfall accumulations.

There is good agreement in seasonal and inter-annual variability between the different gridded precipitation products and the *in-situ* precipitation. The *in-situ* and gridded datasets all show a wet-dry-wet-dry pattern. Focusing on water years 2004 - 2008 (Fig. 3.1, bottom), the even years (WY2004, WY2006, WY2008) show relatively lower precipitation accumulations, and the odd years (WY2005, WY2007) show higher precipitation accumulations.

The reanalysis datasets tend to overestimate the monthly and annual *in-situ* precipitation in the UCRB by around 10% to 20%. This is consistent with the Reichle et al. (2011) study that found MERRA overestimated precipitation in the western U.S. The higher resolution satellite precipitation product (TMPA) underestimates *in-situ* and reanalysis precipitation by more than 40%. The IR rain-retrieval method used by TMPA may possibly be missing lighter precipitation events in mountainous areas, thus resulting in this underestimation (Hirpa et al. 2010). Additionally, the included gauge analysis in TMPA, provided by the Global Precipitation Climatology Centre (GPCC), does adjust for elevation, but could still be underestimating higher elevation precipitation in the basin. Based on the precipitation timeseries, the CFSR is the least correlated with *in-situ* precipitation, and MERRA is highest correlated. The CFSR dataset relies on CMAP precipitation observations in its land surface model, and the CMAP precipitation timeseries is very similar to the TMPA timeseries over the UCRB (not shown). Therefore, the poorer performance of the CFSR precipitation over the UCRB is not due to the inital observational input but rather from some other internal physics within the model and should be considered when using CFSR data in future studies over the region.

3.1.2. EVAPOTRANSPIRATION. Reanalysis and satellite-derived ET over the UCRB are compared in Fig. 3.3. All the gridded products show similar seasonal cycles (with a summer

peak coinciding with warmest temperatures). Reanalysis ET are in good agreement with MPI and PAO ET, while UCB ET estimates can be 25% to 40% higher. Unlike satellite-derived ET, reanalysis data show a consistently repeating double seasonal peak in ET. Looking at long-term monthly averaged MERRA ET (Fig. 3.4), the first ET peak generally occurs in the late spring, immediately following the heaviest precipitation accumulations and as temperatures are rapidly warming. Lower ET values follow during the drier summer months, and then a second ET peak occurs in the late summer, coinciding with the arrival of the NAM. All products (with the exception of the CFSR) agree on inter-annual variability (Fig. 3.3, bottom), which is strongly coupled to precipitation with WY2005 and WY2007 showing relatively higher ET values and WY2004, WY2006, and WY2008 showing lower ET values.

It is difficult to identify one ET product as being more representative than the others for the basin, since reference ET is the only basis for comparison in the UCRB. Mueller et al. (2011) pointed out that good agreement amongst several products may not necessarily mean they are more accurate, but that these products share similar model physics and data forcings. Additionally, one product may stand out as an outlier, but that may not mean it is erroneous (Mueller et al. 2011). The CFSR ET will not be used further in this study as it does not exhibit an accurate pattern in the inter-annual cycle, and its strong positive bias during the cold season (compared to all the other products) may be inaccurate as it is assumed there is very little evaporation during the cold season. MERRA ET will be used for further analysis as it captures the inter-annual variability, and MERRA precipitation is most closely correlated with *in-situ* observations. However, since reanalysis ET could possibly be overestimating actual ET (Jimenez et al. 2011), the MPI ET product will also be used for further analysis.

3.1.3. STORAGE VOLUME CHANGES. One of the largest contributing components to changes in surface storage, and the largest source of seasonal and inter-annual variability, is water stored as snowpack. *In-situ* SWE is shown in the top of Fig. 3.5. At the beginning of the water year (October), virtually no snow is present in the basin. Progressing through time, SWE builds up to its maximum around April or May, then quickly melts off and typically disappears by June.

According to *in-situ* SWE, WY2005 and WY2008 were the highest accumulation years in the analysis, while WY2004 and WY2007 show relatively lower peak SWE values. The variability observed in the SWE peaks doesn't match the wet-dry-wet-dry pattern observed in the precipitation and ET timeseries. WY2004 was drier (and WY2005 was wetter) according to precipitation and SWE. But where precipitation shows a higher accumulation in WY2007, peak SWE is lower. This is the result of an anomalously wet October which led to a large amount of non-frozen precipitation accumulations that didn't translate into storage in snowpack. In WY2008, when peak SWE was high, precipitation was lower as a result of a weak monsoon season at the end of the water year. It is interesting to note that ET is more closely coupled with precipitation and does not respond to higher SWE peaks.

The bottom of Fig. 3.5 shows AMSR-E satellite-derived SWE. Similar to previous studies in the region (De Lannoy et al. 2012), *in-situ* SWE peaks are almost an order of magnitude higher than AMSR-E estimates. The overall purpose of the SNOTEL program (and as a result, the placement of the sites biasing toward higher elevations), was to better predict the upcoming springtime runoff in the western river basins (NRCS NWCC cited 2012). AMSR-E provides more spatial continuity not found with SNOTEL. Looking at Fig. 3.1, average monthly precipitation in the basin for the winter is approximately 3 cm, leading to an approximate winter seasonal total of less than 20 cm. So, AMSR-E may provide

more realistic magnitudes of SWE on a basin-averaged scale, and therefore will be useful for calculating storage volume changes. However, it fails to capture the observed inter-annual variability. Henceforth, satellite-derived SWE will be used for surface water budget calculations, but *in-situ* SWE will still be used to analyze the inter-annual variability in the basin.

When comparing gridded soil moisture products with soil moisture at several of the SCAN sites in eastern UT, large discrepancies are evident in the overall magnitudes of soil moisture, and in the seasonal variability. The gridded products themselves show similar seasonal cycles and inter-annual variability, but the MERRA magnitudes are two to three times larger. The introduction of more soil moisture measuring sites in the UCRB (and longer periods of record) is needed in order to properly validate these gridded soil moisture products. Since that is impossible for this study, only the gridded data are analyzed. In Fig. 3.6, changes in soil moisture are added to changes in SWE and reservoir storage over time. Adding soil moisture can result in a 50% to 100% increase in surface storage changes, with MERRA soil moisture resulting in larger seasonal changes than CPC soil moisture. Annually (not shown), total soil moisture storage displays the same inter-annual variability seen in the precipitation and ET timeseries. Soil moisture changes also respond quickly to precipitation anomalies, which is to be expected as precipitation observations are used to force the CPC soil moisture model. As it is difficult to ascertain which soil moisture product is more accurate for the basin, both will continue to be evaluated.

In Fig. 3.7, storage volume changes (combining AMSR-E SWE with reservoir storage and soil moisture) are compared with changes in GLDAS and CSR satellite-derived ΔTWS. The seasonal cycle is similar for all products, with water storage gains (losses) during the

cold (warm) season. The magnitude and variability of the GLDAS and AMSR-E timeseries are well correlated, while the CSR timeseries displays too much month-to-month variability.

Annual changes in storage volume are compared in the bottom of Fig. 3.7. The annual variability of (reservoir + CPC soil moisture) storage changes matches well with the GLDAS annual changes in ΔTWS. Both show very little change in storage for WY2004 and WY2007, large gains in WY2005, and storage losses in WY2006. WY2005 and WY2006 are consistent with *in-situ* SWE peaks and precipitation variability - there was a gain in storage during the wetter year with a higher peak *in-situ* SWE (WY2005) and a loss in storage during the drier year with a lower peak SWE (WY2006). When *in-situ* SWE peak and precipitation are out-of-phase (WY2007), storage changes are closer to zero. Though the annual magnitudes of (reservoir + MERRA soil moisture) are closer to GLDAS magnitudes, the inter-annual variability is not as well correlated with GLDAS as the (reservoir + CPC soil moisture). The inter-annual variability in the CSR timeseries does not match with any of the other products.

3.1.4. RUNOFF. Variations in streamflow across the UCRB are the result of a combination of man-made regulations and seasonal variability. The Colorado River at the CO-UT state line typically reaches peak streamflows between May and June of each water year (shortly after snow melt begins). Further downstream, at Lee's Ferry, peak streamflows typically occur a little later between June and August. A secondary seasonal peak is observed at the Lee's Ferry site from January - March.

Though flows on the Colorado River are regulated year-round, natural inter-annual variability can still be detected when analyzing the water-year accumulated volume runoff (Fig. 3.8). Upstream, at the CO-UT state line, low accumulations during 2002 can be linked to the major drought in the early 21st century which affected the entire southwestern U.S. Annual

runoff accumulations have been increasing since that period. Downstream at Lee's Ferry, accumulated runoff stays fairly consistent inter-annually, showing more of a man-made signal than a signal from natural variability.

Runoff variability at the CO-UT state line site is better correlated with peak SWE values rather than precipitation. Higher runoff years (WY2005 and WY2008) correspond to higher peak SWEs, whereas a lower runoff year of WY2007 corresponds to a lower peak SWE (even though annual precipitation was high that year). This close relationship between SWE and runoff should be expected, based on the previously stated purpose of SNOTEL. Because of the deliberate choosing of SNOTEL sites (to capture the deeper snow depths), SWE inter-annual variability is better correlated with runoff variability than with precipitation variability.

3.1.5. $\nabla \cdot \mathbf{Q}$. Calculated $\nabla \cdot \mathbf{Q}$ over time from the different reanalysis products are shown in Fig. 3.9. The MERRA and ERA-I show similar seasonal variability. They both show atmospheric divergence over the UCRB in the spring and summer months and atmospheric convergence during the winter (Fig. 3.9, top). This atmospheric seasonal cycle is consistent with the surface water variables and with the climate of the basin. The CFSR shows more erratic month-to-month variability and rarely exhibits atmospheric convergence.

Annually, the CFSR suggests that water vapor is always diverging out of the UCRB region, while MERRA shows several years of divergence (Fig. 3.9, bottom). As all of these years showed surface runoff, it does not make sense to have atmospheric divergence for an entire year. ERA-I is the only reanalysis dataset to consistently show atmospheric convergence with variability only in the magnitude of the convergence. ERA-I displays less atmospheric convergence during years with less precipitation (WY2004, WY2006 and WY2008) and greater atmospheric convergence during the wet year of WY2005. Though

WY2007 was a high precipitation year, the lower snowpack would mean less convergence during the winter, and thus would lead to a year with less atmospheric convergence according the ERA-I.

3.2. Discussion

3.2.1. SURFACE AND ATMOSPHERIC STORAGE ESTIMATES. Using estimates of precipitation, ET, and runoff that are most consistent with each other (in terms of magnitude and variability), changes in surface storage can be estimated over time (using Eq. 2 from Chapter 2) and compared to the changes in surface storage from Fig. 3.7.

in-situ precipitation and accumulated runoff at Lees Ferry will be used for P and R. The question becomes, which product should be used for the ET component. When MERRA ET was input into the calculation, there was frequently an imbalance, and ΔS was negative. MERRA ET appears to be an overestimate (especially when combined with *in-situ* precipitation), and the use of MPI ET leads to a better balance. Therefore, ΔS is calculated using MPI ET. Estimated ΔS is compared with the CSR and GLDAS products in Fig. 3.10 (top). Again, the CSR shows much more month-to-month variability than what is estimated. CSR magnitudes tend to be 50% greater than estimated ΔS while GLDAS magnitudes tend to be 50% less. Based on the seasonal cycle and inter-annual variability, GLDAS appears to better represent surface water storage changes over the UCRB. Rodell et al. (2004a) found that GLDAS data are in better agreement with JPL processed GRACE data (Chambers 2006). Tang et al. (2010) concluded that the data processed by Chambers (2006) significantly underestimated true values in the seasonal cycle of terrestrial water storage (particularly over the Klamath and Sacramento River basins). This should be considered when using GLDAS data over the UCRB.

The bottom of Fig. 3.10 shows the comparison of estimated ΔS with storage changes calculated from changes in (SWE + reservoir + soil moisture). With the use of AMSR-E SWE and CPC soil moisture, calculated changes in storage are well correlated with estimated ΔS in terms of magnitude, seasonal cycle, and inter-annual variability.

In the atmosphere, estimates of precipitation, ET, and $\nabla \cdot \mathbf{Q}$ can be used to estimate changes in atmospheric storage, using Equation (1) in Chapter 2. Estimated $\frac{\partial W}{\partial t}$ is calculated using *in-situ* precipitation, MPI ET, and ERA-I $\nabla \cdot \mathbf{Q}$ (Fig. 3.11). As typical values of total column water vapor over the UCRB would not be greater than 15 kg m^{-2}, annual changes in storage greater than this are unrealistic. Most years of estimated $\frac{\partial W}{\partial t}$ are realistic, though a couple of years show magnitudes greater than 30 kg m^{-2}. Not shown in Fig. 3.11, MERRA $\nabla \cdot \mathbf{Q}$ yields larger imbalances, further supporting the use of ERA-I for budget closure consistency.

3.2.2. LONG-TERM STORAGE. Another way to compare how the different products balance is to total them over long periods. When totaling estimated ΔS (P - ET - R) from WY2003 through WY2008 for the UCRB, there is an overall increase in storage of +176 mm. Yet calculated storage changes in (reservoir + soil moisture) over the same period only yields an increase of +21 mm. Both the GLDAS and CSR products show a loss in storage for the same time period, of -14 mm and -11 mm respectively, neither of which are consistent with observations or models. When looking at long-term atmospheric changes, estimated $\frac{\partial W}{\partial t}$ from WY2003 through WY2008 for the UCRB, there is an overall loss in atmospheric storage of -73 mm (Fig. 3.11).

3.2.3. CONNECTING THE SURFACE AND ATMOSPHERE. Over a long enough period of time, atmospheric convergence/divergence over an area will equal the runoff and change

in storage at the surface. This can help connect the atmospheric water budget with the surface water budget and shed more light on the different products, as shown in Table 3.1. Over the same long-term period (WY2003 through WY2008) total $\nabla \cdot \mathbf{Q}$ from ERA-I shows overall atmospheric convergence, while MERRA shows overall atmospheric divergence. Since surface runoff is positive over that long time period, atmospheric convergence would have had to occur, which MERRA does not show.

Table 3.1 shows that adding estimated ΔS to the runoff results in surface changes that are greater than the atmospheric convergence (by ERA-I). Adding (reservoir + soil moisture) or the CSR and GLDAS to the runoff results in surface changes that are much less than the atmospheric convergence. Estimated ΔS could be too large due to a possible underestimation of the MPI ET product. A systematic increase of 5% to the MPI ET yields a better balance. In Table 3.1, adjustment of ΔS (and adding to runoff) yields a much closer value to atmospheric convergence. The difference between the two would leave a surplus of 13 mm in the atmosphere. This can be accounted for in the adjusted $\frac{\partial W}{\partial t}$, which is now +13 mm after the MPI ET 5% increase (Fig. 3.11).

The issues that remain are with CSR, GLDAS, and MERRA. Both CSR and GLDAS show a loss in surface storage for a time period when a gain in surface storage is expected. Adding the next two years to each (WY2009 and WY2010) results in a switch in sign for CSR. GLDAS numbers stay fairly consistent, with a loss in storage of approximately -10 mm while CSR switches and shows a gain of approximately +10 mm. There is not enough data (as the GRACE satellites were only launched in 2002) to tell if CSR had issues in early years and the data improved for later years. However, even with it switching to show surface storage gains over a long period, the CSR still has issues with month-to-month and inter-annual variability that cannot be overlooked. The GLDAS has better compared with other products in terms

of variability, but with its long-term storage losses, it is either underestimating gains in the winter or overestimating losses in the summer. This disagreement between estimated ΔS, GLDAS, and CSR should be further explored. Discrepancies could possibly be due to the smaller basin size and the coarse resolution of the data. Fersch et al. (2012) found that GRACE estimates also had limitations in basins with smaller water storage changes (less than 25 mm per month). It is beyond the scope of this study to determine how the internal physics of the GLDAS and CSR algorithms affect the estimates over the UCRB, but should be considered for further research.

Finally, the main issue with MERRA is with its long-term $\nabla \cdot \mathbf{Q}$. When compared with the surface runoff, its $\nabla \cdot \mathbf{Q}$ estimates are far off. When calculating a 5-year running mean of $\nabla \cdot \mathbf{Q}$ from WY1999 through WY2008, MERRA consistently shows long-term divergence, while ERA-I always shows convergence which is more realistic for the UCRB.

Table 3.2 provides an inventory of the various datasets for each water budget component. Reanalysis datasets tend to overestimate *in-situ* precipitation while satellite-derived precipitation underestimates. In this region, where there is a fairly dense network of *in-situ* observations that are consistent over time, *in-situ* precipitation data is suggested for future studies. Based on the temporal and spatial resolution, and its consistency with other components in the water budget calculations, the MPI is suggested for ET measurements in the UCRB. Additionally, CPC soil moisture and AMSR-E SWE are also consistent amongst each other in water budget calculations. As ERA-I provides the only $\nabla \cdot \mathbf{Q}$ that is consistently convergent on an annual and long-term basis, it is suggested for future studies of atmospheric water budgets over the UCRB.

TABLE 3.1. Long-term water changes in the atmosphere and the surface, WY2003 - WY2008. The bold values denote a balance between the atmosphere and the surface. A positive value in the atmosphere denotes divergence or addition of storage, while a negative value denotes convergence or loss of storage. At the surface, a positive value denotes excess water to runoff or a gain in storage.

Atmosphere	
ERA-I $\nabla \cdot \mathbf{Q}$	**-347 mm**
MERRA $\nabla \cdot \mathbf{Q}$	+69 mm
Estimated $\frac{\partial W}{\partial t}$	-73 mm
Adjusted $\frac{\partial W}{\partial t}$	**+13 mm**

Surface	
Runoff	+242 mm
Runoff + Estimated ΔS	+418 mm
Runoff + (Reservoir + Soil)	+263 mm
Runoff + CSR ΔTWS	+231 mm
Runoff + GLDAS ΔTWS	+228 mm
Runoff + Adjusted ΔS	**+334 mm**

TABLE 3.2. Summary of the various datasets for each water variable component: precipitation, evapotranspiration, soil moisture, surface storage changes, and water vapor divergence. The suggested dataset for each component is denoted with a ✓*.

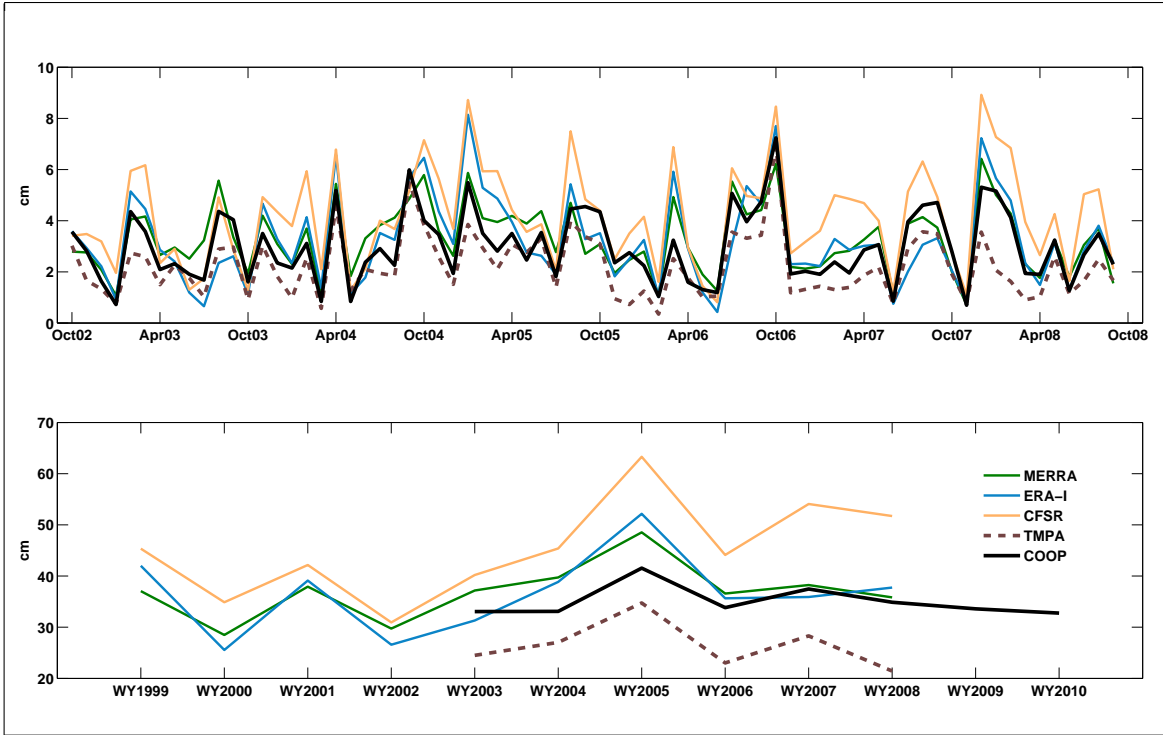| Dataset	P	ET	SM	ΔS	$\nabla \cdot \mathbf{Q}$
MERRA	✓	✓	✓		✓
ERA-I	✓	✓			✓*
CFSR	✓	✓			✓
TMPA	✓				
COOP	✓*				
MPI		✓*			
UCB		✓			
PAO		✓			
SNOTEL				✓	
AMSR-E				✓*	
CPC			✓*		
CSR				✓	
GLDAS				✓	

FIGURE 3.1. Monthly (top) and annual (bottom) precipitation averaged over the UCRB, comparing COOP observations with reanalysis and satellite datasets.
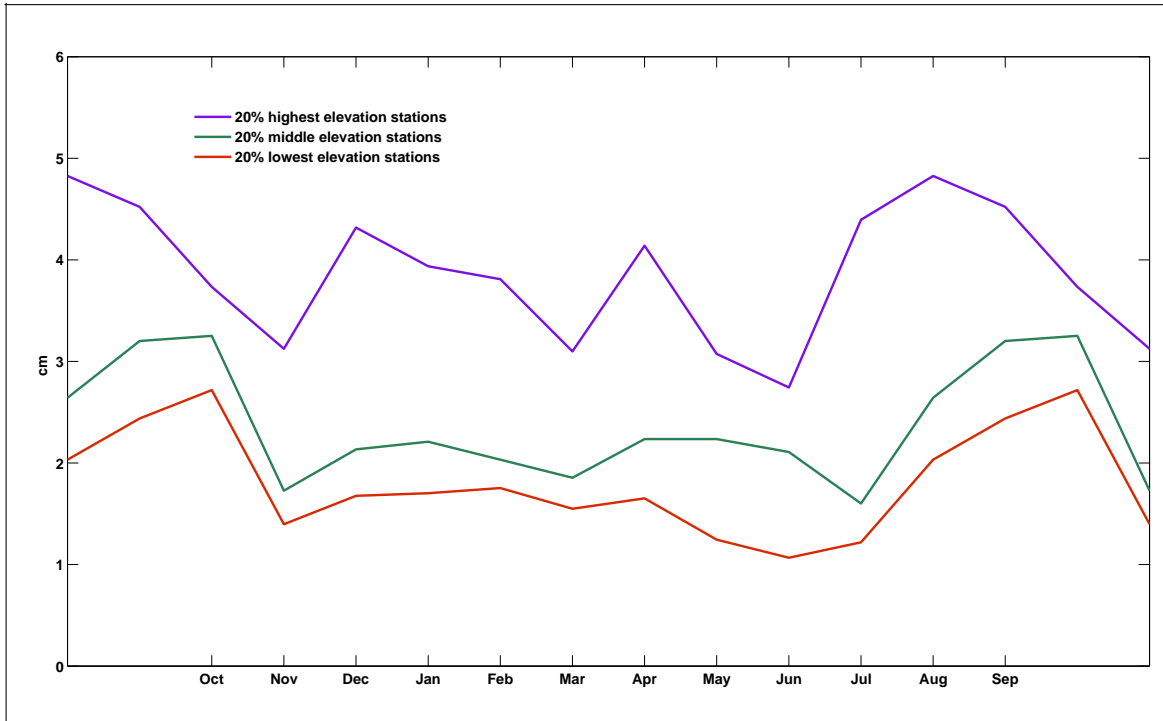
Figure 3.2. Long-term average monthly precipitation, using COOP observatons, for three different elevation bins.
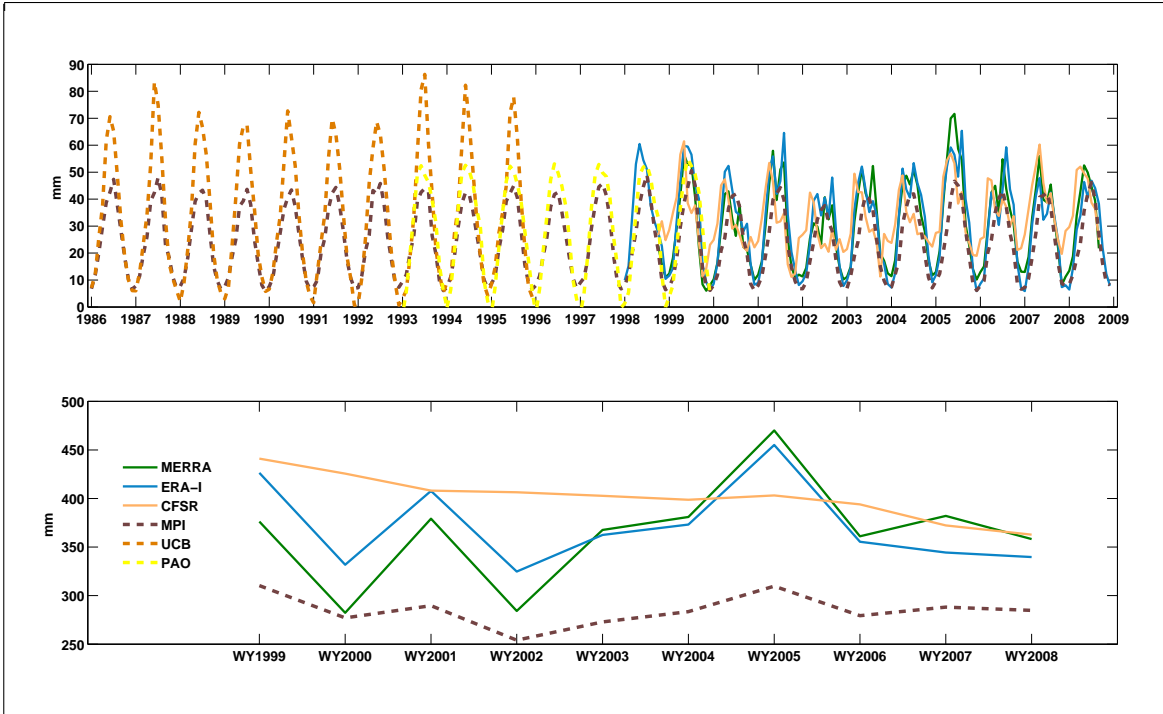
FIGURE 3.3. Monthly (top) and annual (bottom) ET averaged over the UCRB, comparing reanalysis and satellite datasets.
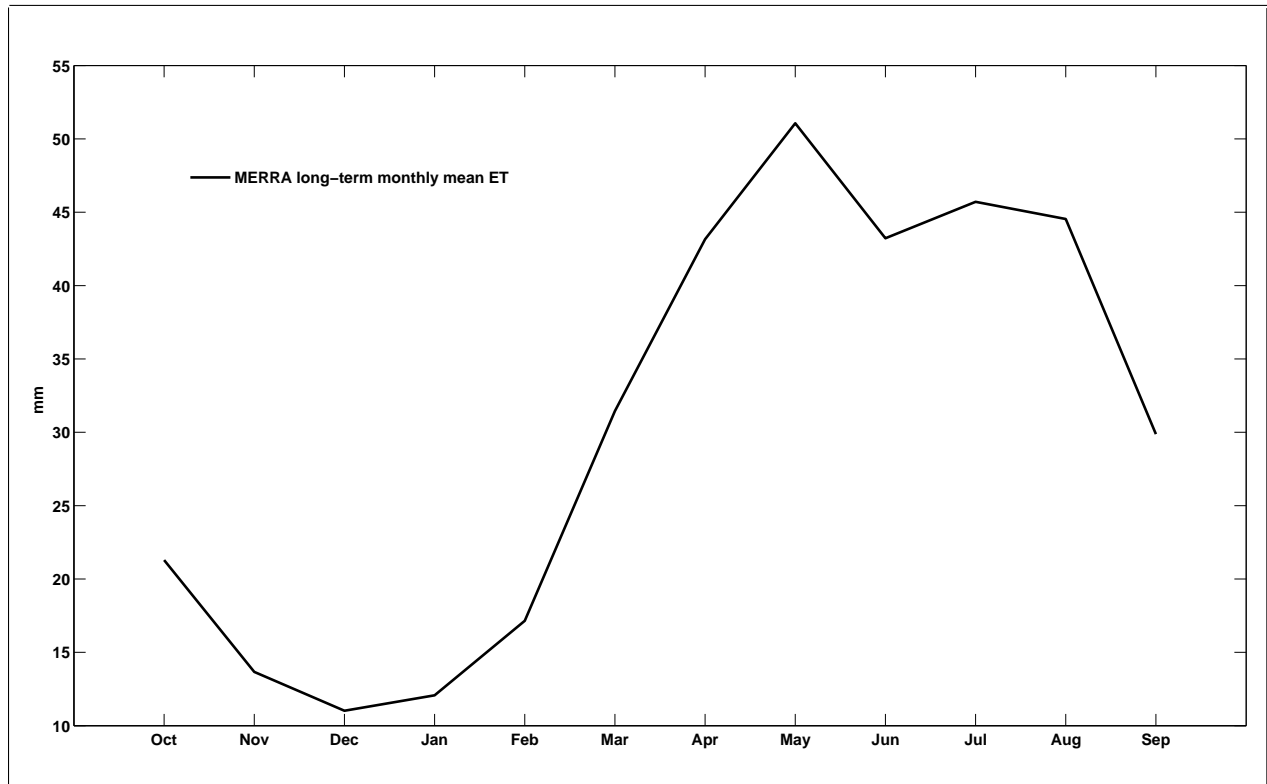
FIGURE 3.4. Long-term average monthly ET averaged over the UCRB using MERRA data.
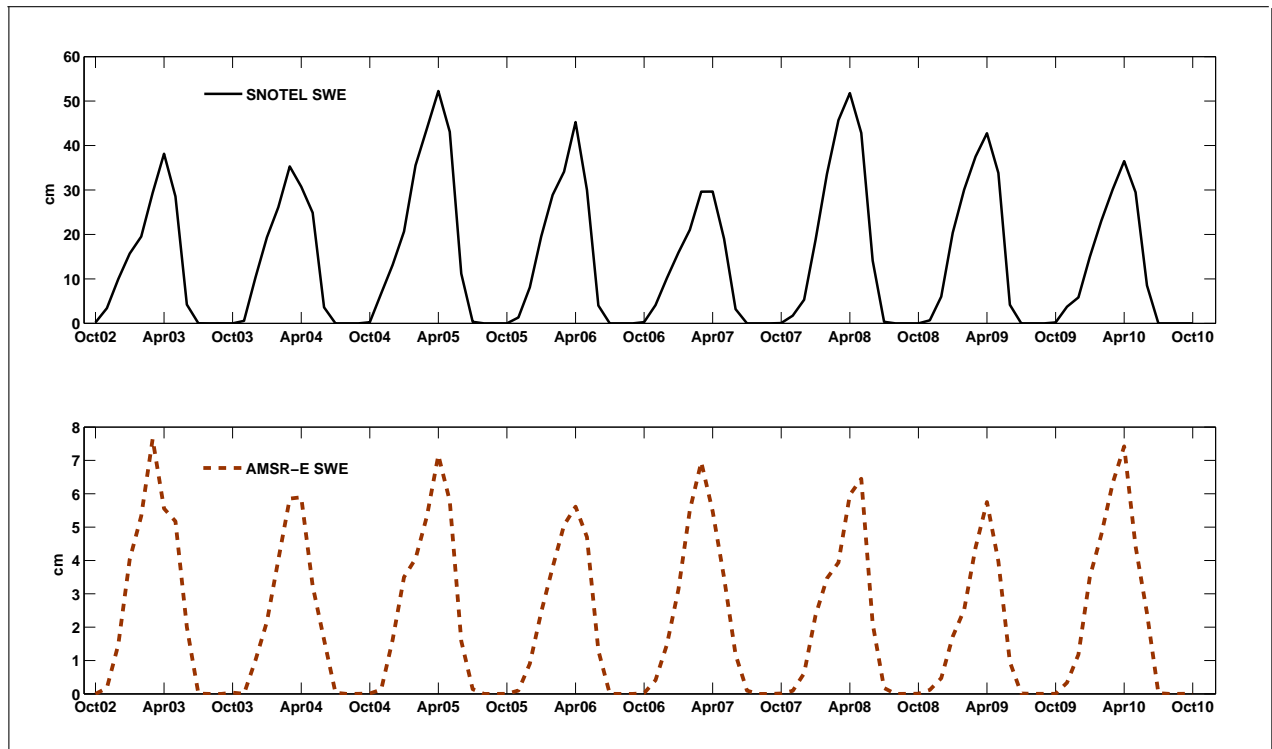
FIGURE 3.5. Monthly SWE averaged over the UCRB, using SNOTEL observations (top) and AMSR-E retrievals (bottom).
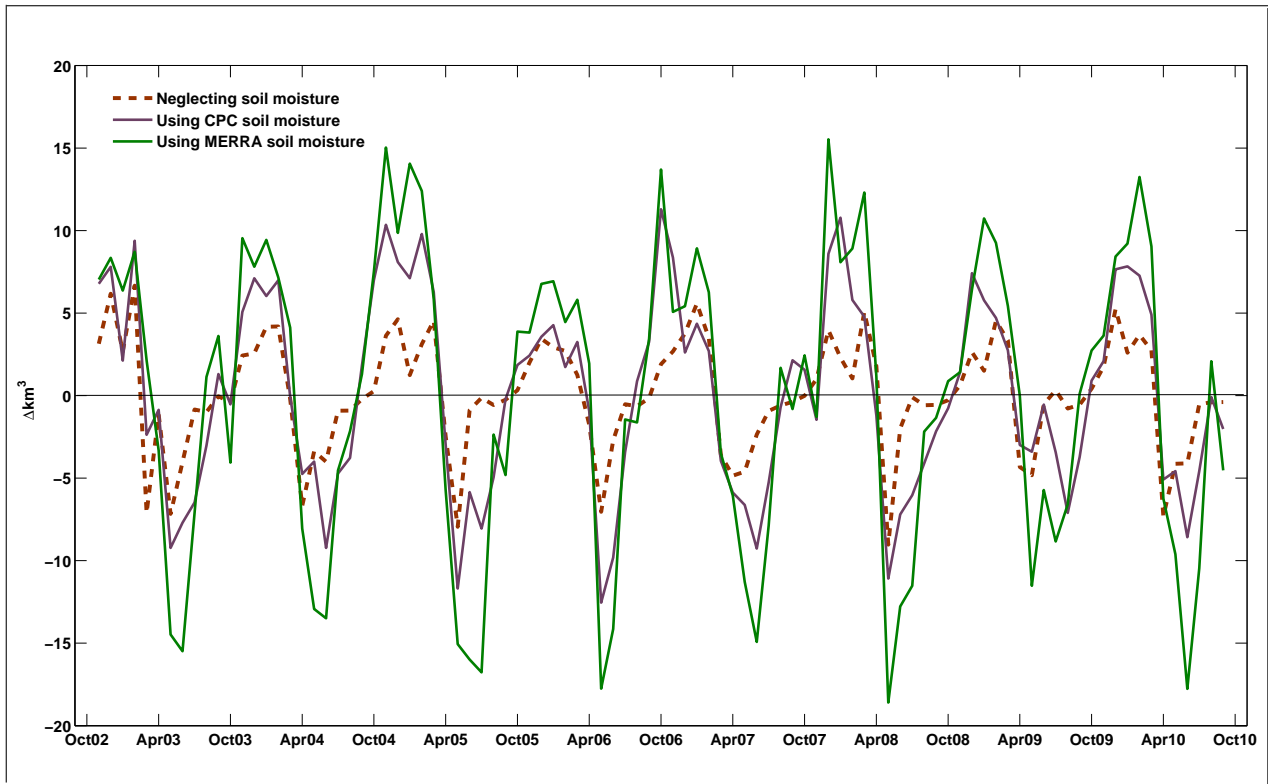
FIGURE 3.6. Comparison of surface storage changes in the UCRB for Δ(SWE + reservoir) (black), Δ(SWE + reservoir + MERRA soil) (green), and Δ(SWE + reservoir + CPC soil) (purple).
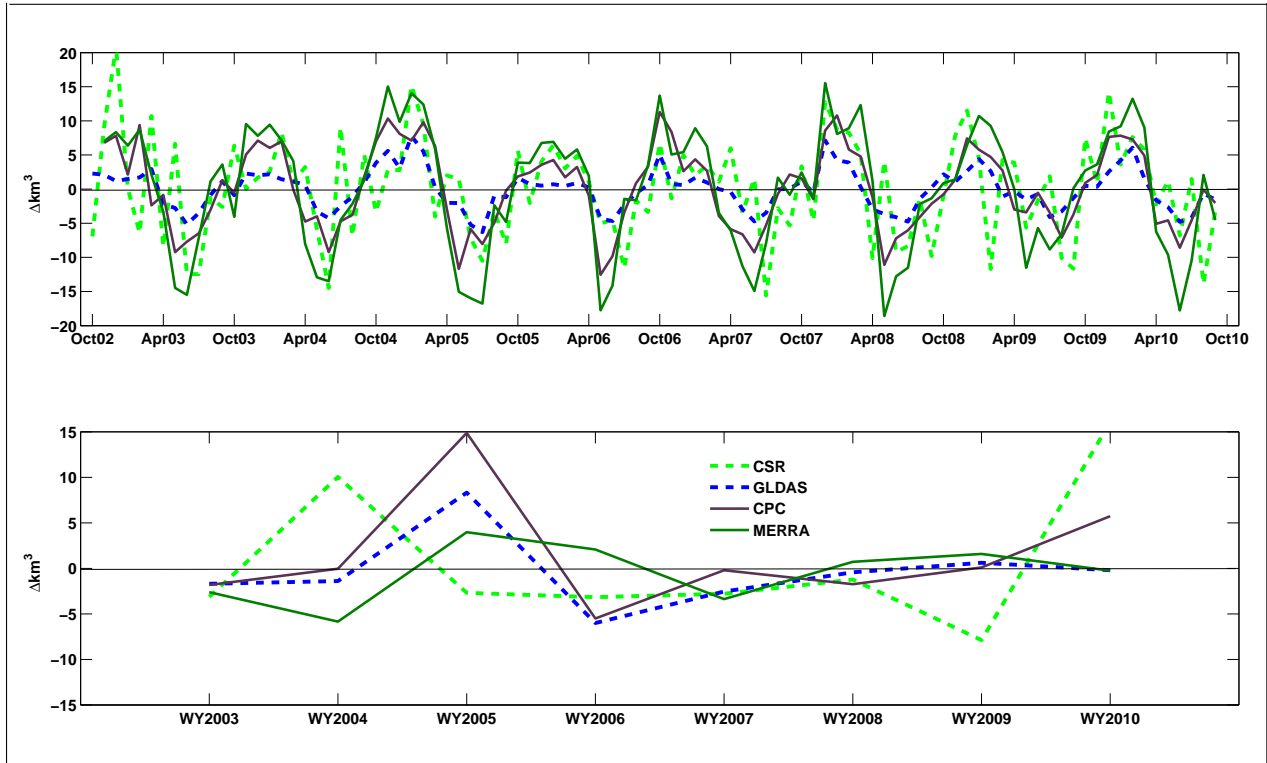
FIGURE 3.7. Monthly (top) and annual (bottom) storage volume changes for the UCRB comparing observations (SWE + reservoir + soil moisture) with satellite ΔTWS estimates from GRACE.
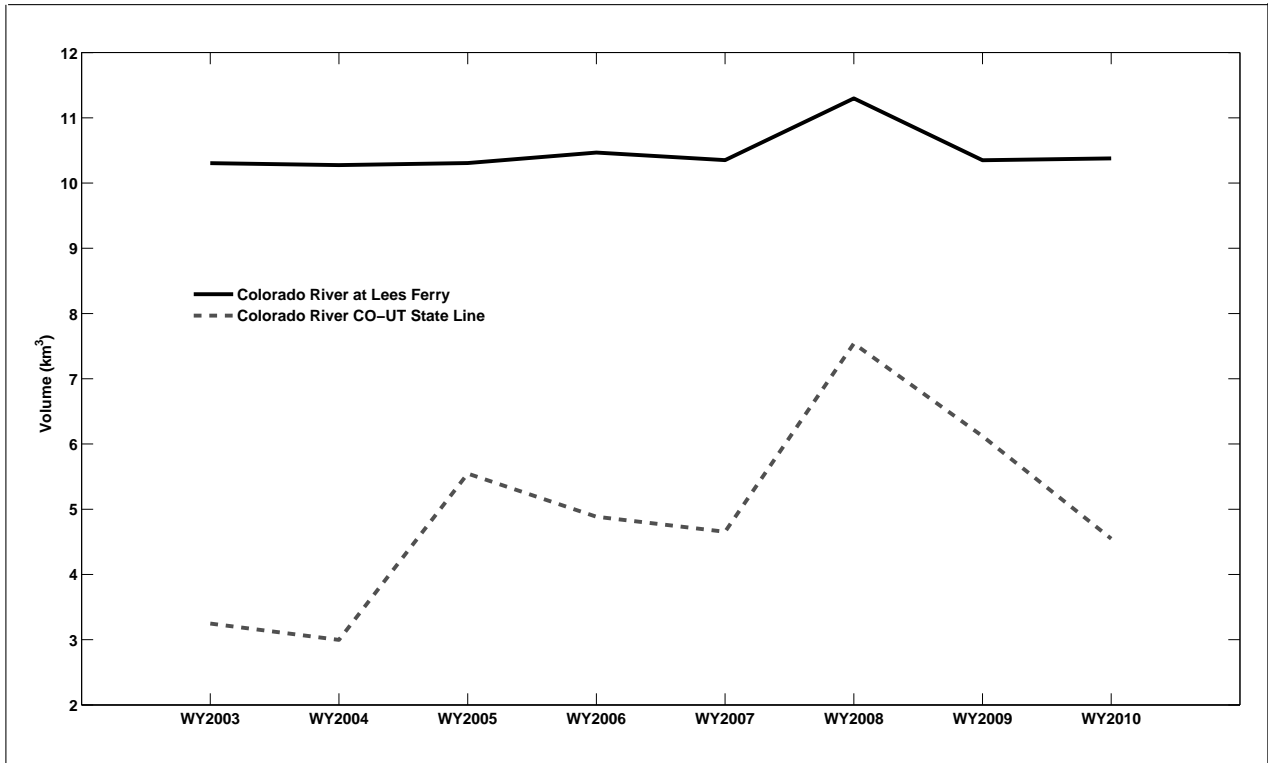
FIGURE 3.8. Annual volume runoff on the Colorado River at the Colorado-Utah state line and at Lee's Ferry.
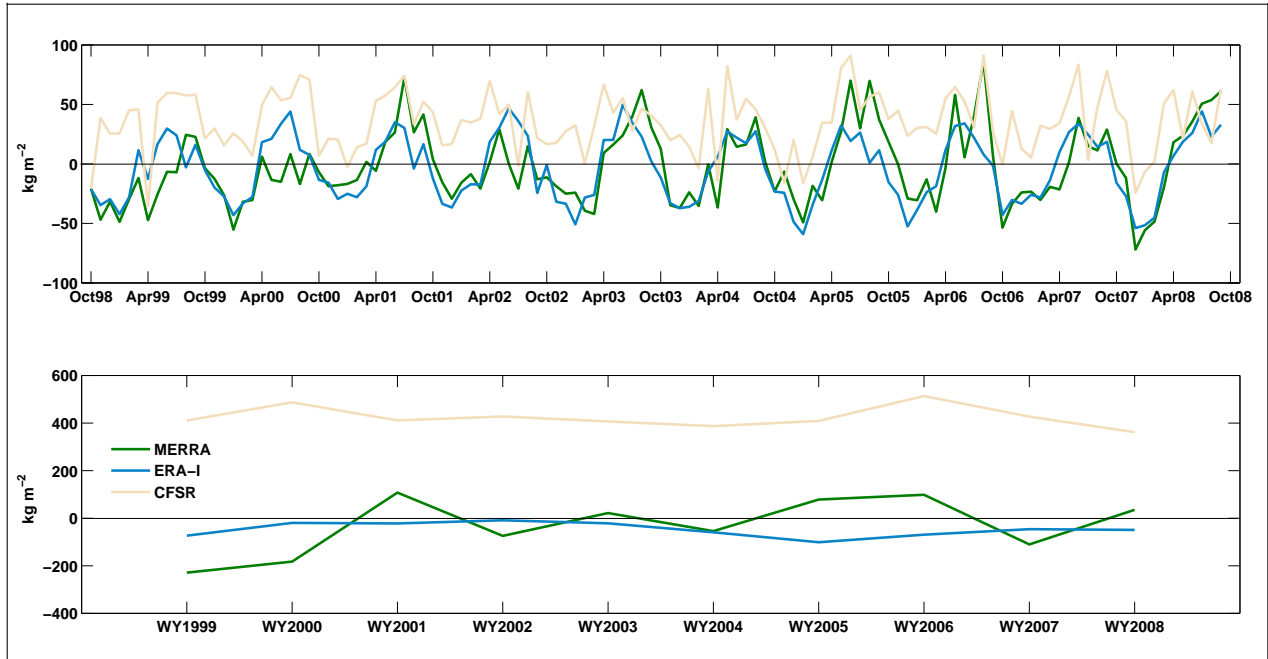
FIGURE 3.9. Monthly accumulation (top) and annual accumulation (bottom) atmospheric $\nabla \cdot \mathbf{Q}$ averaged over the UCRB using reanalysis data.
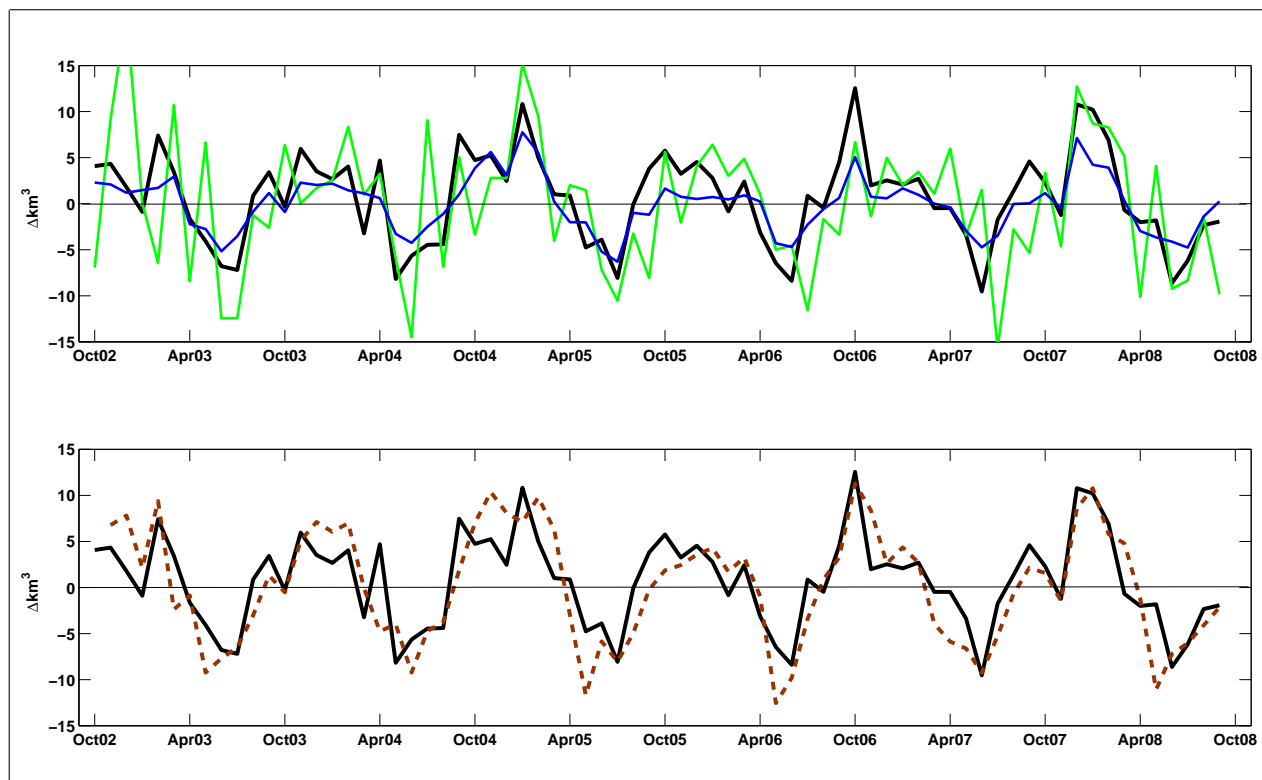
FIGURE 3.10. Comparison of estimated storage changes (*in-situ* P - MPI ET - R, black line) with GLDAS (blue) and CSR (green) in the top panel and with change in (AMSR-E SWE + reservoir + CPC soil moisture) in the bottom panel (maroon dashed).
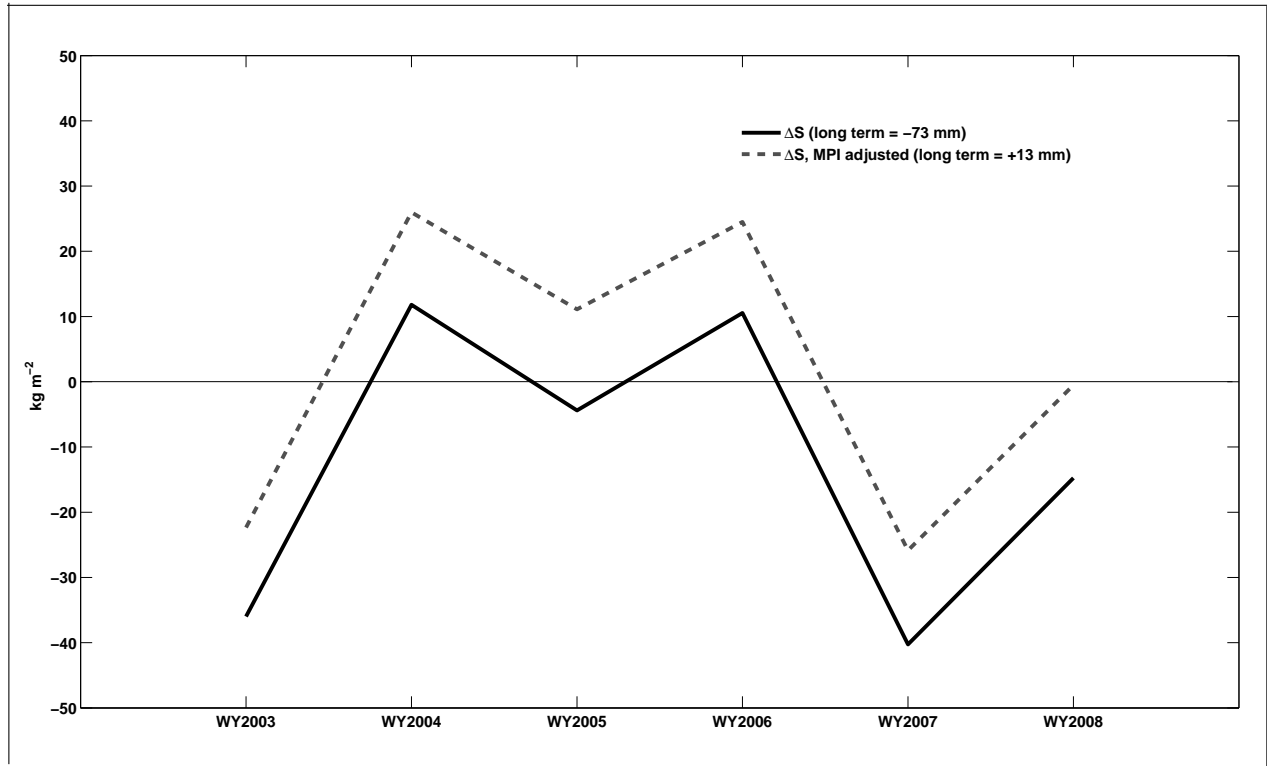
FIGURE 3.11. Annual accumulation of $\frac{\partial W}{\partial t}$ using *in-situ* precipitation, MPI ET, and ERA-I $\nabla \cdot \mathbf{Q}$.

CHAPTER 4

Climate Variability of the UCRB

4.1. Large-scale Teleconnections

Figure 4.1 shows correlations between the sub-basins' October maximum temperature and October SST. The individual sub-basins appear very similar. From previous research regarding relationships with ENSO, more significant correlations were expected for the southern sub-basins, and of opposite sign to the northern sub-basins (Hurkmans et al. 2009; Mo et al. 2009; McCabe and Dettinger 2002), but this study finds that all the sub-basins have almost identical correlation patterns in the ENSO region. All sub-basins are negatively correlated with eastern tropical Pacific Ocean SSTs. This is consistent with the prevailing relationship in the southwestern United States (warmer than average SSTs, El Niño, associated with cooler than average temperatures in the southwest), and opposite the pattern for the Pacific Northwest.

All of the sub-basins also show a significant positive correlation around 35° N Pacific Ocean, wrapped around a negative correlation bullet south of Alaska (i.e. the PDO region, Fig. 4.1). So the cool phase of the PDO (35° N Pacific temperatures are warmer than average) is associated with warmer than average temperatures in all the sub-basins. When ENSO and PDO are in phase, they act to enhance the effects over the UCRB, which has previously been shown. Because of the many similarities among the sub-basins, the correlations for the entire basin yields nearly identical results (not shown).

Correlations between each sub-basin's October SPI and October SST yield similar results to Fig. 4.1 (figure for SPI not shown). The warm (cool) phases of ENSO and PDO are associated with positive (negative) SPIs, or wetter (drier) than average conditions in the

basin. The pattern is not as consistent among all the sub-basins as it was for basin temperatures, suggesting that ENSO and PDO variability more strongly influence temperature than precipitation.

It is important to note that, although the correlations discussed are significant (at the 90% confidence level), correlation magnitudes are generally still no greater than 0.4. Figure 4.2 shows the comparison between the UC sub-basin's October maximum temperature and October SSTs over the area of highest correlation, in the PDO region. Though the relationship is clear, there is still significant scatter - for example, there are many times when the UC's temperature is below average, even when the SSTs in the north Pacific are above average.

Figure 4.3 shows correlations between the UC's maximum temperature and SSTs for each month from November through June (the other sub-basins are not shown but have very similar patterns). Similar to October, November shows negative correlations in the ENSO region and positive correlations in the PDO region (both stronger in the southern sub-basins). During December, January, and February, correlations are displaced southward of the PDO region, with the negative correlation maximum around 35° N and positive correlations wrapped around it to the south and east. In March, a southwest to northeast oriented positive and negative correlation coupling sets up, extending from the tropical western Pacific to the sub-tropical Atlantic. Also of note is a positive correlation region during January across much of the Atlantic ocean and a large area of positive correlation along the eastern Pacific during May. During June, there is very little correlation between SSTs and the basin's maximum temperatures. Correlations between the UC's SPIs and SSTs for each month of the winter do not yield similar results to Fig. 4.3 (figure for SPI not shown) and show little consistency through the months.

Lag correlations between October SST and basin-wide averaged maximum temperature (for November through June) are shown in Fig. 4.4. The ENSO region shows up at a one month lag (due mostly to the southern sub-basins), but at further lags, the ENSO region is not well correlated with winter temperatures in the basin. The PDO region is also correlated with the basin at a one month lag, but not at further lags. In December/January/February, there is a significant positive correlation in the Atlantic - so warmer Atlantic Ocean temperatures in October are well correlated with warmer maximum temperatures in the UCRB in the winter. In March, there is a significant positive correlation in the western Pacific - so warmer western Pacific Ocean temperatures in October are well correlated with warmer maximum temperatures in the UCRB in early spring. A small region east of Iceland is well correlated with UCRB temperatures in April and May, and the Gulf of Alaska is well correlated with UCRB temperatures in June. These areas outside of the ENSO/PDO regions, while interesting, could be exhibiting a connection that may not actually exist. At this time, no physical explanation can be provided for why the basin's temperatures would be modulated by the SSTs in these regions. Although significant, the correlations are still not particularly strong, and therefore may be coincidental.

When looking at lag correlations between October SST and basin-wide averaged SPIs (not shown), the ENSO and PDO regions show as significant for November (as it did with basin temperatures in Fig. 4.4) and March. The remaining months, regions of signficance for basin temperature and basin SPI do not match. Lag correlations with SPI do not show a consistent pattern through the months, and areas of significance for most of the months are small in areal extent.

The significant correlation magnitudes discussed in the previous paragraphs are still generally below 0.4. Additionally, changing the length of time used for the correlation

analysis changes the areas of significant correlations. When looking at just 50 years (1961 - 2010) or 30 years (1981 - 2010), the lagged correlations mentioned in the previous paragraph are not observed, but different areas of significant correlations show up (Fig. 4.5). This suggests that, although the correlations are significant, the results are not robust. Therefore these lag correlations could not be relied upon with any certainty.

4.2. EOF Analysis

Empirical Orthogonal Function (EOF) and Principal Component (PC) analyses are performed to assess the spatial and temporal variability in the UCRB. When calculated for October - June SPIs, the first three EOF modes account for approximately 86% of the variance in the individual sub-basins (76% of the variance when calculated for the entire UCRB, as shown in Fig. 4.6). The first three EOF modes for October - June maximum temperature Z-scores account for 83% of the variance for the UCRB. The first two EOF and PC modes for temperature Z-scores and SPIs are well correlated with each other.

The first EOF mode for SPI (which accounts for around 75% of the variance) shows minimal spatial variability for all of the sub-basins. In Fig. 4.7, when looking at the basin as a whole (57% of the variance), the headwater regions of the Colorado and Green rivers show lower magnitudes of variability than the rest of the basin (though the sign is always the same). The first mode PC time series shows strong year-to-year variability (Fig. 4.6, top). Forty-five out of the 99 winters analyzed are a single season occurrence (wet, dry, or neutral). In this mode, the occurence of consecutive wet winters (two or more years in a row) is very rare, and three or more consecutive dry winters has not occurred. For most of the sub-basins, this mode is not well correlated with any large-scale climate indices, suggesting that variability in the basin may be primarily driven by more localized forcings.

The second EOF mode for SPI accounts for about 8% of the variance in the sub-basins, 14% for the entire UCRB. The mode two PC time series (Fig. 4.6, middle) for both SPI and temperature are well correlated with ENSO/PDO variability; temperatures are better correlated with the ENSO index and SPIs are better correlated with the PDO index. When looking at the EOF for the entire basin (Fig. 4.8), the northern portion of the basin is of opposite sign from the southern portion of the basin. However, when looking at the individual sub-basins for SPI, an elevation dependence is evident - the higher elevations are of opposite sign from the lower elevations (see elevations in Fig. 1.1).

The third EOF mode for SPI accounts for about 4% of the variance in the sub-basins (5% for the entire UCRB) and is not associated with any of the large-scale climate indices. Shown in the bottom of Fig. 4.6, the earlier period of the PC time series exhibits a decadal variability: negative in the 1910s and 1920s, positive in the 1930s and 1940s, negative in the 1950s, and positive in the 1960s. This pattern is not evident in the final 40 years of the PC time series, which are more variable. The spatial pattern across the UCRB exhibits an east-west gradient (Fig. 4.9). However, when looking at the individual sub-basins, the Gun, Dol, UG, and Y-W sub-basins show a north-south gradient, and the UC sub-basin shows no clear spatial pattern. The third EOF mode for temperature (3% of the variance for the entire UCRB) shows spotty spatial variability, and the PC time series shows an increasing trend from 1911 to mid-1940s and a decreasing trend from mid-1940s to 2010 (Fig. 4.6).

4.3. Sub-seasonal Characteristics

In order to better analyze the mechanisms that control the variability of the UCRB, it is important to understand each month's impact on the season as a whole and how that changes for wet or dry seasons. Figs. 4.10 and 4.11 break down each sub-basin into its monthly

statistics for wet and dry seasons. In this section, percent of average precipitation (monthly and seasonal) will be used instead of SPI. This is done to allow for a better analysis of the characteristics and magnitude of the variability. The SPI method normalizes precipitation values (making the mean and median equal, and setting the magnitude of variability equal for all points), whereas using percent of average will show if a sub-basin tends to be dry or wet more often and will also show which sub-basins are generally more variable. In this section, dry refers to precipitation less than 90% of average, and wet refers to precipitation greater than 110% of average.

When looking at each month's contribution to the seasonal total (Fig. 4.10), March and April are the largest contributors for the northern sub-basins (UC, Gun, UG, Y-W). October is the largest contributor to the seasonal total for the southern sub-basins (Dol, LG, DD, SJ). When combined with the analysis from Section 4.1, this is an important result. For the northern sub-basins, the largest contributing months are during a time (in the spring) when there is very little correlation (and no lag correlations) between precipitation and large-scale forcings (such as ENSO or PDO). Therefore, a long-term prediction at the beginning of the season would have little skill. There could, however, be more skill for the southern sub-basins, where October is the largest contributing month, and October climate also has the strongest correlation to large-scale forcings.

For all of the sub-basins, June contributes the smallest percentage to the seasonal total (and usually little to no snow accumulation, Fig. 4.10). During the winter months, each sub-basin varies in the smallest contributing month. In general, February is the least sensitive to variability - so it contributes much more to dry season totals and much less to wet season totals. The southern sub-basins exhibit much higher variability throughout all the months.

Looking at Fig. 4.11, for most of the sub-basins, spring months are generally wet during wet seasons. February is the least sensitive month to wet seasons, and can be either wet or dry. During dry seasons, October is usually drier than average for most of the sub-basins. Additionally, October can be dry during a wet season. The occurrence of a wet October is much more common in a wet season than a dry one, therefore a wet October could be a good predictor for the season as a whole. Overall (especially for the southern sub-basins) there is a higher frequency of occurrence of dry months. Therefore, the occurrence of a dry month does not necessarily aide in the prediction a dry or wet season.

Both Figs. 4.10 and 4.11, and the results of Section 4.1, point to the greater importance of October over the other months. October has a stronger correlation to ENSO and PDO (which can be predicted to a certain degree of accuracy over a longer time period). As October is the largest contributing month to the southern sub-basins' seasonal precipitation total, the predicted ENSO/PDO phases for October could give a better idea of what might happen over the southern sub-basins. Additionally, the occurrence of a wet October greatly increases the possibility of a wet season overall for all of the sub-basins.

4.4. Case Study

Section 4.1 showed that large-scale climate variability and basin varibiability are correlated, but the connection isn't clear or robust. To further examine this, two seasons with similar ENSO and PDO signals are examined. Though the large-scale climate indicies are similar for the two seasons, the basin's response is very different. The time series in Fig. 4.12 show that the 2002 (top, a dry year) and 1997 (bottom, a wet year) winters were very similar in the ENSO region. Both seasons start with slightly below average SSTs, increasing to the ENSO cold phase in the winter months. By the spring, both seasons were in the warm

phase of ENSO. Their PDO time series (not shown) also share similarities. Both seasons start in the PDO cold phase and end in the warm phase by the end of the summer. Their springs are slightly different, as the 1997 season is in the warm phase by May while the 2002 season stays in the cold phase through the spring.

From Section 4.1, correlations between SST and the basin show that the cold ENSO phase in the fall is generally associated with negative SPIs and above average temperatures. The cold phase of the PDO would act to enhance this relationship. Table 4.1 shows the monthly SPIs and departure from average temperature for the basin during the two seasons. The 2002 season starts as expected with warmer than average temperatures and negative SPIs in October. The 1997 season does not begin this way though (it shows below average temperature and positive SPI). This example shows the basin's sensitivity to other driving factors (aside from large-scale ocean variability) that can have an impact.

There are two interesting points to note regarding the October of the 1997 season. First, although the fall months tend to show the strongest correlations with the ENSO/PDO regions, it is not uncommon for the basin to behave differently than statistically expected. Second, it supports the idea in Section 4.3 that a wet October could be a good indicator for a wet season. In fact, the 1997 season would have been better predicted by the occurrence of a wet October, rather than the occurrence of the cold ENSO phase.

For the 1997 season, the largest contributing months to the seasonal total were March and April. This is consistent with what most commonly occurs in the basin (particularly the northern sub-basins). The largest contributing month for the 2002 season was November.

Neither statistics nor the monthly analysis can explain why winter 2002 was drier than average and winter 1997 was wetter than average. Without understanding why these two seasons are different, seasonal prediction can't be improved upon. Because the seasonal and

monthly statistics can't adequately explain the differences, a more detailed analysis (daily and synoptic scale) is necessary.

SNOTEL snowpack data is used to look at the daily statistics of each season. From the beginning of the water year to the last day of snowmelt season, the 1997 snowpack period lasted 295 days, and the 2002 snowpack period lasted 253 days. The 1997 snowpack period only had 14 more accumulation days than 2002 though (accumulation day defined as one day's snowpack greater than the previous day's, in Chapter 2). Focusing on the distribution of just the accumulation days (Fig. 4.13), accumulations less than 2.5 mm are the most common for both seasons. However, those lowest accumulations account for more than 80% of all the accumulation days in 2002, and less than 60% of the accumulation days in 1997. The 1997 accumulation season has a much higher frequency of higher accumulations than 2002.

In the 2002 season, there were only two days when snowpack accumulation was greater than 10 mm; these occurred in November, the only positive SPI month in the October - June season (Table 4.1). In the 1997 season, for the period of October - April, most of the months had more than one day with accumulations greater than 10 mm; the only months that didn't have multiple large accumulation days were February and March (the only negative SPI months as seen in Table 4.1). An analysis of daily SWE accumulations over ten years (2001 - 2010) shows that wetter years tend to have closer to 10 large accumulation days during the winter, while the drier winters generally have five or fewer large accumulations.

The existence of just a few more significant accumulations cannot be easily predicted by looking at longer-term global patterns. Because large accumulation days define the difference between wet and dry seasons, it is important to know what causes large accumulations in the basin. Heavy basin snowfall requires three components - upward vertical motion, instability

and a source of moisture. The upward vertical motion, or lift, comes from the rising air that is forced upward due to orographic influences. This lifting mechanism can become even stronger in the presence of unstable air, which is needed for larger accumulating events. This unstable air (warmer air below colder air) can be provided in several different ways, including frontal passage or the passage of a baroclinic trough. What exactly provides the instability for an individual heavy storm over the basin is not easy to predict on a short timescale (i.e. one week), thus adding to the extreme difficulty of seasonal prediction for the area. The moisture for the basin is most often provided by maritime polar (mP) airmasses that travel from the northern Pacific across the western United States. These airmasses are modified as they pass over the complex terrain of the western U.S., so the amount of moisture available when they reach the basin is variable with each system. Also, the exact position of fronts and surface lows associated with the airmass can cause widely varying results in the basin. Closer examination of specific storms will provide more information.

January 26 - 27, 1997 were two of the largest accumulation days in the 1997 winter season, with a two-day total accumulation of 32 mm. Before the start of this event, a surface low moved southward, staying on the northern fringes of the UCRB, while a weak surface high pressure set up over the southern part of the basin (Fig. 4.14, top left). The pressure gradient over the basin would have resulted in westerly flow across the basin, and a very strong high pressure region across the midwest United States would have blocked the surface low from quickly moving away from the basin. Two-day storm totals show widespread precipitation over much of the western United States, with the heaviest amounts in northern California and dry over Washington (Fig. 4.14, top right). Surface analysis does not show evidence of the passage of a strong cold front and 500 hPa heights were mainly zonal over the region. So, it is difficult to determine the storm's major source of instability over the basin.

January 27 - 28, 2002 exhibited a similar synoptic set-up to the 1997 storm. A surface low pressure center settled over eastern Wyoming, with a weak surface high pressure over the southern part of the basin (Fig. 4.14, bottom left). With the pressure gradient and location of fronts around the basin, a similar westerly flow would have resulted across the basin. But the two-day total snowpack accumulation over the basin was less than 4 mm. Precipitation totals show that precipitation was not as widespread or as intense (Fig. 4.14, bottom right). Frontal passage had also not occurred during this time period; but the 500 hPa heights do show a large trough to the west, bringing southwesterly flow into the basin (unlike the zonal flow from the 1997 example).

Though the orographic component was present for both of the storms, the accumulations for the 2002 storm were much less. It is difficult to determine with certainty the reasons for this, but there are a couple of possibilities. In the reanalysis (Fig. 4.14, left), pressure gradients appear to be somewhat stronger in the 1997 storm. This could mean that the 2002 storm did not have a strong enough westerly component to generate the upward motion needed for larger accumulations. Additionally, the southwesterly flow aloft could have brought in warmer air than what was at the surface, acting to stabilize the region. Another possiblity is that the modified mP airmass over the area for the 1997 storm could have had more moisture associated with it. The entire western region received less precipitation in the 2002 example, suggesting that the airmass itself was not as strong of a moisture source. Also, the presence of the strong high pressure in the eastern U.S. could have played a role in making the 1997 storm longer duration. Perhaps the low pressure center in the 2002 example was allowed to pass by too quickly for larger accumulations to occur.

Even though there are similarities between the two storms, minor differences changed the overall results, leading to very different outcomes over the basin. Looking at the other

storms in 1997, there is much diversity in the synoptic scale patterns that result in larger accumulations. Essentially, no two storms were the same. The case study shows that the region is particularly sensitive to the exact position of synoptic patterns and is also dependent on the moisture content and modification of the airmasses moving over it. This is likely why there isn't a stronger correlation with large-scale forcings.

TABLE 4.1. Basin-averaged monthly statistics for 1997 (wet year) and 2002 (dry year). The first two columns are one-month standardized precipitation index (SPI), the last two columns are departure from average temperature for the month.

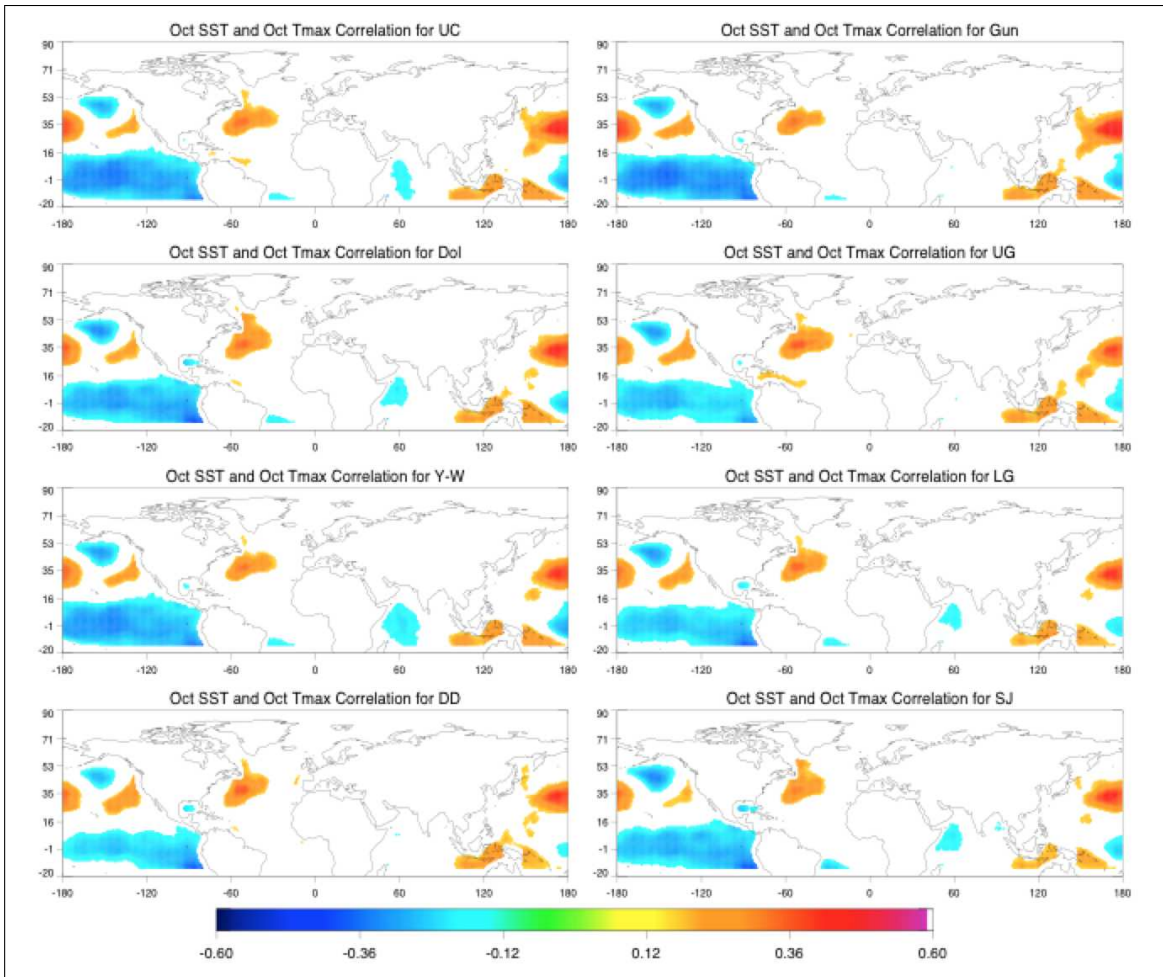| Month	1997 P	2002 P	1997 T	2002 T
October	+0.59	-0.66	-0.87	+1.17
November	+1.00	+0.38	+0.82	+2.25
December	+0.37	-0.23	+0.97	-0.89
January	+1.32	-0.99	+0.55	-0.00
February	-0.20	-1.59	-0.67	-1.11
March	-1.44	-0.44	+1.80	-1.06
April	+1.23	-0.79	-1.85	+2.51
May	+0.50	-1.36	+0.96	+0.86
June	+0.60	-1.08	+0.47	+2.66

FIGURE 4.1. Correlation between October SST and each sub-basin's October maximum temperature. Only significant correlations ($p < .10$) are shaded.
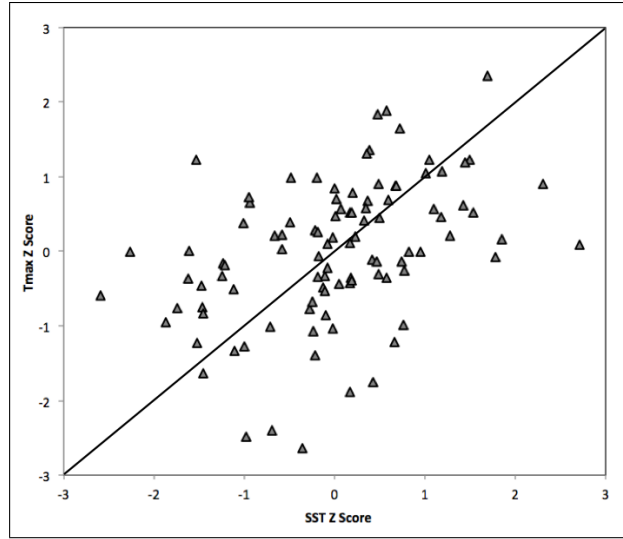
FIGURE 4.2. Comparison of Upper Colorado sub-basin's October maximum temperature Z-scores and October SST Z-scores at 33.5° N and 172.5° E. Correlation, $\rho = 0.47$.
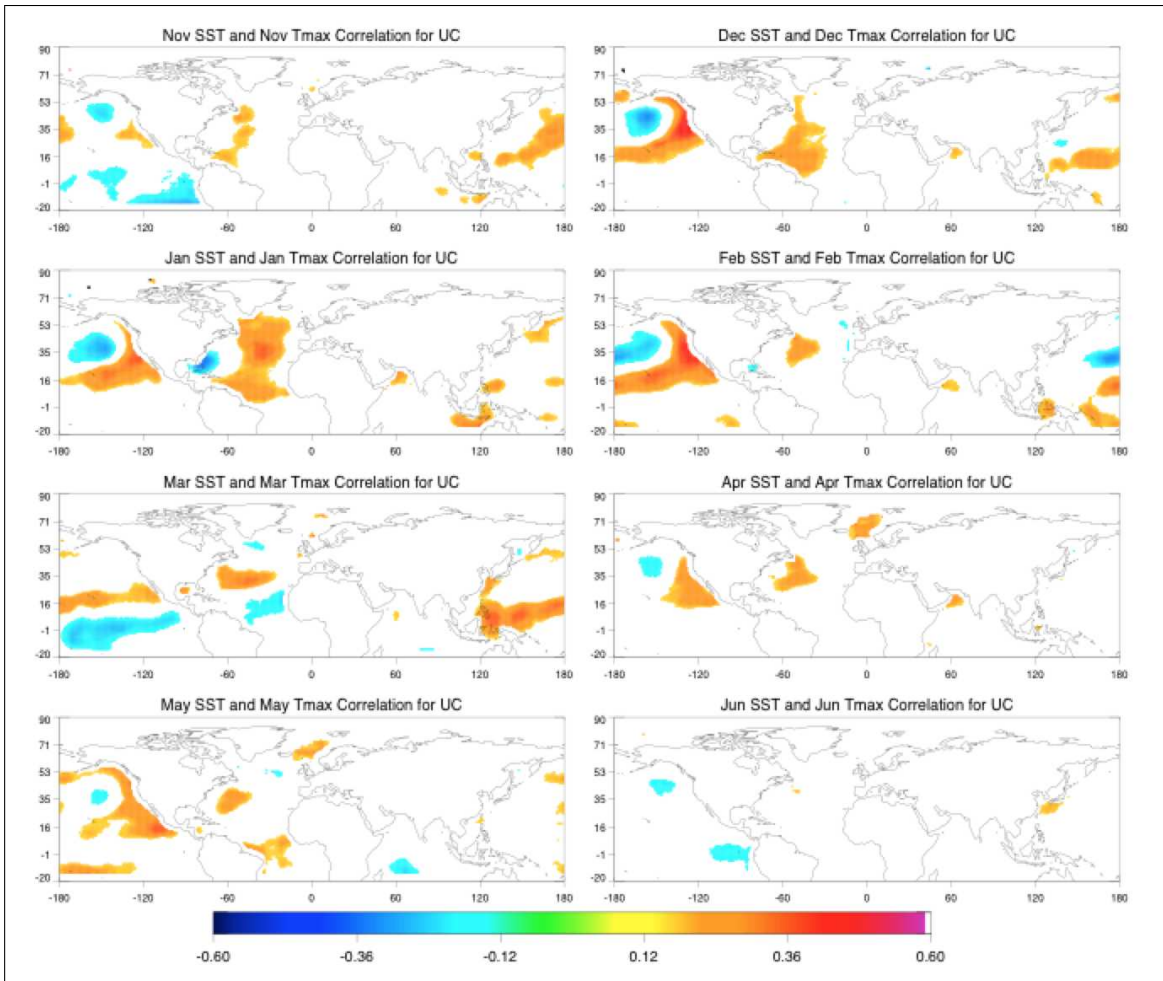
FIGURE 4.3. Zero lag correlations for each month (Nov. - Jun.) between SST and Upper Colorado sub-basin maximum temperature. Only significant correlations ($p < .10$) are shaded.
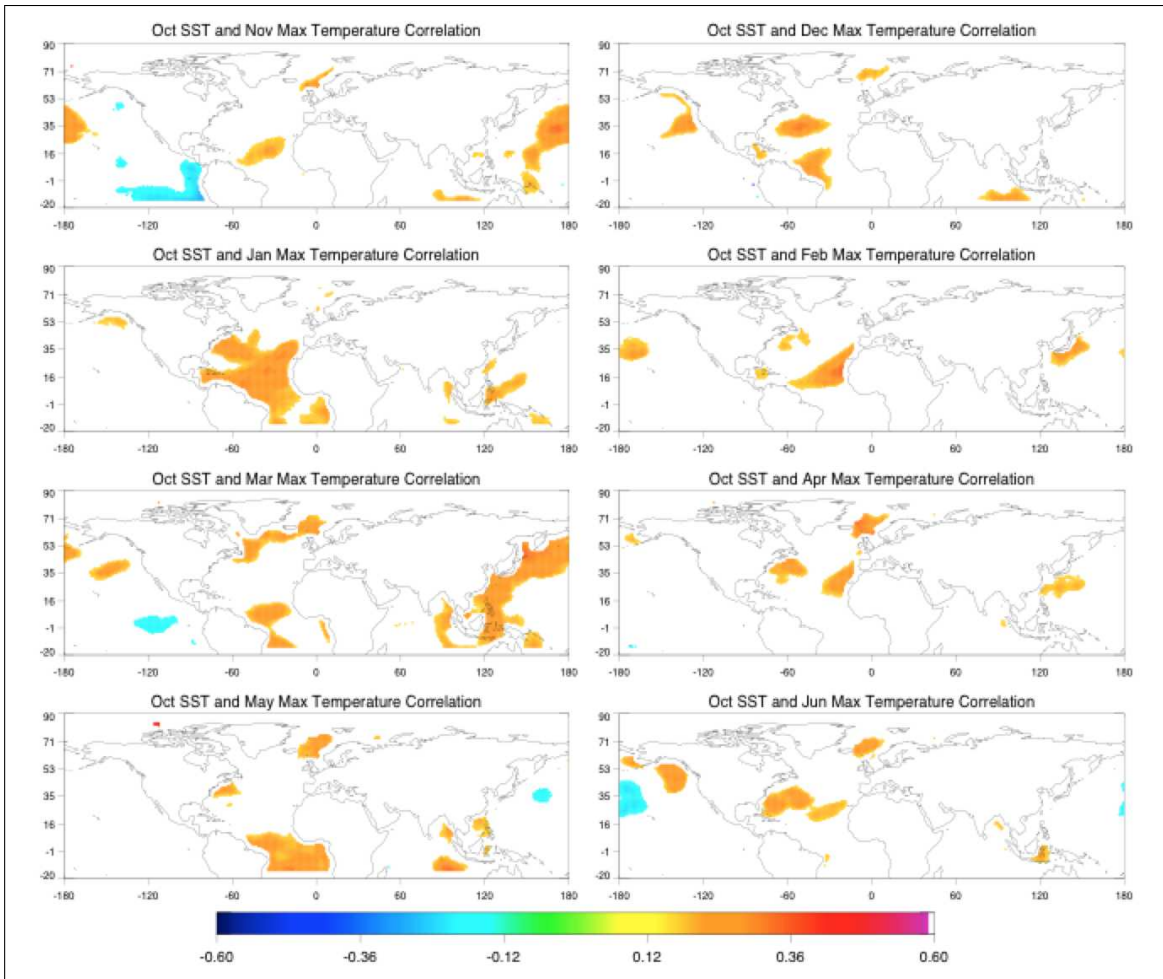
FIGURE 4.4. Lag correlations between October SST and UCRB averaged maximum temperature for subsequent months. Only significant correlations ($p < .10$) are shaded.
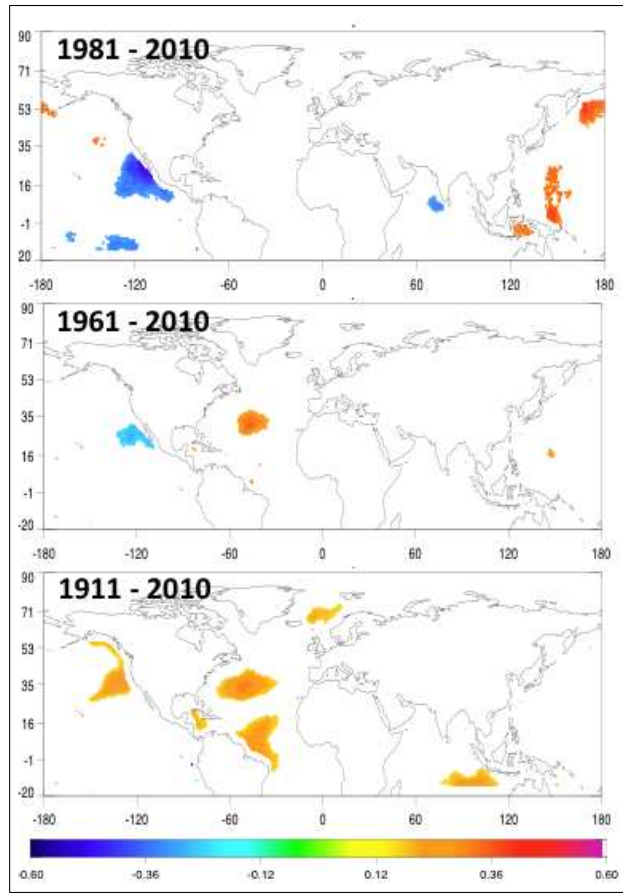
FIGURE 4.5. Lag correlation between October SST and UCRB averaged December maximum temperature using three different time periods. Only significant correlations ($p < .10$) are shaded.
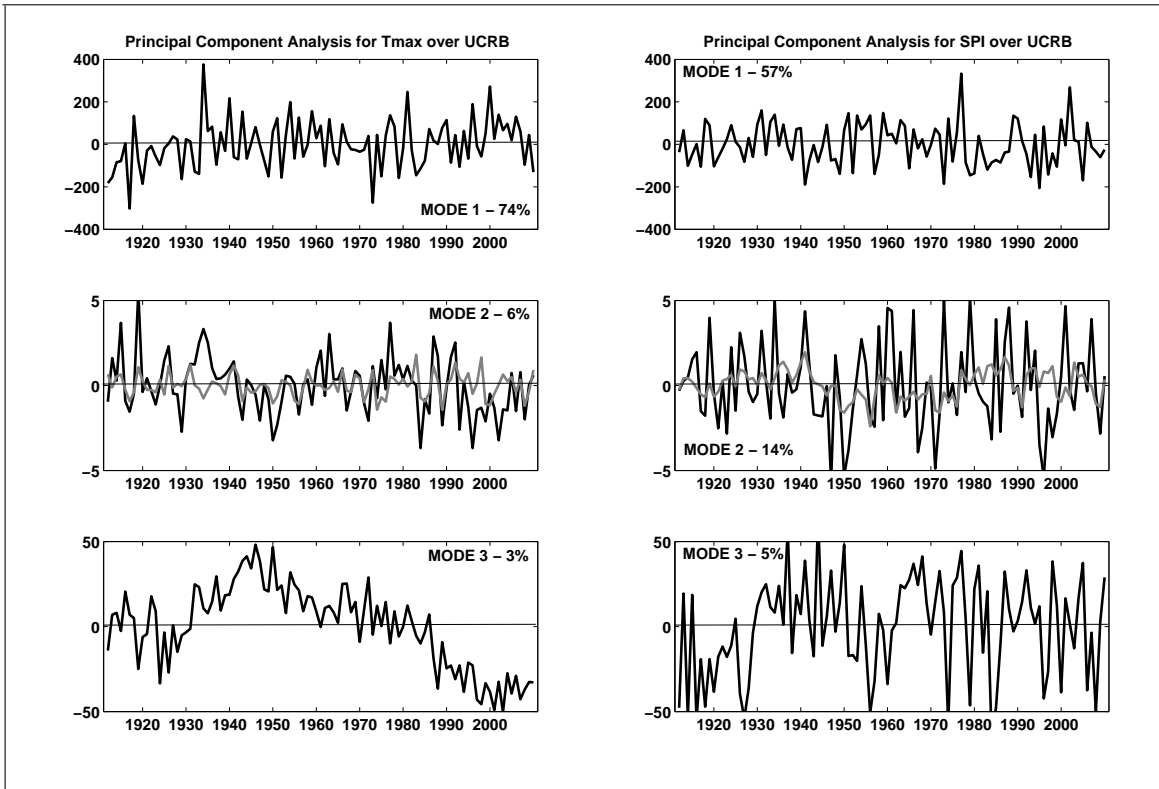
FIGURE 4.6. Principal component time series for October - June maximum temperature (left) and SPI (right) over the UCRB, showing the first three modes of variability. The second mode PC is overlaid with October - June averaged ENSO (left) and PDO (right) indices in grey.
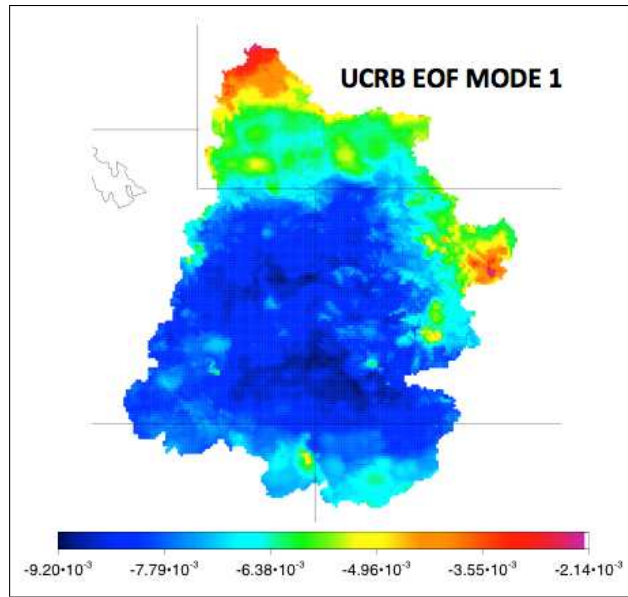
FIGURE 4.7. First mode EOF for October - June SPI over the UCRB.
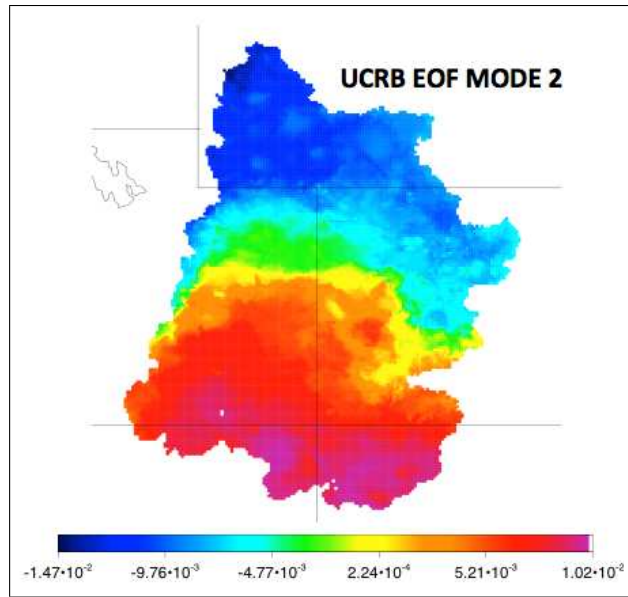
FIGURE 4.8. Second mode EOF for October - June SPI over the UCRB.
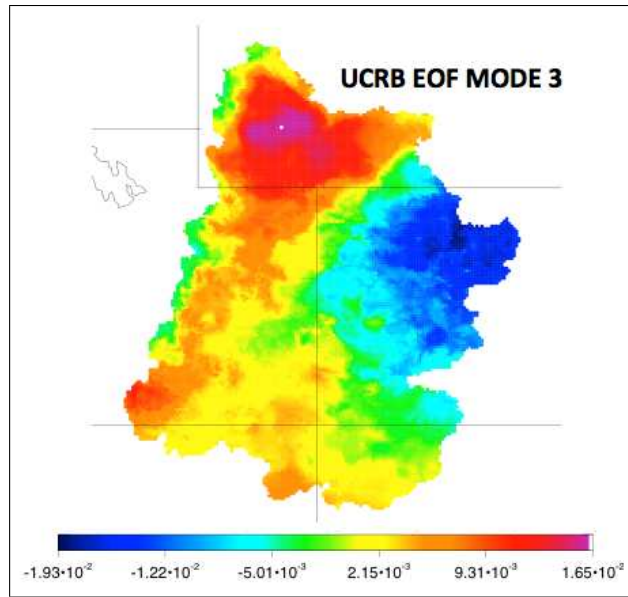
FIGURE 4.9. Third mode EOF for October - June SPI over the UCRB.
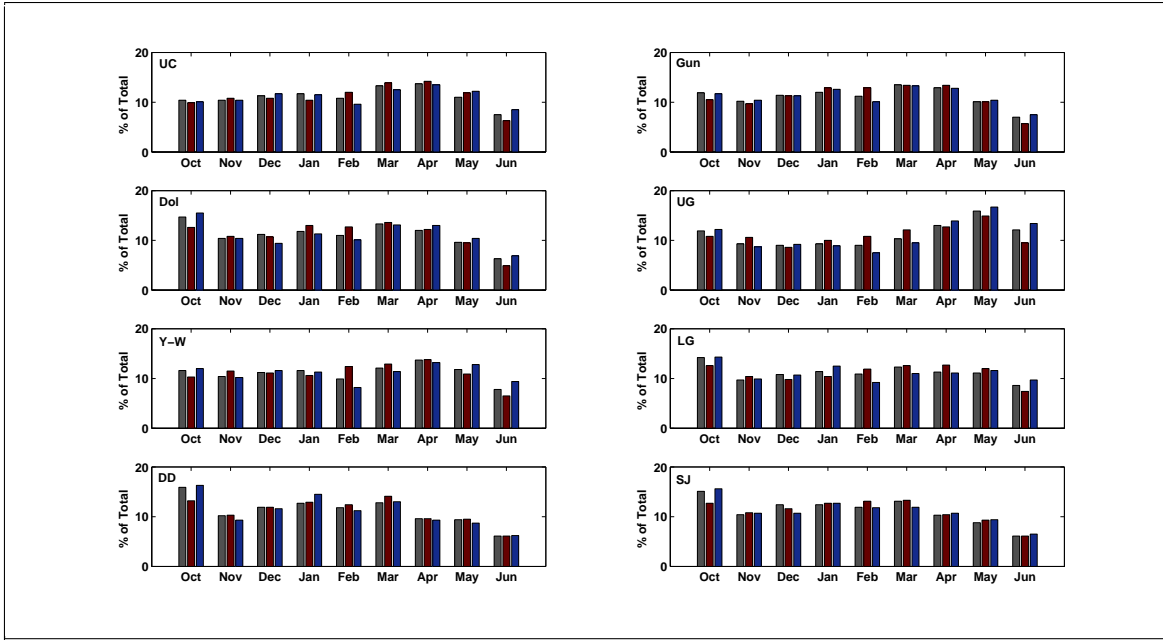
FIGURE 4.10. For each sub-basin, every month's percent contribution to the seasonal total for average years (grey), dry years (maroon), and wet years (blue).
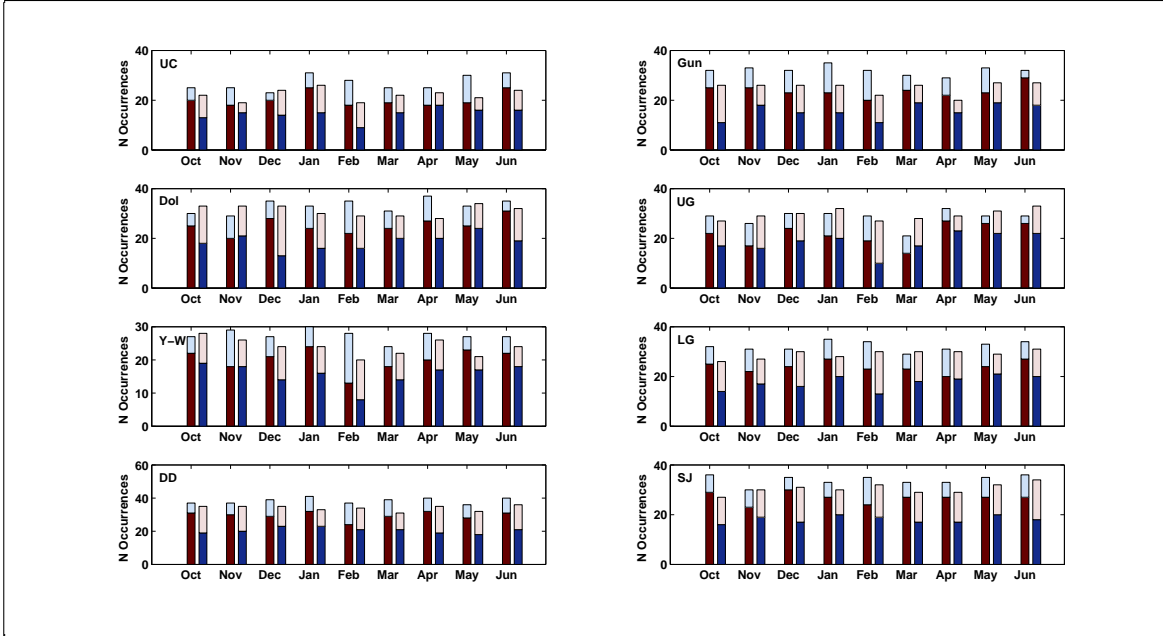
FIGURE 4.11. For each sub-basin, number of occurrences of wet and dry months during dry seasons (left bars) and wet seasons (right bars).
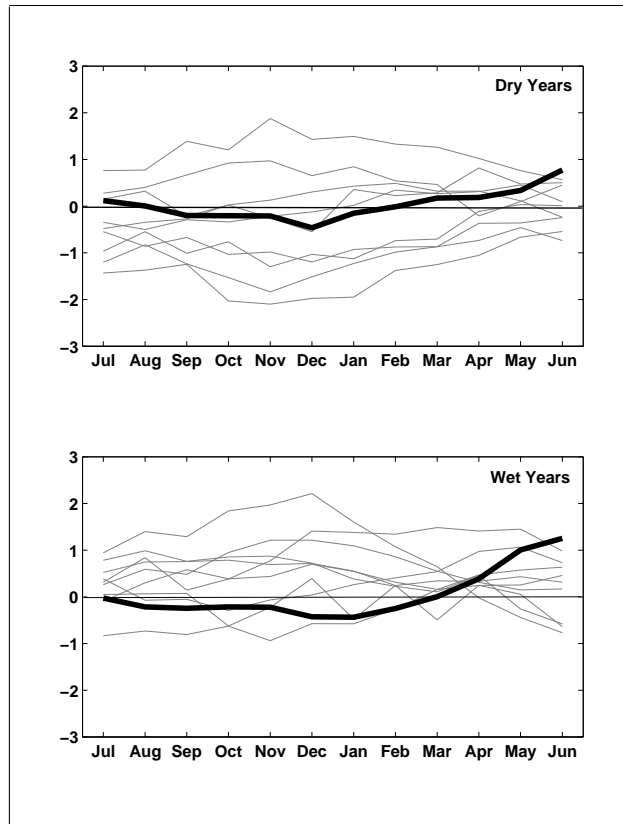
FIGURE 4.12. Monthly SST anomalies in the ENSO region for the UCRB's ten driest (top) and ten wettest (bottom) seasons. The thick black lines represent the two similar winters in the wet and dry years (2002-top and 1997-bottom).
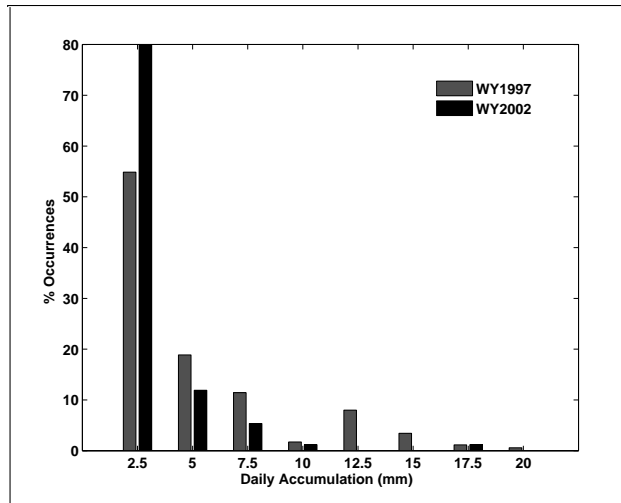
FIGURE 4.13. Frequency distribution of basin-averaged daily snow water equivalent accumulations during WY1997 (grey) and WY2002 (black).
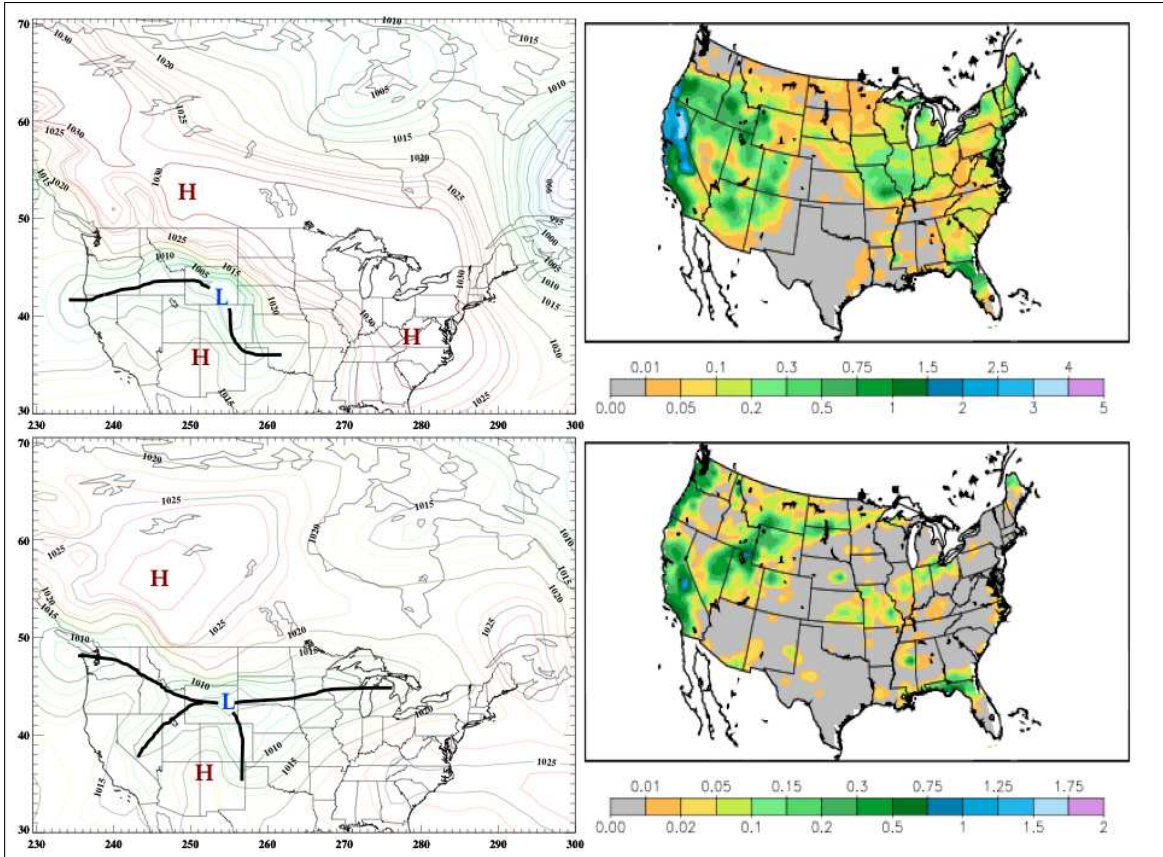
FIGURE 4.14. Top maps are mean sea level pressure in hPa (left) and precipitation accumulation in inches (right) for January 26 - 27, 1997. Bottom maps are same as top but for January 27 - 28, 2002. Mean sea level pressure maps were generated using ECMWF ERA-I 6-hourly dataset, with highs and lows denoted and fronts/troughs outlined in black; precipitation maps were provided by the Midwestern Regional Climate Center.

Water Budget of the Western U.S.

5.1. Water Balance

Average annual totals of precipitation, ET, $\nabla \cdot \mathbf{Q}$, and runoff are shown in Fig. 5.1. Precipitation accumulations exhibit high spatial variability (Fig. 5.1a); the lower elevation HUC4s and areas of the southwest can receive less than 200 mm in a year, while the higher elevation basins receive between 700 mm and 1600 mm. It is not uncommon for parts of Pacific Northwest to accumulate 2000 mm or more in one year.

Average annual ET patterns are similar to precipitation patterns, with higher ET amounts generally coinciding with areas of higher precipitation totals (Fig. 5.1b). Basins with the highest annual ET are found around the Pacific Northwest and extending southward along the California coastline. The lowest ET extends northward from the desert southwest in southern California and Arizona into the Great Basin in Nevada. Several basins in central California show relatively higher ET amounts and relatively lower precipitation - this is likely due to the dominance of croplands and irrigation.

Figure 5.1c shows annual $\nabla \cdot \mathbf{Q}$, with positive (negative) values denoting divergence (convergence).The Pacific Northwest, northern California, and the higher elevations of Idaho, Montana, Wyoming, and Colorado show net convergence, annually. Widespread annual divergence is found over the Great Basin in Nevada and southern Utah, and the desert southwest of southern California and Arizona.

In Fig. 5.1d, annual runoff along the coastal Pacific Northwest is up to an order of magnitude greater than the runoff totals for much of the rest of the western United States, with values greater than 1000 mm. In the northern Rocky Mountains (Idaho/Montana), annual

runoff is between 300 and 400 mm, with central Rocky Mountain values (Colorado/Wyoming) between 50 and 150 mm. The desert and lower elevation basins can experience less than 50 mm of runoff, annually.

The spatial variability of the annual water budget components show that, in general, areas with higher precipitation and ET coincide with areas of convergence and higher runoff. Areas dominated by divergence and low runoff receive less precipitation and evaporate less moisture into the atmosphere.

5.1.1. ATMOSPHERIC WATER BUDGET. Using Eq. 3 in Chapter 2, average annual percent residual errors for the atmosphere (ε_A) are presented in Fig. 5.2. Although a few basins show smaller errors, many of the basins show large percent residual errors, ranging in magnitude between 30% to over 100%. There is a mixture of positive and negative errors, but which component primarily contributes to the sign of the error can be different.

Several regions stand out with consistent errors. Southern California, southern Arizona, and southern Nevada show large negative residual errors. Since annual precipitation is small, these errors are primarily due to small ET values contributing to the atmospheric moisture and large amounts of divergence moving moisture out of the region.

Another region of note is the Upper Colorado River region, primarily the headwater basins in western Colorado and western Wyoming. These basins show large positive residual errors. Precipitation is slightly greater than ET in this region, which would lead to a negative residual. However, the large magnitude of convergence over the region results in the large positive residual error seen in Fig. 5.2.

There are several basins with large positive residual errors, inland from the coast in Oregon and central California. These areas receive much less precipitation than the coastal

region, but they experience high amounts of ET and some convergence - both of which contribute to the large errors.

The Pacific Northwest shows mainly negative residual errors, although the relative magnitude of these errors is smaller than in other areas. Although the region experiences high ET rates and consistent convergence, the large magnitude of precipitation overwhelms the other water budget components, thus leading to the negative residuals.

One possible reason for the large errors observed in Fig. 5.2 could be the shape of the basins and the selection of grid points from each dataset. The obscure geometry of some of the basins may not match well with the rectangular geometry of the chosen grid points within the basin boundaries; this problem could be magnified with the use of lower resolution datasets.

Using the same data and methodology, ε_A is calculated for square areas of varying size ($3°$ by $3°$ box size example shown in Fig. 5.3), to determine if the magnitude of errors can be reduced by using a shape that is consistent with the shape of the grids in the datasets. Some of the boxes in Fig. 5.3 continue to show large residual errors. Many of the boxes (e.g., the box in central California) do show an overall reduction in error: This is largely due to the box containing portions of basins with large positive residuals combined with portions of basins with large negative residuals. Increasing the box sizes to $5°$ by $5°$ results in further reductions in the error magnitudes (not shown). Over one specific area (the Colorado River region), increasing the box size several times, from $3°$ by $3°$ up to $9°$ by $9°$, systematically led to smaller error magnitude. So a better balance is achieved simply by bounding the data within a square over a larger area.

Another issue with the errors in atmospheric balance could be due to low resolution, particularly with the reanalysis data. Due to the smaller size of some of the basins, basin-averaged $\nabla \cdot \mathbf{Q}$ could be calculated using only a couple of grid points (compared to around 10 grid points with the MPI ET data and hundreds of grid points with the PRISM precipitation data). To analyze this further, $\nabla \cdot \mathbf{Q}$ is calculated for all the basins using NARR data, which is at a much higher resolution than the ERA-I data.

Results using NARR data in Fig. 5.4, also show large residual errors, many times with the opposite sign of the errors shown in Fig. 5.2. When looking at NARR $\nabla \cdot \mathbf{Q}$ over the region (Fig. 5.4, right), increasing the resolution leads to much finer detail, especially around the higher elevations. Overall, the basic locations of divergence and convergence are similar to the depiction with the lower resolution ERA-I. The biggest difference between the ERA-I and NARR $\nabla \cdot \mathbf{Q}$ is the magnitude of convergence/divergence. NARR shows much larger magnitudes, thus leading to much larger residual errors seen in Fig. 5.4 (left). Differences in signs between the HUC4s when comparing residual errors from the two different datasets are likely the result of the differing resolutions, and exact locations of the grids around coastlines and mountains. Although the ERA-I data are at a lower resolution, the ERA-I data result in a better overall atmospheric balance throughout the region.

5.1.2. SURFACE WATER BUDGET. Using Eq. 4 in Chapter 2, average annual percent residual errors for the surface (ε_S) are presented in Fig. 5.5. Overall, errors across the region are smaller than the atmospheric errors seen in Fig. 5.2, possibly because ε_S is more dependent on direct measurements within the region, and also suggesting that the divergence term may be responsible for the larger atmospheric errors. The northern Rockies, Upper Colorado River Basin, the Great Basin, and the Pacific coastline all show very small surface residual errors.

The basins in Arizona stand out in Fig. 5.5 for having relatively larger positive residual errors. It is expected that runoff for that region will be very low, so the positive residuals could be due to inaccuracies in the change in storage. Changes in storage could be too small because the CPC soil moisture doesn't account for enough gained, or because ground water and reservoir storage are not taken into account. It is also possible that the positive residual error is the result of a low bias with MPI ET in the region, which was previously observed in Chapter 3, over the UCRB. In fact, increasing the MPI ET would actually decrease the surface and atmospheric errors over that area.

Several basins east of the Pacific coastal basins (in central Washington, Oregon, and California) show large negative residual errors. The land cover of several of these basins show large areas of croplands and pasture. Because of the lower precipitation in these areas, croplands are heavily irrigated, leading to an imbalance between low precipitation and large ET. This does not explain the large errors for all of those basins though.

5.2. Hydroclimate Zones

Figure 5.6 allows for a spatial analysis of the surface and atmospheric balance for all the basins. Of the 44 HUC4 basins, 13 have relatively small magnitude residual errors (ε_A and ε_S), thus show better atmospheric and surface balance. Many basins balance at the surface (small ε_S), but don't balance in the atmosphere (larger ε_A). These are mainly confined to the southern Utah, southern Nevada, and Southern California, with another prominent region around northwest Colorado and southwest Wyoming. A good balance at the surface with larger imbalances in the atmosphere suggests that the errors are associated with ERA-I data.

Thirteen basins don't balance at the surface or in the atmosphere (larger ε_S and ε_A). One such region of imbalance is over Arizona. Many of the HUC4 basins just east of the Pacific coastal basins also show an imbalance at both the surface and atmosphere. If the imbalances are of opposite sign (positive ε_S with negative ε_A, or vice versa), the imbalances are harmonious, and the error can likely be narrowed down to one of the common components in both equations (precipitation or ET). These basins are shaded in light red in Fig. 5.6. When the imbalances are the same sign (both positive or both negative), they are contradictory, and the errors cannot be narrowed down to one dataset. In Fig. 5.6, these are shaded in dark red.

Most of the basins in Arizona are shaded light red, so their imbalances are consistent with each other. Errors in precipitation are assumed to be small since 1) annual precipitation totals are very small in magnitude, and 2) the PRISM dataset is derived from a dense network of directly observed precipitation measurements. Therefore, the imbalances over Arizona are due to a systematic underestimate of ET in the MPI dataset. Increasing ET would lead to a better balance at the surface and in the atmosphere.

Two other HUC4s show consistent imbalances in the surface and atmosphere (Fig. 5.6, light red shaded). One is in central California and the other is in central Oregon. Looking at the land cover over both of these basins (not shown), both show large areas of cropland. Even though runoff and precipitation are low for both basins, the predominant irrigation throughout both results in large ET. For both basins, one can assume that all components of the budget equations are relatively accurate, but that manmade runoff (e.g., water through canals) is a missing component in the equations.

Several HUC4 basins in Fig. 5.6 are shaded dark red, denoting inconsistency between the surface and atmospheric imablances. Residual errors for three of these basins, located

in southern California and one in southern Oregon, are negative for both the surface and atmosphere. For one basin, along the border of California and Arizona, residual errors are positive for both the surface and atmosphere. For all of these basins, both the MPI and the ERA-I datasets could be contributing to the errors.

In studying the patterns in Fig. 5.6, five general regions begin to stand out. 1) The HUC4 basins bordering the Pacific Ocean balance well at the surface and somewhat well in the atmosphere. 2) HUC4 basins that border the coastal basins do not balance as well. 3) The northern Rocky Mountains, extending southward through the Great Basin show overall good surface and atmospheric balance. 4) The basins in Arizona don't balance well at the surface or in the atmosphere. 5) The Colorado River headwaters region balances well at the surface, but does not balance in the atmosphere. Using topographical and land cover maps (not shown), analyzing the climatology of the entire region, and constraining the boundaries based on the above general regions, five hydroclimate zones are defined in Fig. 5.7 for the western U.S. The boundaries of each zone are delineated based on topography, consistency among land cover, and hydrologic boundaries. The surface and atmospheric balance is generally homogeneous within each zone. Although the climatology may differ across a zone, the climatological variability is mostly similar within the zone.

Figure 5.8 shows the seasonal and interannual variability of precipitation, ET, and $\nabla \cdot \mathbf{Q}$ for each named hydroclimate zone, and are described in detail in the following sections.

5.2.1. PACIFIC COAST. This zone contains all of the HUC4 basins that border the Pacific Ocean. The region is predominantly evergreen forest, and its temperate climate is moderated by the neighboring ocean. While the northern portion of the zone receives much more precipitation than the southern portion, the variability throughout is comparable. The Pacific Coast zone experiences strong convergence for much of the year. Precipitation peaks

in the cold season (November, December, and January), with very low accumulations during the summer, while ET peaks in the summer. Seasonal cycles of precipitation, ET, and $\nabla \cdot \mathbf{Q}$ are in good agreement with each other and suggest an efficient hydrologic cycle.

The interannual variability of precipitation and $\nabla \cdot \mathbf{Q}$ are somewhat similar. The lowest precipitation years coincide with the years of least convergence, and the years with higher precipitation generally match with the years of greater convergence. ET interannual variability does not match well with precipitation.

In Fig. 5.6, the basins of the Pacific Coast zone exhibit a good balance at the surface (small ε_S). The northern portion shows relatively lower atmospheric residual error, but the southern portion does not balance as well in the atmosphere. This can likely be attributed to the directional orientation of the southern HUC4s. The basins follow a northwest to southeast line, which does not match well with the north-south orientation of the ERA-I grid boxes. A higher resolution reanalysis could solve this issue, and indeed, in Fig. 5.4, two of the basins do come closer to balancing when using the NARR dataset.

5.2.2. INTERMOUNTAIN WEST. This zone is a diverse region which lies just east of the Pacific Coast zone. The western portion of the zone is primarily cropland and evergreen forest. This gives way to rangeland, with the Sierra Nevada mountains to the south and the Columbian Plateau to the north. Aside from higher annual precipitation accumulations over the Sierra Nevadas, this drier zone comprising the lee side of the coastal mountains receives much less precipitation. Peak precipitation occurs in December, January, and February, with the lowest accumulations from June through September. Peak ET occurs in the early summer, and for most of the year precipitation is greater than ET. Atmospheric convergence occurs over the Intermountain West zone for the fall and winter, while divergence dominates from May through September.

In general, the interannual variability of precipitation, ET, and $\nabla \cdot \mathbf{Q}$ are consistent with each other, although there are some discrepancies. For example, WY2006 shows the highest precipitation accumulation and the greatest magnitude of convergence, but the largest amount of ET occurred in WY2005.

This zone displays the most errors in terms of atmospheric and surface water balance (Fig. 5.6). Error type is mixed throughout this zone, with some portions balancing in the atmosphere but not the surface, while other areas balance at the surface but not the atmosphere. Several regions in the Intermountain West zone don't balance well at the surface or atmosphere. While part of this can be explained due to irrigated crops, for other areas, it's more difficult to determine the reasoning. For this zone, it appears that there are issues with multiple datasets.

5.2.3. INTERIOR PLATEAU. This zone is mostly high elevation, made up of the northern Rocky Mountains and the Great Basin, and primarily forest and rangeland. The largest precipitation accumulations occur in the northern portion of this zone, with much lower accumulations across the Great Basin. A double seasonal precipitation peak occurs - one in December/January, and the other during April/May. ET peaks around May, June, and July, and convergence and divergence are equally split for six months of the year. Overall the Interior Plateau experiences much lower seasonal variability.

Precipitation and ET interannual varibiability match fairly well with each other, and $\nabla \cdot \mathbf{Q}$ mostly matches, although there are a few minor discrepancies.

All of the Interior Plateau zone balances well at the surface with only small magnitude in residual error (Fig. 5.6). Some parts of the region (mostly located in the more arid Great Basin) don't balance as well in the atmosphere, suggesting issues with the ERA-I dataset. Overall though, the region shows a good atmospheric balance as well.

5.2.4. SOUTHWEST. This zone has two distinct regions - the higher elevation forested region to the northeast, and the lower elevation rangeland region to the southwest. Annual precipitation throughout the region is lower than most of the rest of the western U.S. While there is a slight precipitation peak in February, the most notable precipitation peak occurs in the late summer and is associated with the North American Monsoon (Vera et al. 2006), now referred to as the NAM. The NAM is also clearly identifiable with a late summer peak in ET and a dip in the $\nabla \cdot \mathbf{Q}$ toward convergence in July. Atmospheric flow over the Southwest zone is primarily divergent except for December through February.

The interannual variability of precipitation and ET match very well, with the highest (lowest) precipitation years coinciding with the highest (lowest) ET years. The variability of $\nabla \cdot \mathbf{Q}$ matches somewhat, but is not as consistent.

The majority of basins in this zone do not balance well at the surface or in the atmosphere (Fig. 5.6). As stated previously, the imbalances between the two are consistent with each other, and systematically increasing the magnitude of ET for the region would result in a better balance for both the surface and atmosphere. Because ET variability is highly correlated with observed precipitation variability in this zone, and correctly captures the NAM, the MPI ET product can be assumed to be a good dataset to use over the region, it just exhibits a bias in magnitude.

5.2.5. DIVIDE ROCKIES. This is the highest elevation zone, covering the southern Rocky Mountains. The region is mostly evergreen forest, with isolated areas of tundra. Although the Divide Rockies is the smallest zone in areal extent, the headwaters of several rivers (including the Colorado River) begin in this zone. Annual precipitation peaks in April, with a secondary peak associated with the NAM in the late summer. Seasonal ET is at its peak in June and July, but it does not show evidence of the NAM. Conditions are primarily

convergent over the Divide Rockies, except for the occurrence of weak divergence during June and July.

Precipitation and ET interannual variability are highly correlated over the Divide Rockies. $\nabla \cdot \mathbf{Q}$ displays much less interannual variability and is not as highly correlated with precipitation and ET. The year with the lowest amount of convergence does coincide with the lowest precipitation and ET year, but the year with the most convergence is not consistent with the highest precipitation and ET year.

The Divide Rockies comes very close to balancing at the surface, but there are large positive residual errors in the atmospheric balance over the zone (Fig. 5.6). This imbalance points to the possibility that ERA-I overestimates the amount of convergence that is calculated over this region.

5.3. Discussion

To more thoroughly analyze the variability and water budget of each zone, Figs. 5.9 and 5.10 show monthly means of the atmospheric and surface water budget components, averaged over every zone.

In Fig. 5.9, the Pacific Coast, Intermountain West, and Interior Plateau zones all show similar seasonal cycles of $\nabla \cdot \mathbf{Q}$ and (ET - P). Over the Pacific Coast, the seasonal variability of (ET - P) is greater than that of $\nabla \cdot \mathbf{Q}$, resulting in atmospheric water deficits (surplus) in the cold (warm) months. The greatest error occurs in December - January when either 1) not enough convergence is estimated, or 2) not enough ET is estimated. The Intermountain West zone comes very close to balancing throughout the entire year. Although the individual HUC4 basins show imbalances, the average of the entire zone balances well. Over the Interior Plateau, $\nabla \cdot \mathbf{Q}$ is always greater than (ET - P), so the zone always shows an atmospheric

water deficit. In the winter, the errors are very small, with larger errors in the spring and summer. Larger errors could be because ET is under estimated, or too much divergence is calculated. Over the Southwest, the seasonal cycles of both (ET - P) and $\nabla \cdot \mathbf{Q}$ show negative values in the winter and summer, with positive values in the spring. The zone always shows an atmospheric water deficit throughout the year, although errors are very low during the winter and spring. Errors are largest coinciding with the timing of the NAM. (ET - P) should be less than zero during this time when ET is suppressed (and it is, according to Fig. 5.9), but there should also be atmospheric convergence (Fig. 5.9 only shows divergence during this time). The Divide Rockies zone shows a similar seasonal cycle as the first three zones. But, since (ET - P) is always greater than $\nabla \cdot \mathbf{Q}$, there is always an atmospheric surplus. This zone shows large errors in the winter. This could be due to an overestimate of ET, but this is unlikely since ET values are calculated as very low in the cold months. It is more likely that convergence has been over estimated during the cold months.

In Fig. 5.10, the Pacific Coast's seasonal cycle of runoff matches the (P - ET) seasonal cycle. The calculated and observed surface storage components are well correlated, with a surface storage surplus in the cold months and a deficit in the warm months. The sesaonal cycle suggests a strong connection between precipitation and runoff for the Pacific Coast zone.

The Intermountain West and Interior Plateau zones show peak (P - ET) in the winter, with peak runoff occurring a couple months later and coinciding with the "demand" season (demand referring to the warm season months when ET is much greater than precipitation). For both zones, there is good agreement between calculated and observed surface storage changes during the winter. In the Intermountain West, errors are larger during the spring and early summer, when the calculated storage deficit is larger than the observed. This leads

to an overall deficit imbalance. The annual and seasonal imbalances can be attributed to the large amounts of ET resulting from the areas of irrigation in that zone. For the Interior Plateau, the calculated surface changes come very close to balancing, annually.

For the Southwest zone, the runoff seasonality matches well with the (P - ET) seasonality, both peaking during the winter and during the NAM. Because runoff is extremely low, (P - ET) are closely correlated with surface storage changes. Calculated surface storage changes are in good agreement with observed changes during the spring and fall months, but there is larger error in the winter and summer. As has been speculated earlier for this zone, increasing the ET in both the winter and summer would lead to a much better seasonal and annual surface balance.

Peak runoff perfectly coincides with the peak demand season over the Divide Rockies. But calculated and observed surface storage changes don't correlate as well. In the winter, the observed storage surplus is greater than the calculated surplus (pointing to a discrepancy between the precipitation and SWE). In the summer, this is offset by the calculated storage deficit being greater than the observed deficit (likely due to runoff). The two offsetting errors leads to small error in the annual surface balance for the zone.

There are several interesting points to note based on the analysis of Figs. 5.8 - 5.10:

• Combining equations 3 and 4 from Chapter 2, and assuming surface storage changes are relatively smaller, then atmopsheric divergence of water vapor will essentially balance with surface runoff. Since the Pacific Coast and Divide Rockies zones show the largest amounts of convergence, they should also have the highest runoff magnitudes. This is the case for the Pacific Coast zone, but runoff for the Divide Rockies zone is not as high as expected (further evidence that the ERA-I estimates too much convergence for the Divide Rockies).

• The Southwest zone always shows divergence, and this is supported by very low annual runoff values.

• The Pacific Coast and Southwest zones display the largest magnitudes of interannual variability. The Interior Plateau has the lowest magnitudes of interannual variability of all the zones.

• Previous studies have found that winter precipitation in the Pacific Northwest is highly sensitive to climate change (Regonda et al. 2005). Because the winter temperatures are so close to freezing, a minor shift in the climate results in large changes in seasonal peak SWE (Mote 2003), which has previously been connected to long-term decreasing trends in runoff (Hamlet and Lettenmaier 1999). However, Fig. 5.10 shows that the seasonal and interannual variability of precipitation and runoff are strongly correlated, with no consideration given to SWE. In Table 5.1, it is clear that there is a strong interannual relationship between runoff, precipitation, and SWE. But the strongest match is between runoff and precipitation, which show the same wettest and driest years (as opposed to SWE mismatching one of the wettest years).

• The water budget of the Divide Rockies (a much colder zone, therefore not as sensitive to climate change) is very sensitive to seasonal variability (Fig. 5.10). In Chapter 3, it was found that UCRB runoff is more strongly correlated with SWE variability than precipitation. Table 5.1 supports this conclusion for the Divide Rockies zone, where wettest and driest years mostly match for SWE and runoff, but don't match as well to precipitation. Due to the timing of snowpack, runoff, and the demand season, in conjunction with the relationship between snowpack and runoff variability, the Divide Rockies' sensitivity to variability has the greatest impact on water resources in the region.

TABLE 5.1. Above and below average water years (denoted as "wet" and "dry", respectively) with respect to seasonal peak SWE, total Runoff, and total Precipitation for the Pacific Coast and Divide Rockies zones.

Pacific Coast		
	wet	dry
SWE	1999,2008	2001,2005
R	1999,2006	2001,2005
P	1999,2006	2001,2005

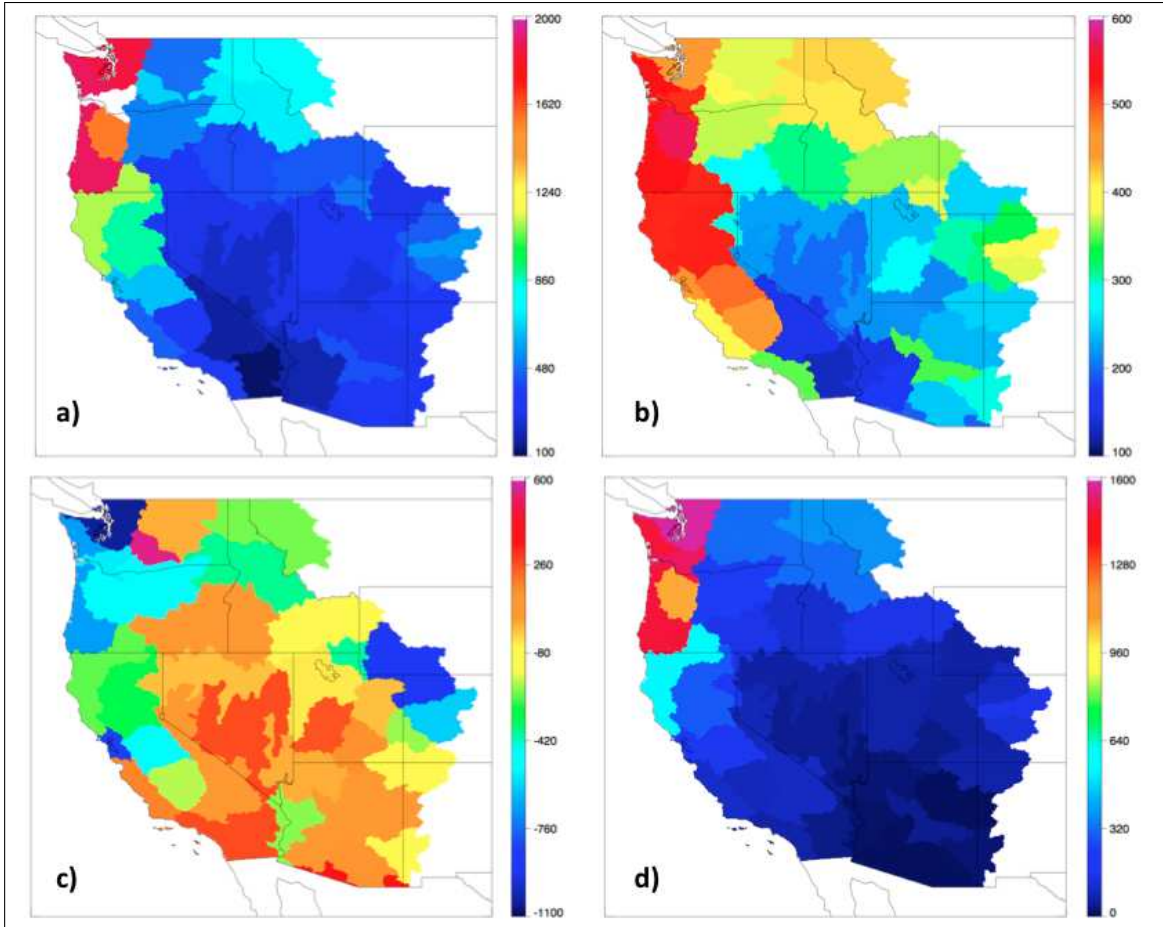| Divide Rockies		
	wet	dry
SWE	2006,2008	2002,2007
R	2006,2008	2002,2004
P	1999,2005	2000,2002

FIGURE 5.1. Average annual HUC4 PRISM precipitation (a), MPI evapotranspiration (b), ERA-I $\nabla \cdot \mathbf{Q}$ (c), and USGS surface runoff (d), all in units of mm.
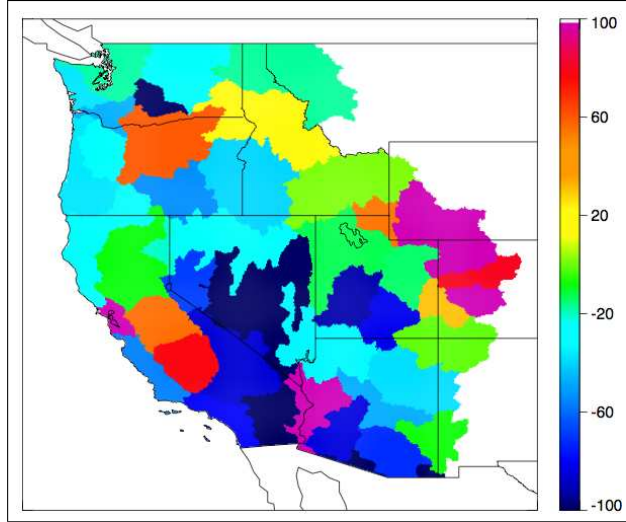
FIGURE 5.2. Atmospheric percent residual error, ε_A, for each HUC4, using ERA-I data.
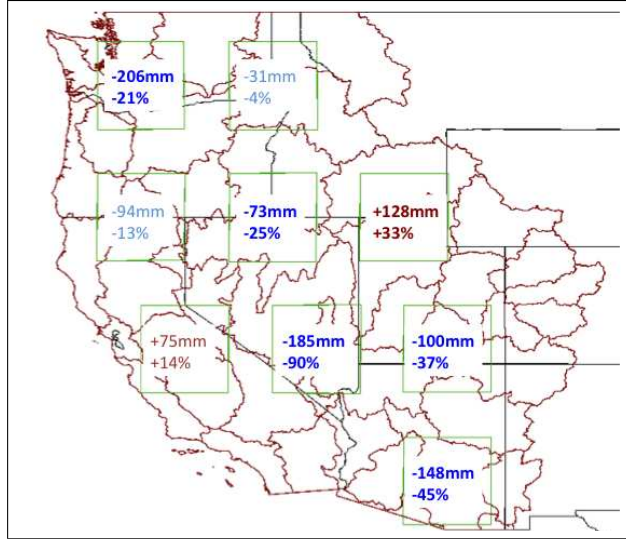
FIGURE 5.3. Atmospheric percent residual error, ε_A, for 3° by 3° boxes, using ERA-I data.
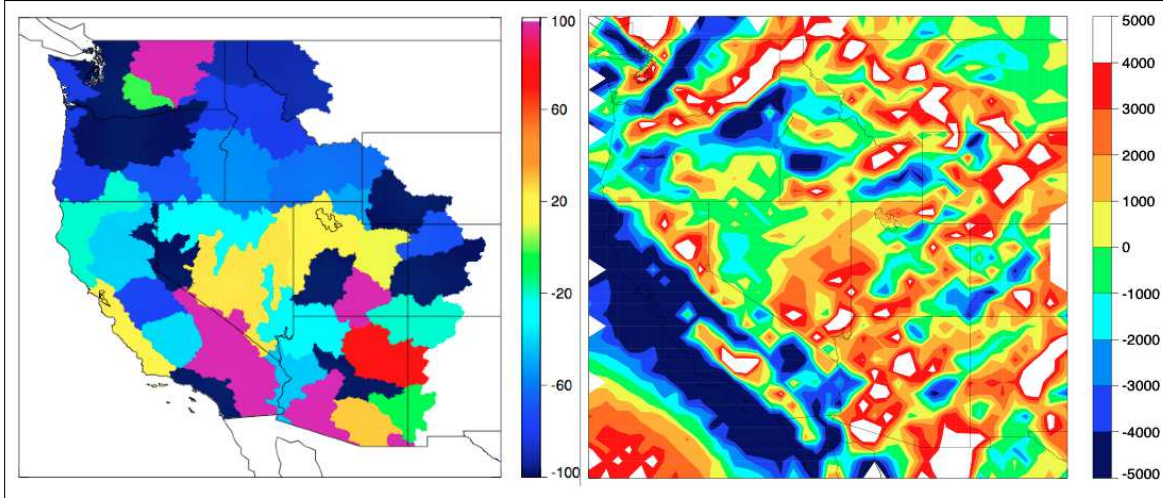
FIGURE 5.4. (Left) Atmospheric percent residual error, ε_A, for each HUC4, using NARR data, and (Right) NARR $\nabla \cdot \mathbf{Q}$ in mm.
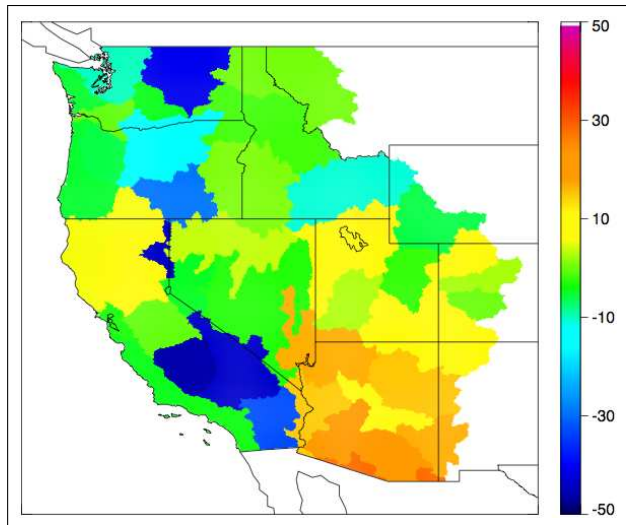
FIGURE 5.5. Surface percent residual error, ε_S, for each HUC4.
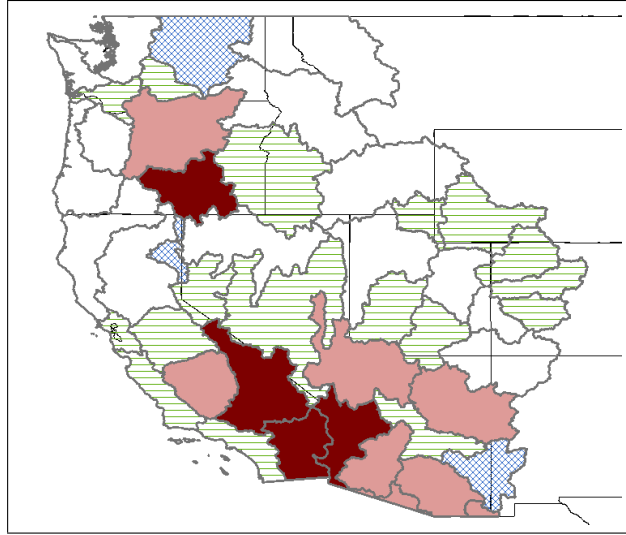
FIGURE 5.6. Designation of HUC4 basins that balance or don't balance. Non-shaded basins balance at both the surface and atmosphere. Basins with green lines balance at the surface, but not in the atmosphere. Blue hatched basins balance in the atmosphere, but not at the surface. Red basins don't balance at the surface or atmosphere (light red denotes similar imbalance between surface and atmosphere, dark red denotes opposite imbalances).
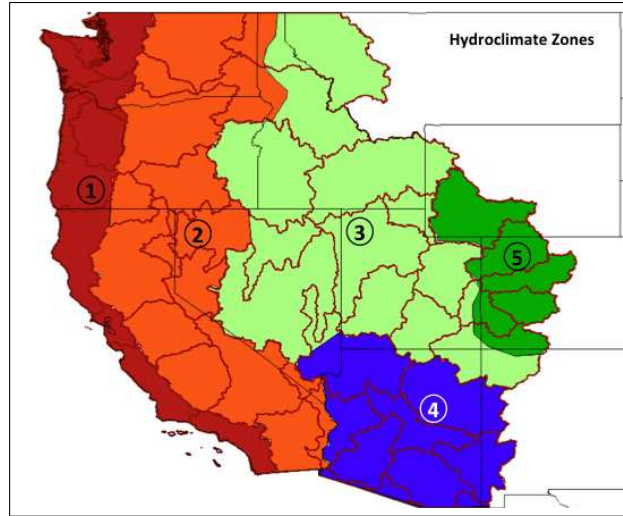
FIGURE 5.7. Boundaries of the five defined hydroclimate zones: 1) Pacific Coast, 2) Intermountain West, 3) Interior Plateau, 4) Southwest, and 5) Divide Rockies.
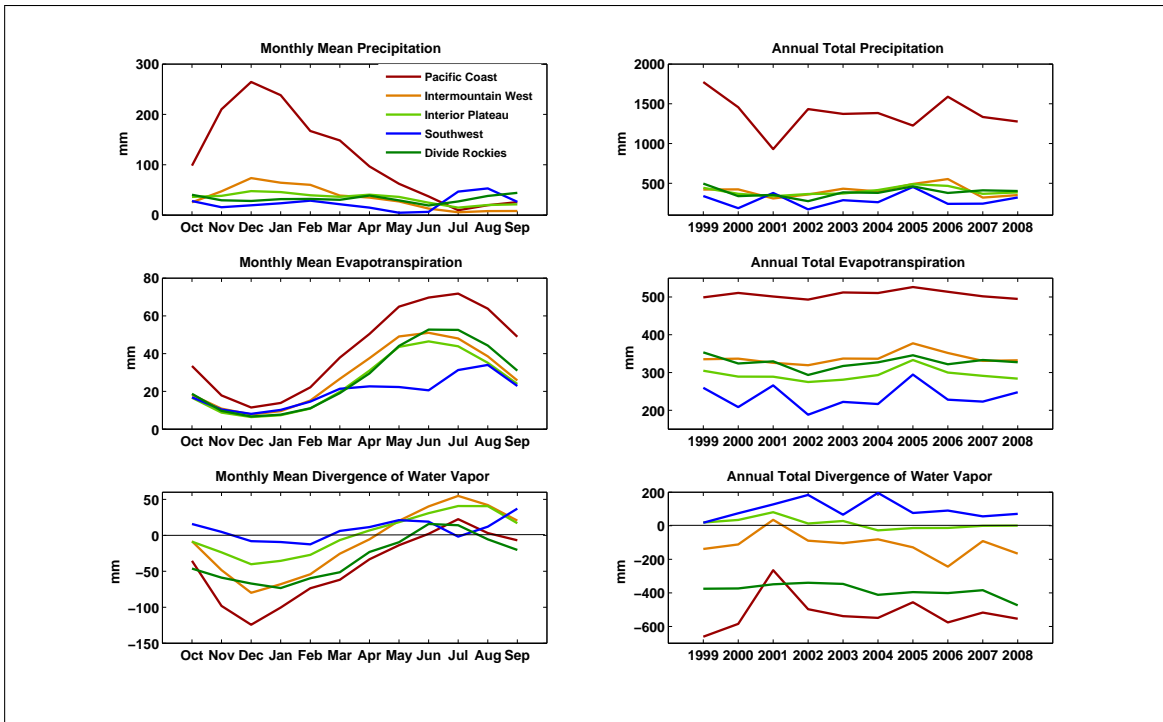
FIGURE 5.8. Monthly mean (left side) and annual total (right side) precipitation, ET, and $\nabla \cdot \mathbf{Q}$, for each of the hydroclimate zones.
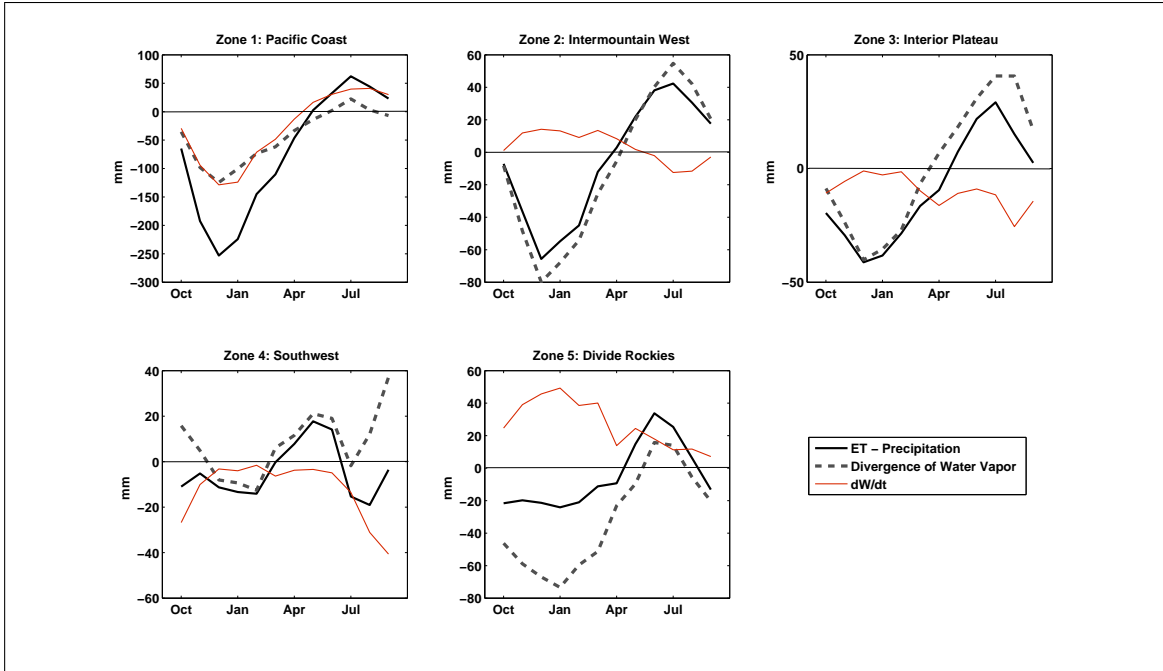
FIGURE 5.9. Monthly mean atmospheric balance components for each hydro-climate zone. Monthly atmospheric balance equation is $dW/dt = (ET - P) - \nabla \cdot \mathbf{Q}$.
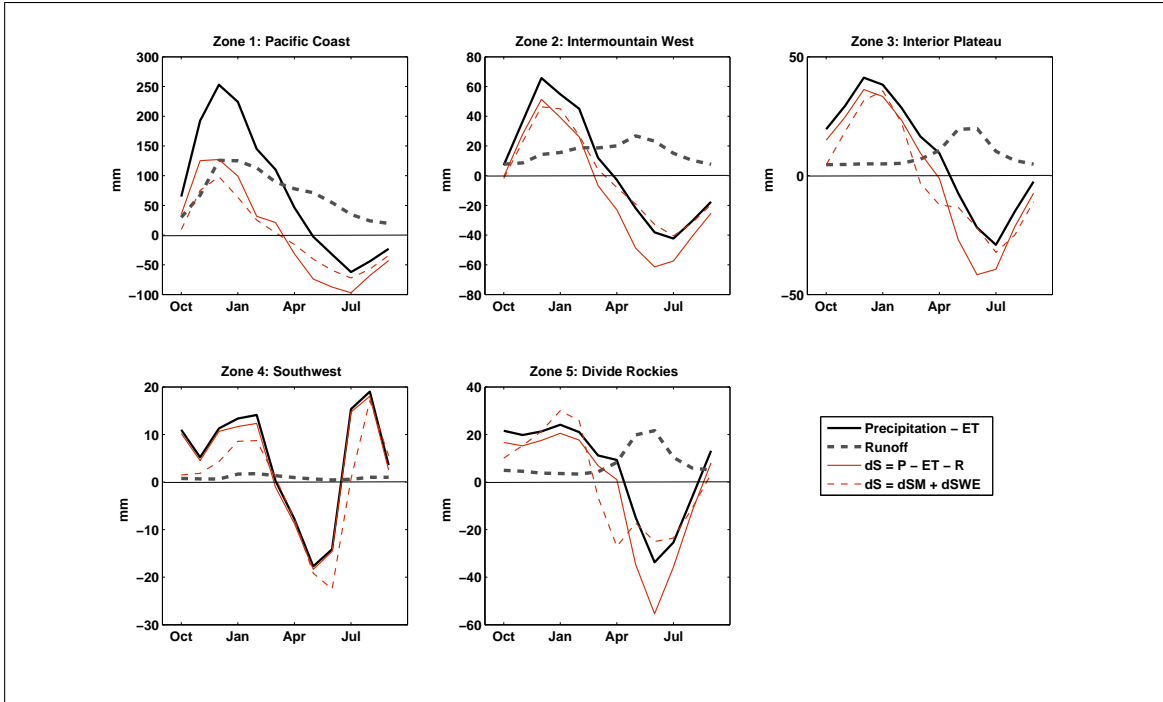
FIGURE 5.10. Monthly mean surface balance components for each hydrocli-
mate zone. Calculated $dS = P - ET - R$, and observed dS is the sum of
changes in soil moisture and snow water equivalent.

CHAPTER 6

Conclusions

6.1. Chapter 3 Summary

Utilizing *in-situ*, reanalysis, and satellite-derived datasets, each component of the surface and atmospheric water budgets is analyzed for the Upper Colorado River Basin. In general, all products capture the seasonal cycle of each water budget component.

In terms of interannual variability, there is a strong relationship between precipitation, ET, and soil moisture, while total runoff is more strongly correlated with SWE peaks. This key finding indicates that water years with greater amounts of rain but lower snowpack will result in increased ET lost to the atmosphere and lower surface runoff.

Using estimates of precipitation, ET, and runoff that are consistent amongst each other, estimated change in surface storage is calculated. The magnitude and inter-annual variability of estimated ΔS is comparable to GLDAS and to calculated changes in (AMSR-E SWE + reservoir + soil moisture). When estimates of precipitation, ET, and $\nabla \cdot \mathbf{Q}$ are used to estimate changes in atmospheric storage, there are generally small changes in annual atmospheric storage.

Several key results were found when analyzing long-term storage changes (shown in Table 2):

- The estimated long-term ΔS shows a large gain in surface storage while long-term changes in (reservoir + soil moisture) leads to a small gain in surface storage. Both the CSR and GLDAS actually show surface storage losses for the same time period.

- Long-term $\nabla \cdot \mathbf{Q}$ is convergent for ERA-I and divergent for MERRA. Adding surface runoff to either estimated ΔS or changes in (reservoir + soil moisture) yields a surplus of

surface water. This means atmospheric convergence occurred (i.e. the ERA-I $\nabla \cdot \mathbf{Q}$ yields more accurate results).

• Increasing MPI ET by 5% leads to a closer balance between ERA-I $\nabla \cdot \mathbf{Q}$ and surface runoff + estimated ΔS. The 5% increase also leads to a better balance in $\frac{\partial W}{\partial t}$.

6.2. Chapter 4 Summary

When looking at correlations between SSTs and each sub-basin's variability, there are only minimal differences. Overall, every sub-basin shows similar correlations with SSTs. Basin temperature and precipitation are significantly correlated with SSTs in the ENSO and PDO regions during October and November. Beyond November, there's little to no significant correlation or lag correlations in the ENSO and PDO regions. Although significant, correlations and lag correlations are rarely above 0.4. Additionally, when changing the time period used, lag correlations are not spatially consistent, and therefore the results are not considered robust.

An EOF and PC analysis of the individual sub-basins, as well as the entire basin as one, was used to shed light on the dominant modes of variability in the region. The first mode EOF shows little spatial variability, and the PC time series exhibits high year-to-year variability. The second mode is correlated with ENSO and PDO and shows a north-south gradient. When looking at the individual sub-basins, the second EOF mode shows an elevation dependence. The third PC mode is not correlated with any large-scale climate indices and is different for temperature and precipitation. While the EOF and PC analysis does point to a relationship with ENSO and PDO (in the second mode), it mainly shows that the variability in the basin is more sensitivie to individual cold season patterns, rather than large-scale climate variations.

The results from both the correlation and EOF analyses indicate that although the UCRB does have some relationship with ENSO and PDO, the variability in the basin is more dominated by year-to-year variability not explained by large-scale long-term climate regimes. Because of this, an accurate seasonal prediction for the basin is very difficult.

A more detailed investigation of the sub-seasonal characteristics in each sub-basin yielded several interesting results. For the northern sub-basins, March and April are generally the largest contributors to the seasonal total, while October is usually the largest contributor for the southern sub-basins. The southern sub-basins exhibit more variability (monthly and seasonally) than the northern sub-basins. Overall, February shows the least variability, regardless of if the season is wet, dry, or average.

Both the SST correlations and the monthly analysis point to the importance of October. For the southern sub-basins, October precipitation is the largest contributor to the seasonal total, and October is also more strongly correlated with ENSO/PDO. Additionally, a wet October increases the likelihood of a wet season. October was generally found to be an important month for the hydroclimate of the UCRB. When cold season precipitation falls as rain instead of snow (more likely to happen early in the season, like October), the seasonal total could be wetter than average but overall runoff will be reduced due to lower peak snowpack. The results for October do show that it could provide some information about the rest of the season (particularly after a wet October), but the correlations are still not strong enough to solely depend on statistics for an accurate prediction.

A case study looked in-depth at the 1997 and 2002 seasons - both showed similar ENSO and PDO conditions, but 1997 was a wet season while 2002 was dry. The ENSO and PDO conditions (both mainly in the cold phase during the winter), could indicate warm and dry conditions across the basin (based on the results from Section 3). The majority of the months

during the 2002 season were warmer and drier. Although there were warmer than average months during the 1997 season, most of the months were wet.

There was only a minimal difference in the number of snow accumulation days between the seasons, however 1997 had a much greater frequency of large accumulation days (greater than 10 mm). This result supports a previous study that concluded the basin's water balance was more dependent on large accumulating and longer duration winter storm events (Rasmussen 1968).

An analysis of a 1997 storm with the largest 24-hour accumulation of the season (at 19 mm) showed a slow moving surface low along the northern part of the basin, with fronts surrounding the basin to the east and to the north and a surface high to the south. The prevailing flow across the basin was westerly. A similar synoptic pattern was found during the 2002 season, but minor differences resulted in a much lower accumulating storm (less than 4 mm). When evaluating the synoptic conditions for several other larger accumulating storms during both seasons, diverse results could be found. Modification of airmasses, precise positioning of troughs and fronts, and the speed and intensity of the troughs can ultimately affect the amount of accumulation over the basin, thus showing that local factors (controlling the instability and moisture availability over the basin), not large-scale drivers (SST), are responsible for the variability across the basin.

Basin variability has proven to be complex and diverse. Its relationship with large-scale climate variability, although present, is weak and not recommended for use as a predictor. Additionally, the basin's sensitivity to even small variations in monthly patterns and synoptic systems leads to the conclusion that accurate seasonal prediction is not realistic at this time.

6.3. Chapter 5 Summary

A bigger picture analysis of the water budget over the western United States was performed. This qualitative analysis allows for identification of strengths and weaknesses of different datasets' measurements of the water budget components over different regions. It also allows for the definition of five self-similar hydroclimate zones.

The atmospheric water budget over each HUC4 does not balance well for many of the basins. Large negative errors occur over the southwest, and large positive errors are found over the southern Rocky Mountains and across central Oregon and central California. Using a higher resolution dataset to calculate $\nabla \cdot \mathbf{Q}$ does not result in smaller error, and it is determined that, overall, the ERA-I dataset is the most accurate for the western U.S. Surface water budget over the region yields generally much smaller errors. Larger errors in Arizona are attributed to a systematic bias in the MPI ET dataset, while larger errors in several basins in central Washington and central California are the result of heavy irrigation not being taken into account in any of the datasets.

Based on a visual inspection of the west's different balances and imbalances, several regions begin to become evident. This leads to the creation of five hydroclimate zones. Their boundaries are defined by compositing similarities in topography, land cover, and climate variability. The Pacific Coast zone balances well at the surface and the atmosphere, and it displays a large amount of interannual variability amongst all the water budget components. The Intermountain West zone shows a large mixture of imbalances throughout the region, indicating that several different dataset issues exist. The Interior Plateau zone mostly balances well at the surface and the atmosphere, with a few larger errors in the atmosphere (the result of inaccuracies in the ERA-I dataset). It also shows the least amount of interannual variability of all the zones. The Southwest zone does not balance well at the surface or in

the atmosphere. However, systematically increasing the MPI ET values during the winter and summer would lead to a better annual balance at both the surface and atmosphere. Interannual variability in this zone is very large. The Divide Rockies zone balances well at the surface, but does not balance in the atmosphere. These imbalances are the result of ERA-I's tendency to overestimate winter convergence over the region.

Analysis of the water budget's seasonal variability for each zone shows some notable results. The North American Monsoon is observed in every water budget component for the Southwest zone. For the Pacific Coast zone, the seasonal cycle of the atmospheric and surface water components match well, and a strong relationship between precipitation and runoff variability is evident. The Intermountain West, Interior Plateau, and Divide Rockies zones all show an offset between the highest (P - ET) values and peak runoff - in other words, higher runoff occurs during the "demand" season (when ET is much greater than P). The Divide Rockies zone shows a much stronger relationship between SWE and runoff variability, and the water resources of this zone are much more vulnerable to variability.

6.4. Conclusions

This research has identified self-consistent datasets to use for water budget analysis over the complex topography of the Upper Colorado River Basin. It has also pinpointed the weaknesses of several satellite-derived and reanalysis datasets over the region. These datasets were expanded for use over the entire western U.S. to determine the datasets' strengths and weaknesses.

The definition of five hydroclimate zones highlights areas with similar climatological hydrologic variability. These five zones show that MPI exhibits overall accurate ET measurements with the exception of Arizona, where ET is underestimated. The ERA-I dataset

(while lower resolution) performs fairly well at estimating $\nabla \cdot \mathbf{Q}$, although it tends to over-estimate convergence near the Continental Divide region.

Some notable results have been found over the UCRB:

• Total runoff is more strongly correlated with SWE than with precipitation.

• Although significant correlations are found, relationships between UCRB variability and large-scale climate indices are not particularly strong.

• October shows the strongest possibility of indicating future conditions. It shows the most significant correlation with ENSO/PDO; whether it rains or snows in this month can greatly affect the overall runoff in the spring; and a wet October could increase the possibility of an overall wet winter season.

• Winter season moisture totals are dependent on only a few larger storms. The difference between a wet and dry season is largely the result of a difference in the frequency of a few large accumulating events.

Bibliography

Abatzoglou, J. T., 2011: Influence of the PNA on declining mountain snowpack in the western United States. *Inter. J. Climatol.*, **31**, 1135–1142.

Ault, T. R., and S. S. George, 2010: The magnitude of decadal and multidecadal variability in North American precipitation. *J. Climate*, **23**, 842–850.

Aziz, O. A., G. A. Tootle, S. T. Gray, and T. C. Piechota, 2010: Identification of Pacific Ocean sea surface temperature influences of Upper Colorado River Basin snowpack. *Water Resour. Res.*, **46**, W07536, doi:10.1029/2009WR008053.

Bao, X., and F. Zhang, 2012: Evaluation of NCEP/CFSR, NCEP/NCAR, ERA-Interim and ERA-40 reanalysis datasets against independent sounding observations over the Tibetan Plateau. *J. Climate*, doi:10.1175/JCLI-D-12-00056.1.

Barnett, T., R. Malone, W. Pennell, D. Stammer, B. Semtner, and W. Washington, 2004: The effects of climate change on water resources in the west: introduction and overview. *Climate Change*, **62**, 1–11.

Bosilovich, M. G., F. R. Robertson, and J. Chen, 2011: Global energy and water budgets in MERRA. *J. Climate*, **24**, 5721–5739.

Cayan, D. R., 1996: Interannual climate variability and snowpack in the western United States. *J. Climate*, **9**, 928–948.

Chambers, D. P., 2006: Evaluation of new GRACE time-variable gravity data over the ocean. *Geophys. Res. Lett.*, **33**, L17603, doi:10.1029/2006GL027296.

Changnon, D., T. B. McKee, and N. J. Doesken, 1993: Annual snowpack patterns across the Rockies: long-term trends and associated 500-mb synoptic patterns. *Mon. Wea. Rev.*, **121**, 633–647.

Christensen, N. S., and D. P. Lettenmaier, 2007: A multimodel ensemble approach to climate change impacts on the hydrology and water resources of the Colorado River Basin. *Hyrol. Earth Syst. Sci.*, **11**, 1417–1434.

Clark, G. M., 2010: Changes in patterns of streamflow from unregulated watersheds in Idaho, western Wyoming, and northern Nevada. *JAWRA*, **46**, doi: 10.1111/j.1752-1688.2009.00416.x.

Daly, C., R. P. Neilson, and D. L. Phillips, 1994: A statistical-topographic model for mapping climatological precipitation over mountainous terrain. *J. Appl. Meteor.*, **33**, 140–158.

De Lannoy, G. J. M., R. H. Reichle, K. R. Arsenault, P. R. Houser, S. Kumar, N. E. C. Verhoest, and V. R. N. Pauwels, 2012: Multiscale assimilation of Advanced Microwave Scanning Radiometer-EOS snow water equivalent and Moderate Resolution Imaging Spectroradiometer snow cover fraction observations in northern Colorado. *Water Resour. Res.*, **48**, W01522, doi:10.1029/2011WR010588.

Decker, M., M. Brunke, Z. Wang, K. Sakaguchi, X. Zeng, and M. G. Bosilovich, 2012: Evaluation of the reanalysis products from GSFC, NCEP, and ECMWF using flux tower observations. *J. Climate*, **25**, 1916–1944.

Dee, D. P., and Coauthors, 2011: The ERA-Interim reanalysis: configuration and performance of the data assimilation system. *Quart. J. Roy. Meteor. Soc.*, **137**, 553–597.

Dettinger, M. D., and D. R. Cayan, 1995: Large-scale atmospheric forcing of recent trends toward early snowmelt runoff in California. *J. Climate*, **8**, 606–623.

Entekhabi, D., I. Rodriguez-Iturbe, and R. L. Bras, 1992: Variability in large-scale water balance with land surface-atmosphere interaction. *J. Climate*, **5**, 798–813.

Fan, Y., and H. van den Dool, 2004: Climate Prediction Center global monthly soil moisture data set at 0.5 ° resolution for 1948 to present. *J. Geophys. Res.*, **109**, D10102, doi:10.1029/2003JD004345.

Fersch, B., H. Kunstmann, A. Bardossy, B. Devaraju, and N. Sneeuw, 2012: Continental-scale water storage variation from global and dynamically downscaled atmospheric water budgets in comparison with GRACE-derived observations. *J. Hydrometeor.*, **13**, 1589–1603.

Fisher, J. B., K. P. Tu, and D. D. Baldocchi, 2008: Global estimates of the land-atmosphere water flux based on monthly AVHRR and ISLSCP-II data, validated at 16 FLUXNET sites. *Remote Sensing of Environment*, **112**, 901–919.

Franz, K. J., H. C. Hartmann, S. Sorooshian, and R. Bales, 2003: Verification of National Weather Service ensemble streamflow predictions for water supply forecasting in the Colorado River Basin. *J. Hydrometeor.*, **4**, 1105–1118.

Groisman, P. Y., T. R. Karl, R. W. Knight, and G. L. Stenchikov, 1994: Changes in snow-cover, temperature, and radiative heat balance over the Northern Hemisphere. *J. Climate*, **7**, 1633–1656.

Haiden, T., and G. Pistotnik, 2009: Intensity-dependent parameterization of elevation effects in precipitation analysis. *Adv. Geosci.*, **20**, 33–38.

Hamlet, A. F., and D. P. Lettenmaier, 1999: Effects of climate change on hydrology and water resources in the Columbia River Basin. *JAWRA*, **35**, 1597–1623.

Hamlet, A. F., P. W. Mote, M. P. Clark, and D. P. Lettenmaier, 2007: Twentieth-century trends in runoff, evapotranspiration, and soil moisture in the western United States. *J. Climate*, **20**, 1468–1486.

Harpold, A., P. Brooks, S. Rajagopal, I. Heidbuchel, A. Jardine, and C. Stielstra, 2012: Changes in snowpack accumulation and ablation in the intermountain west. *Water Resources Res.*, **48**, doi: 10.1029/2012WR011949.

Hirpa, F. A., M. Gebremichael, and T. Hopson, 2010: Evaluation of high-resolution satellite precipitation products over very complex terrain in Ethiopia. *J. Appl. Meteor. Climatol.*, **49**, 1044–1051.

Hoerling, M., and J. Eischeid, 2007: Past peak water in the Southwest. *Southwest Hydrol.*, **6**, 18–19.

Huang, J., H. M. van den Dool, and K. P. Georgakakos, 1996: Analysis of model-calculated soil moisture over the United States (1931 - 1993) and applications to long-range temperature forecasts. *J. Climate*, **9**, 1350–1362.

Huffman, G. J., and Coauthors, 2007: The TRMM Multisatellite Precipitation Analysis (TMPA): quasi-global, multiyear, combined-sensor precipitation estimates at fine scales. *J. Hydrometeor.*, **8**, 38–55.

Hurkmans, R., P. A. Troch, R. Uijlenhoet, P. Torfs, and M. Durcik, 2009: Effects of climate variability on water storage in the Colorado River Basin. *J. Hydrometeor.*, **10**, 1257–1270.

Jimenez, C., and Coauthors, 2011: Global intercomparison of 12 land surface heat flux estimates. *J. Geophys. Res.*, **116**, D02102, doi:10.1029/2010JD014545.

Jung, M., M. Reichstein, and A. Bondeau, 2009: Towards global empirical upscaling of FLUXNET eddy covariance observations: validation of a model tree ensemble approach using a biosphere model. *Biogeosciences*, **6**, 2001–2013.

Kelly, R. E., 2009: The AMSR-E snow depth algorithm: Description and initial results. *J. Remote Sens. Soc. Jpn.*, **29**, 307–317.

Kennedy, A. D., X. Dong, B. Xi, S. Xie, Y. Zhang, and J. Chen, 2011: A comparison of MERRA and NARR reanalyses with DOE ARM SGP data. *J. Climate*, **24**, 4541–4557.

Kim, T. W., B. Valdes, B. Nijssen, and D. Roncayolo, 2005: Quantification of linkages between large-scale climatic patterns and precipitation in the Colorado River Basin. *J. Hydrol.*, **321**, 173–186.

Kustas, W. P., and Coauthors, 1991: An interdisciplinary field study of the energy and water fluxes in the atmosphere-biosphere system over semiarid rangelands: description and some preliminary results. *Bull. Amer. Meteor. Soc.*, **72**, 1683–1705.

Lorenz, C., H. Kunstmann, B. Devaraju, M. J. Tourian, N. Sneeuw, and J. Riegger, 2014: Large-scale runoff from landmasses: a global assessment of the closure of the hydrological and atmospheric water balances. *J. Hydrometeor.*, in press.

MacDonald, R. J., J. M. Byrne, S. W. Kienzle, and R. P. Larson, 2011: Assessing the potential impacts of climate change on mountain snowpack in the St. Mary River watershed, Montana. *J. Hydrometeor.*, **12**, 262–273.

McCabe, G. J., and M. D. Dettinger, 2002: Primary modes and predictability of year-to-year snowpack variations in the western United States from teleconnections with Pacific Ocean climate. *J. Hydrometeor.*, **3**, 13–25.

McCabe, G. J., and D. M. Wolock, 2007: Warming may create substantial water supply shortages in the Colorado River Basin. *Geophys. Res. Lett.*, **34**, L22708, doi:10.1029/2007GL031764.

McKee, T. B., N. J. Doesken, and J. Kleist, 1993: The relationship of drought frequency and duration of time scales. *9th Conference on Applied Climatology*, Anaheim, CA, 179—186.

Mesinger, F., and Coauthors, 2006: North American Regional Reanalysis. *Bull. Amer. Meteor. Soc.*, **87**, 343–360.

Miller, W. P., and T. C. Piechota, 2008: Regional analysis of trend and step changes observed in hydroclimatic variability around the Colorado River Basin. *J. Hydrometeor.*, **9**, 1020–1034.

Mo, K. C., J. E. Schemm, and S. Yoo, 2009: Influence of ENSO and the Atlantic Multidecadal Oscillation on drought over the United States. *J. Climate*, **22**, 5962–5982.

Mote, P. W., 2003: Trends in snow water equivalent in the Pacific Northwest and their climatic causes. *Geophys. Res. Lett.*, **30**, 1601–1604.

Mueller, B., and Coauthors, 2011: Evaluation of global observations-based evapotranspiration datasets and IPCC AR4 simulations. *Geophys. Res. Lett.*, **38**, L06402, doi:10.1029/2010GL046230.

Nolin, A. W., 2012: Perspectives on climate change, mountain hydrology, and water resources in the Oregon Cascades, USA. *Mountain Res. and Develop.*, **32**, 35–46.

Nowak, K., M. Hoerling, B. Rajagopalan, and E. Zagona, 2012: Colorado River Basin hydroclimatic variability. *J. Climate*, **25**, 4389–4403.

NRCS NWCC, cited 2012: SNOTEL data network - general information. [Available online at http://www.wcc.nrcs.usda.gov/snow/about.html.].

Pederson, G. T., S. T. Gray, T. Ault, W. Marsh, D. B. Fagre, A. G. Bunn, C. A. Woodhouse, and L. J. Graumlich, 2011: Climatic controls on the snowmelt hydrology of the northern Rocky Mountains. *J. Climate*, **24**, 1666–1687.

Peixoto, J. P., and A. H. Oort, 1992: *Physics of Climate*. Springer, 520 pp.

Rasmussen, J. L., 1968: Atmospheric water balance of the Upper Colorado River Basin. Ph.D. thesis, Colorado State University, 111 pp. [Available from http://lib.colostate.edu/repository]

Rayner, N. A., D. E. Parker, E. B. Horton, C. K. Folland, L. V. Alexander, D. P. Rowell, E. C. Kent, and A. Kaplan, 2003: Global analyses of sea surface temperature, sea ice, and night marine air temperature since the late nineteenth century. *J. Geophys. Res.*, **108**, doi:10.1029/2002JD002670.

Redmond, K. T., and R. W. Koch, 1991: Surface climate and streamflow variability in the western United States and their relationship to large-scale circulation indices. *Water Resour. Res.*, **27**, 2381–2399.

Regonda, S. K., B. Rajagopalan, M. Clark, and J. Pitlick, 2005: Seasonal cycle shifts in hydroclimatology over the western United States. *J. Climate*, **18**, 372–384.

Reichle, R. H., R. D. Koster, G. J. M. De Lannoy, B. A. Forman, Q. Liu, S. P. P. Mahanama, and A. Toure, 2011: Assessment and enhancement of MERRA land surface hydrology estimates. *J. Climate*, **24**, 6322–6338.

Reichle, R. H., R. D. Koster, J. Dong, and A. A. Berg, 2004: Global soil moisture from satellite observations, land surface models, and ground data: implications for data assimilation. *J. Hydrometeor.*, **5**, 430–442.

Rienecker, M., and Coauthors, 2011: MERRA: NASA's Modern-Era Retrospective Analysis for Research and Applications. *J. Climate*, **24**, 3624–3648.

Rodell, M., J. S. Famiglietti, J. Chen, S. I. Seneviratne, P. Viterbo, S. Holl, and C. R. Wilson, 2004a: Basin scale estimates of evapotranspiration using GRACE and other observations. *Geophys. Res. Lett.*, **31**, L20504, doi:10.1029/2004GL020873.

Rodell, M., and Coauthors, 2004b: The Global Land Data Assimilation System. *Bull. Amer. Meteor. Soc.*, **85**, 381–394.

Saha, S., and Coauthors, 2010: The NCEP climate forecast system reanalysis. *Bull. Amer. Meteor. Soc.*, **91**, 1015–1057.

Sapiano, M. R. P., and P. A. Arkin, 2009: An intercomparison and validation of high-resolution satellite precipitation estimates with 3-hourly gauge data. *J. Hydrometeor.*, **10**, 149–166.

Seaber, P. R., F. P. Kapinos, and G. L. Knapp, 1987: *Hydrologic Unit Maps: U.S. Geological Survey*. Water-Supply Paper 2294, 63 pp.

Seager, R., and Coauthors, 2007: Model projections of an imminent transition to a more arid climate in southwestern North America. *Science*, **316**, 1181–1184.

Sheffield, J., B. Livneh, and E. F. Wood, 2012: Representation of terrestrial hydrology and large-scale drought of the continental United States from the North American Regional Reanalysis. *J. Hydrometeor.*, **13**, 856–876.

Stewart, I. T., D. R. Cayan, and M. D. Dettinger, 2005: Changes toward earlier streamflow timing across western North America. *J. Climate*, **18**, 1136–1155.

Swenson, S. C., and J. Wahr, 2006: Post-processing removal of correlated errors in GRACE data. *Geophys. Res. Lett.*, **33**, L08402, doi:10.1029/2005GL025285.

Switanek, M. B., P. A. Troch, and C. L. Castro, 2009: Improving seasonal predictions of climate variability and water availability at the catchment scale. *J. Hydrometeor.*, **10**, 1521–1533.

Tang, Q., H. Gao, P. Yeh, T. Oki, F. Su, and D. P. Lettenmaier, 2010: Dynamics of terrestrial water storage change from satellite and surface observations and modeling. *J. Hydrometeor.*, **11**, 156–170.

Tootle, G. A., and T. C. Piechota, 2006: Relationships between Pacific and Atlantic ocean sea surface temperatures and U.S. streamflow variability. *Water Resour. Res.*, **42**, W07411, doi:10.1029/2005WR004184.

Trenberth, K. E., and C. J. Guillemot, 1998: Evaluation of the atmospheric moisture and hydrological cycle in the NCEP/NCAR Reanalyses. *Climate Dyn.*, **14**, 213–231.

Trenberth, K. E., D. P. Stepaniak, and J. M. Caron, 2000: The global monsoon as seen through the divergent atmospheric circulation. *J. Climate*, **13**, 3969–3993.

Vera, C., and Coauthors, 2006: Toward a unified view of the American monsoon systems. *J. Climate*, **19**, 4977–5000.

Werner, K., D. Brandon, M. Clark, and S. Gangopadhyay, 2004: Climate index weighting schemes for NWS ESP-based seasonal volume forecasts. *J. Hydrometeor.*, **5**, 1076–1090.

Zaitchik, B. F., M. Rodell, and R. H. Reichle, 2008: Assimilation of GRACE terrestrial water storage data into a land surface model: Results for the Mississippi River Basin. *J. Hydrometeor.*, **9**, 535–548.